

**A MULTI-PROXY STUDY OF THE KIZILIRMAK RIVER TERRACES AND
ITS DELTA, NORTHERN TURKEY: IMPLICATIONS FOR TECTONICS,
SEDIMENTATION, SEA LEVEL AND ENVIRONMENTAL CHANGES**



Ph. D. THESIS

Christopher BERNDT

**Department of Solid Earth Sciences
Geodynamics Programme**

APRIL 2019

**A MULTI-PROXY STUDY OF THE KIZILIRMAK RIVER TERRACES AND
ITS DELTA, NORTHERN TURKEY: IMPLICATIONS FOR TECTONICS,
SEDIMENTATION, SEA LEVEL AND ENVIRONMENTAL CHANGES**



Ph. D. THESIS

**Christopher BERNDT
(602142002)**

Department of Solid Earth Sciences

Geodynamics Programme

**Thesis Advisor: Prof. Dr. Attila ÇİNER
Thesis Co-Advisor: Assoc. Prof. Cengiz YILDIRIM**

APRIL 2019

İSTANBUL TEKNİK ÜNİVERSİTESİ ★ AVRASYA YER BİLİMLERİ
ENSTİTÜSÜ

**KIZILIRMAK NEHİR TERASLARI VE DELTASININ ÇOKLU-PROKSİ
YÖNTEMİ İLE ÇALIŞMASI: TEKTONİK, SEDİMENTASYON, DENİZ
SEVİYESİ VE ÇEVRESEL DEĞİŞİKLİKLER İLE İLGİLİ ÇIKARIMLAR**

DOKTORA TEZİ

Christopher BERNDT
(602142002)

Katı Yer Bilimleri
Jeodinamik Programı

Tez Danışmanı: Prof. Dr. Attila ÇİNER
Eş Danışman: Doç. Dr. Cengiz YILDIRIM

NİSAN 2019

Christopher Berndt, a Ph.D. student of İTÜ Eurasia Institute of Earth Sciences, student ID 602142002, successfully defended the dissertation entitled “A MULTI-PROXY STUDY OF THE KIZILIRMAK RIVER TERRACES AND ITS DELTA, NORTHERN TURKEY: IMPLICATIONS FOR TECTONICS, SEDIMENTATION, SEA LEVEL AND ENVIRONMENTAL CHANGES”, which he prepared after fulfilling the requirements specified in the associated legislations, before the jury whose signatures are below.

Thesis Advisor : **Prof. Dr. Attila ÇİNER**
İTÜ Avrasya Yer Bilimleri Enstitüsü




Co-advisor : **Doç. Dr. Cengiz YILDIRIM**
İTÜ Avrasya Yer Bilimleri Enstitüsü



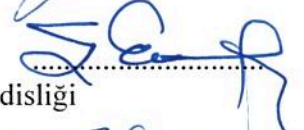
Jury Members : **Doç. Dr. Tolga GÖRÜM**
İTÜ Avrasya Yer Bilimleri Enstitüsü



Doç. Dr. Kadir ERİŞ
İTÜ Jeoloji Mühendisliği Bölümü



Prof. Dr. Şükrü ERSOY
Yıldız Teknik Üniversitesi, İnşaat Mühendisliği



Prof. Dr. Faruk OCAKOĞLU
Eskişehir Osman Gazi Üniversitesi, Jeoloji Mühendisliği



Prof. Dr. Tuncer DEMİR
Akdeniz Üniversitesi, Coğrafya Bölümü



Date of Submission : 20 March 2019

Date of Defence : 19 April 2019





To my mom,



FOREWORD

First, I would like to thank my supervisor Prof. Attila Çiner for giving me the opportunity to work as a member of his research team, his great support in all academic, fieldwork, financial and organizational matters. I am further thankful for his significant support to improve my scientific skills and his great help for housing and personal issues.

Furthermore, I would like to thank my co-supervisor Doç. Dr. Cengiz Yıldırım for his great scientific support in several ways and for improving the critical way of thinking.

I further thank Dr. Peter Frenzel for his great advisory, scientific and technical support and Friedrich Schiller University of Jena to provide housing during my secondments.

In addition, I would like to thank Prof. Dr. Aral Okay, Prof. Dr. Namık Çağatay and Prof. Dr. Ercan Özcan for providing access to their laboratories for the sample preparation. I also thank Statik Mühendislik for the sediment core recovery, the Eastern Mediterranean Centre for Oceanography and Limnology for the geochemical data acquisition of the sediment core and support during preparation, Prof. Dr. Nafiye Güneç Kıyak and Dr. Tuğba Öztürk for sample preparation and OSL signal measurement and BETA Analytic Inc. for radiocarbon dating.

I am very thankful as well to Gülgün Ertunç for her efficient organizational support during the fieldworks and I thank Dr. Orkan Özcan for his support during fieldwork as well as for data acquisition and preparation. I further thank Prof. Dr. Mehmet Akif Sarıkaya, and Ali Aksu with his drilling team for their help during fieldwork. I am grateful to Prof. Dr. Evren Erginal and ACME Analytical Laboratories Ltd. for their measurements of elemental contents.

I also thank Prof. Dr. Robin Lacassin, Dr. David Fernandez-Blanco, Dr. Giovanni de Gelder (IPG Paris), and Prof. Helmut Echtler (GFZ Potsdam) as well as Prof. Aral Okay, Prof. Kadir Eriş, Dr. Cengiz Zabcı, Oğuz Göğüş, Ömer L. Şen for their friendly, very helpful and constructive scientific conversations and discussions.

I also would like to thank the ALerT members for the helpful training activities and excursions to strengthen my scientific background. Moreover, I also thank Manfred Strecker for his great support and suggestions during the writing and review process of my second chapter.

I also thank my mom for her extraordinary and selfless support as well as Christelle Guilbaud for her encouraging support.

Last, I am very grateful to the European Union, the Turkish state and Istanbul Technical University for providing me these opportunities.

This study was funded by the European Commission as part of the Marie-Curie-ITN ALerT project (Grant FP7-PEOPLE- 2013-ITN, number 607996).

MARCH 2019

Christopher BERNDT



TABLE OF CONTENTS

	<u>Page</u>
FOREWORD.....	ix
TABLE OF CONTENTS	xi
ABBREVIATIONS.....	xiii
SYMBOLS.....	xv
LIST OF TABLES	xvii
LIST OF FIGURES.....	xix
SUMMARY	xxv
ÖZET	xxix
1. INTRODUCTION	1
2. QUATERNARY UPLIFT OF THE NORTHERN MARGIN OF THE CENTRAL ANATOLIAN PLATEAU: NEW OSL DATES OF FLUVIAL AND DELTA-TERRACE DEPOSITS OF THE KIZILIRMAK RIVER, BLACK SEA COAST, TURKEY.....	5
2.1 Introduction.....	5
2.2 Regional Setting.....	8
2.3 Data and Methods	12
2.3.1 Geomorphic mapping and analysis.....	12
2.3.2 OSL sampling and dating.....	14
2.4 The Kızılırmak Fluvial Terrace Sequence	14
2.4.1 Geomorphology and stratigraphy of strath terraces.....	14
2.4.2 Geomorphology and stratigraphy of fill terraces.....	19
2.4.3 Geomorphology and stratigraphy of coastal terraces.....	23
2.5 Result	26
2.5.1 OSL age determination	26
2.5.1.1 OSL ages of the strath terraces	27
2.5.1.2 OSL ages of the fluvial fill terraces	27
2.6 Discussion.....	29
2.6.1 Tectonic versus climatic processes	29
2.6.2 Timing and rate of long-term uplift	30
2.6.3 Implications for plateau margin deformation and lateral plateau growth.....	36
2.7 Conclusions.....	37
3. HOLOCENE MARGINAL MARINE OSTRACOD SUCCESSIONS FROM THE KIZILIRMAK RIVER DELTA; IMPLICATIONS FOR DEPOSITIONAL ENVIRONMENTS AND SEA-LEVEL CHANGES AT THE SOUTHERN BLACK SEA COAST	39
3.1 Introduction.....	39
3.2 Regional Setting.....	40
3.2.1 Regional Black Sea oceanography.....	42
3.2.2 Ecological conditions of the eastern delta plain	43
3.3 Methodology	44
3.4 Results.....	46
3.4.1 Sediment core description.....	46

3.4.2 Elemental content.....	47
3.4.3 Radiocarbon dating	49
3.4.4 Ostracoda	50
3.4.4.1 Ostracods from the samples of the recent delta plain	50
3.4.4.2 Faunal associations of the sediment core.....	50
3.4.4.3 Abundances and diversity	54
3.4.4.4 Cluster analysis	54
3.4.4.5 Principal component analysis and assemblages.....	55
3.4.5 Morphological analysis.....	58
3.5 Discussion.....	58
3.5.1 Environmental control on the ostracod assemblages and sediment chemistry.....	58
3.5.2 Holocene environments compared to recent delta lakes.....	62
3.5.3 Processes forming the lagoons of the Kızılırmak Delta.....	63
3.5.4 Holocene environmental development of the eastern Kızılırmak Delta plain.....	65
3.5.5 Relative water depth estimation.....	67
3.5.6 Holocene sea level and climate of the Black Sea region	69
3.5.6.1 Middle Holocene wet period and rapid rising sea levels	69
3.5.6.2 From the Middle Holocene climatic optimum to the semiarid Late Holocene	73
3.6 Conclusions.....	75
4. INTRASPECIFIC LENGTH VARIATION AND SHELL THICKNESS OF THE OSTRACOD <i>CYPRIDEIS TOROSA</i> (JONES, 1850) AS A POTENTIAL TOOL FOR PALAEO-SALINITY CHARACTERIZATION	77
4.1 Introduction.....	77
4.2 Materials and Methods.....	80
4.3 Results.....	81
4.3.1 Length variation	81
4.3.2 Valve thickness	83
4.4 Discussion.....	84
4.4.1 Valve size-salinity relationship.....	85
4.4.2 Valve thickness	89
4.5 Conclusions.....	91
5. CONCLUSIONS AND FUTURE PROSPECTS	93
REFERENCES.....	97
APPENDIX.....	121
CURRICULUM VITAE.....	125

ABBREVIATIONS

A	: Adult ostracod valve
A-1	: Ostracod valve in penultimate ontogenetic stage
ALeRt	: Anatolian pLateau climatE and Tectonic hazards
ALOS	: The Advanced Land Observing Satellite
ASTER	: Advanced Spaceborne Thermal Emission and Reflection
(ka) cal BP	: Calibrated (thousand) years before present
c	: Clay
CSF	: Cloth Simulation Filter
CONISS	: Constrained incremental sum of squares cluster analysis
DEM	: Digital Elevation Model
dGPS	: Differential Global Positioning System
DSM	: Digital Surface Model
DTM	: Digital Terrain Model
EAFZ	: East Anatolian Fault Zone
EBA	: Early Bronze Age
EMCOL	: Eastern Mediterranean Centre for Oceanography and Limnology
fs	: Fine sand
GPS	: Global Positioning System
gen. et sp. inc.:	Genus and species name not determined
HPD	: High Probability Density Range
ITN	: Initial Training Network
ITRAX-XRF	: X-ray fluorescence core scanner
KD	: Kızılırmak Delta
Lat/Long	: Latitude/Longitude
LBA	: Late Bronze Age
LGM	: Last Glacial Maximum
LV	: Left valve
MBA	: Middle Bronze Age
Mg	: Magnitude

MIS	: Marine Isotope Stage
MP	: Megapixel
ms	: Middle sand
MT	: Marine Terrace level
n_A	: Number of adult specimens
n_{A-1}	: Number of specimens in penultimate ontogenetic stage
n_{total}	: Number of total specimens
NAFZ	: North Anatolian Fault Zone
OSL	: Optically-Stimulated Luminescence
PC	: Principal component
R	: Regression
RV	: Right valve
SAR	: Single-Aliquot regenerative dose
SEM	: Scanning Electron Microscope
SfM	: Structure-from-Motion
SH_{max}	: Highest horizontal stress
sp.	: Species level not determined
spp.	: Genus includes more than one species
SPA	: Sieve-pore shape analysis
SRTM	: Shuttle Radar Topography Mission
ST	: Strath Terrace
T	: Relative transgression
t	: possible terrestrialization
T[...]	: Terrace level
u	: Silt
U	: Unit
UAV	: Unmanned Automated Vehicle
UTM	: Universal Transverse Mercator coordinate system
¹⁴C yrs BP	: Radiocarbon years before present
WGS84	: World Geodetic System 1984

SYMBOLS

^{14}C	: Carbon-14 isotope
Ca	: Calcium
D_e	: Equivalent dose
D_r	: Radiation dose rate
$\delta^{18}\text{O}$: Ratio of stable isotopes oxygen-18 and oxygen-16
$\delta^{13}\text{C}$: Ratio of stable isotopes carbon-13 and carbon-12
Fe	: Iron
H₂O₂	: Hydrogen peroxide
HCl	: Hydrochloric acid
K	: Potassium-40 isotope
Li	: Lithium
Sr	: Strontium
T_D	: Test dose
Th	: Thorium
Ti	: Titanium
U	: Uranium



LIST OF TABLES

	<u>Page</u>
Tab. 2.1 : Results of the OSL signal measurements (in decreasing order by age), cosmic dose, measurements of the radioactive elements (U, Th, and K) and carbonate content used to determine the environmental dose. The OSL ages highlighted in gray are considered outliers and were not included in the mean-age calculations.	28
Table 3.1 : Samples of sediment core BW with mean core depth in m and recent samples (KD).	45
Table 3.2 : Radiocarbon dating results (Beta Analytics, USA).	50
Table 3.3 : Ostracod taxa of sediment core BW. The systematic follows Brandão et al. (2018).	52
Table 3.4 : Categorization of the four main assemblage types and their sub-assemblages.	57



LIST OF FIGURES

	<u>Page</u>
Figure 2.1 : (a) Tectonic overview of the Eastern Mediterranean region (ALOS 3D WorldDEM; modified from Robertson et al., 2012 and Emre et al., 2012); GPS-derived slip rates are taken from Tatar et al. (2012) (NAFZ) and Ozener et al. (2010) (EAFZ); black arrows denote plate motions; the red arrow marks the direction of the greatest horizontal stress (SHmax) acting upon the NAFZ and the Central Pontides (Yıldırım et al., 2011); (b) ASTER DEM of the eastern Central Pontides with main faults (Demir, 2005; Yıldırım et al., 2011; Emre et al., 2012; Yıldırım et al., 2013a; b; Espurt et al., 2014; Hippolyte et al., 2016); isobaths are shown with 200 m contours; (c) Copernicus Sentinel-2 image (2015) of the study area with sampling locations indicated by numbered red dots; 1 - İkiztepe (T3: IKZ1; T6: IKZ2), 2 - Aktekke (T1: AK2; T4: AK1), 3 - Selemelik (TX: SE1; T7: SE2; ST1: SE3), 4 - Yakıntaş (T3: YAK), 5 - Hıdırellez (T6: HIR), 6 - Kızılırmak (T0: KIZ), 7 - Kolay (ST1/T6: KOL). This and all following maps are based on a UTM 32N projection of the WGS84 coordinate system; the grids depict latitude and longitude.	6
Figure 2.2 : Geologic map of the eastern Central Pontides with faults and folds (modified after Demir, 2005; Uğuz and Sevin, 2009; Emre et al., 2012). The main features are the parallel ridges in folded Cretaceous and Eocene flysch units that form the local basement of the southern terraces. Pre-Quaternary units north of the Eocene flysch are not exposed.....	9
Figure 2.3 : Earthquakes between 1904 and 2017 recorded by the Kandilli Observatory and Earthquake Research Institute of Boğaziçi University (2017). The dashed circles highlight the most active seismogenic zones; large-magnitude earthquakes occurred exclusively offshore.....	10
Figure 2.4 : Outcrop conditions at and close to a representative suite of sampling locations in the study area. (a) Kolay sampling site; (b) SE3 sampling site; (c) SE2 sampling site; (d) outcrop 500 m SE of the AK2 sampling site at low sun-angle conditions to highlight internal bedding; (e) outcrop approximately 100 m S of IKZ1; (f) IKZ2 sampling site and post-sedimentary normal faulting; (g) YAK sampling site.....	13
Figure 2.5 : (a) Terrace sequences at the lower sectors of the Kızılırmak River and its delta, with strath terraces inside the narrow river valley in the south, alluvial fill terraces inside river valleys, delta terraces forming the delta platform (esp. T5 and T7), and coastal terraces at the northern margins of the delta platform (hatched); (b) SW-NE oriented maximum elevation profiles across the eastern delta platform with a complete terrace sequence; (c) detailed SW-NE oriented maximum elevation profile of the Gerzeliler OSL sampling site; (d) overview of the locations of Figs. 2.6-2.11.....	15

Figure 2.6 : Map (a) and topographic profile (b) across the sampling location at Kolay.....	16
Figure 2.7 : Map (a) and topographic profile (b) of the Selemelik sampling site (c1, c2, and c3 are sections of the profile).	18
Figure 2.8 : Map (a) and topographic profiles (b, c) of the Aktekke sampling sites.	19
Figure 2.9 : Map (a) and topographic profile (b) of the Hıdırellez sampling site. Only the deposits of terrace levels T7 and T8 are exposed at the confluence of the Gökçesu and Kızılırmak Rivers. Since large parts of terrace T7 were covered by dense vegetation, no high-resolution DSM data could be acquired. Instead, a combination of publicly available data was used to further map this terrace.....	21
Figure 2.10 : Map (a) and topographic profile (b) of the İkiztepe sampling site. The delta terrace T7 is partly modified by the formation of terraces T6 and MT3 on both sides of the ridge. The area was affected by a SE-dipping normal fault that abuts the T6 surface. The İkiztepe archeological site is located on MT3.	22
Figure 2.11 : (a) Map of the Gerzeliler sampling site at the mouths of distributaries draining the eastern Kızılırmak Delta platform; (b) profile across the Gerzeliler sampling site.	24
Figure 2.12 : Elevation/time plot of the OSL dating results. The inferred positions for terraces corresponding to MIS 5e and MIS 7 have been added to illustrate extrapolated terrace elevations; the lower delta platform at 58 m (T5) is assigned to MIS 7, and an extensive coastal terrace with a pronounced shoreline angle at an elevation of 42 m (MT3) is correlated with MIS 5e. The time ranges highlighted in gray correspond to odd numbers of MIS (Lisiecki and Raymo, 2005). The sea level curves emphasize differences between the reconstructions of past sea level oscillations in the Black Sea (red: Shmuratko, 2001; green: Bintanja et al., 2005; blue pentagons represent sea level estimations based on the constant uplift model).	31
Figure 2.13 : (a) Spatial and vertical distribution of terrace flights and sampling sites along the lower reaches of the Kızılırmak River. Marine isotope stages and colors are correlated with the ages of terrace formation according to the uplift model; (b) Terrace flights with two MIS correlations document the timing of primary deposition and subsequent overprint by incision and renewed terrace formation.....	33
Figure 2.14 : Reconstruction of the delta terrace formation since MIS 14, with an accompanying map of the individual delta and terrace stages (a-j). Sea level stages in the Black Sea are taken from Zubakov and Borzenkova (1990); the position of the inferred reverse fault is shown according Robinson et al. (1996). Terrace formation occurs during low and high sea level stands; changes are displayed on a vertical scale. The upward-facing vertical arrow below the delta represents protracted regional uplift of the Pontide wedge. The black arrows on the maps to the left of the charts indicate small exposed terrace flights. The red lines (maps c-e) indicate prevailing active normal faulting.	35
Figure 3.1 : (a) Overview of the Kızılırmak Delta and its location in Turkey; Area of the delta wetlands and the sediment core location (BW). (b) Geology, geomorphology and sampling sites. Holocene: Recent delta plain,	

Pleistocene: elevated riverine, deltaic and marine terraces of former delta plains, Eocene: volcanoclastics. Atbaşı Fm.: volcanics, Paleocene: volcanics, Upper Cretaceous: volcanics and carbonates. Recent samples: KD-1: Karaboğaz Lake, KD-4: Sahilkent estuary, KD-7: Liman Lake, KD-9: NE-delta beach..... 41

Figure 3.2 : Ecological conditions (salinity, temperature and water depth; pH for all lakes ca. 8.1 to 9–10) of the Recent delta lakes and the recent occurrence of ostracods (collected in 1995 and 1996; Ustaoglu et al., 2012). Satellite image by Sentinel-2 30.11.201 [modified]. White dot indicates the location of the sediment core BW (this study)..... 43

Figure 3.3 : Lithological profile with grain size classes, samples of the sediment core BW and marked radiocarbon samples and ITRAX-XRF measurements of Ca, Sr/Ca and Ca/Fe..... 48

Figure 3.4 : Calibrated radiocarbon ages according to the depth with added conventional (blue) and calibrated (red) date of Bottema et al. (1995).. 49

Figure 3.5 : (Scale bars: 100 µm) (1) *Candona neglecta* Sars, 1887, male LV, exterior. (2) *Pseudocandona marchica* (Hartwig, 1899), adult LV, exterior. (3) *Cyclocypris ovum* (Jurine, 1820), adult carapace from left. (4) *Physocypris kraepelini* G. W. Müller, 1903, adult LV, interior. (5) *Heterocypris salina* (Brady, 1868), adult LV, exterior. (6) *Ilyocypris bradyi* Sars, 1890, adult RV, exterior. (7) *Ilyocypris gibba* (Ramdohr, 1808), adult LV, exterior. (8) *Cyprideis torosa* (Jones, 1850), female LV, exterior. (9) *C. torosa*, male LV, exterior. (10) *C. ?torosa*, instar A-1, RV, exterior. (10a) ornamentation. (11) *C. torosa*, adult RV, sieve pore. (12) *Cyprideis pontica* Krstic, 1968, female LV, exterior. (13) *Tyrrhenocythere amnicola* (Sars, 1888), adult RV, exterior. (14) *Amnicythere longa* (Negadaev, 1955), adult LV, exterior. (15) *Amnicythere quinetuberculata* (Schweyer, 1949), adult LV, exterior. (16) *Euxinocythere bacuana* (Liventan, 1929), adult LV, exterior. (17) *Euxinocythere crebra* (Suzin, 1959), adult RV, exterior. (18) *Limnocythere inopinata* (Baird, 1843), juvenile RV, exterior. (19) *Metacypris cordata* Brady and Robertson, 1870, adult LV, exterior. (20) *Cytheromorpha fuscata* (Brady, 1869), female RV, exterior. (21) *Loxoconcha bulgarica* Caraion, 1960, adult LV, exterior. (22) *Loxoconcha gibboides* Livental, 1949, adult RV, exterior. (23) *Loxoconcha rhomboidea* Fischer, 1855, adult RV, exterior. (24) *Xestoleberis aurantia* (Baird, 1838), adult RV, interior. (25) *Xestoleberis cornelii* Caraion, 1963, adult LV, exterior; (26) *Darwinula* sp., juvenile LV, exterior. (27) gen. et sp. inc., exterior..... 51

Figure 3.6 : Abundance (valves/100 g), principal ostracod-associations and diversity of Ostracoda along the sediment core. Red lines indicate the overall mean and grey bars the major peat level between 8.23 and 8.33 m below surface..... 53

Figure 3.7 : Cluster analysis (Method: *Coniss*) with ostracod units, cluster, assemblage and sub-assemblage classification..... 55

Figure 3.8 : Principal components that account for 90% of the variance [%] (PC 1: 74%, PC 2: 16%) representing main influencing factors (components). Sample names are given by their depth and colours refer to the units (brown: lower unit, blue: middle unit and green: upper unit). (a) Components 1 and 2, (b) Components 2 and 3..... 56

- Figure 3.9** : Distribution of the ecological groups, salinity (based on sieve pore-analysis) and principal components along the sediment core. Thin scale lines indicate sample depths..... **57**
- Figure 3.10** : Water depth range estimations based on the ostracod fauna (*Tyuleneva et al., 2014; R – regression, T – transgression, t – possible terrestrialization). Dark grey ranges before 7 ka cal BP are ranges of higher probability of the surrounding rectangle and light grey rectangles with dashed margins indirectly dated..... **68**
- Figure 3.11** : Sea level variability between 8 and 2 ka cal BP. (a) Reconstruction of the absolute Black Sea level (this study; c. f. Fig. 3.10) and comparison to the Mediterranean Sea (Seeliger et al., 2017) and the sea level indications (peat) for the Danube Delta (blue: Giosan et al., 2006), Taman Peninsula (light green: Brückner et al., 2010 and dark green: Bolikhovskaya et al., 2018) and Rioni River delta (grey: non-peat estimations and brown: peat levels; yellow: Laermans et al., 2018). (b) Timeframe of Yanko-Hombach (2007). (c) Black Sea level reconstructions (data from Erginal et al., 2013). (d) Sea level curves from the Mediterranean Sea, North Sea and Northern Atlantic (USA) (compilation of Ramsey and Baxter, 1996; Behre, 2003, Brückner et al., 2010 and references therein). Grey shade indicates the total range of sea level curves of Greece (Vött, 2007)..... **70**
- Figure 3.12** : (a) Holocene environments of the Kızılırmak Delta (2 to 8 ka cal BP) (this study; marine: blue and limnic: yellow). (b) Stalagmite $\delta^{13}\text{C}$ of Sofular Cave (black) and $^{238}\text{U}/^{234}\text{U}$ (red) (SW Black Sea coast; data from Göktürk et al., 2011). (c) Simplified climate oscillations of the Holocene of Europe (Schönwiese, 1995). (d) Climate and sea level variation of Taman Peninsula (NE Black Sea coast; modified from Bolikhovskaya et al., 2018). (e–g) Wet (black) and very dry phases of the lakes Eski Acıgöl and Nar Gölü (e; Central Anatolia; Turner et al., 2008; Berger et al., 2016), Tecer Lake (f; Northern Anatolia; Kuzucuoğlu et al., 2011) and Western Anatolian lakes (g; based on Akçer Ön, 2011 and Ocakoğlu et al., 2013). (h) Occupation phases of İkiztepe (based on Alkim et al., 1988; Alkim et al., 2003 and Welton, 2010). The red vertical barrens in (d) and (f) refer to the basis of the related record. **71**
- Figure 4.1** : Natural-colored image (a) and geological-geomorphological map (b) of the Kızılırmak Delta with sediment core (BW) (modified from Berndt et al., 2019). **79**
- Figure 4.2** : Sediment core BW with lithology appearance of larger shells of *C. edule* and gravel, sedimentological (A–D) and ecological zonation (blue: Marine, green: Lacustrine), radiocarbon ages, ostracod ecology, reconstructed salinity, length and height measurements of female adult and instar A-1 *C. torosa* valves, valves thickness variation, sample names according to their depth below surface, total number of *C. torosa* valves (n_{total}), number of adult *C. torosa* valves (n_A) and number of valves of the instar A-1 (n_{A-1}) (modified from Berndt et al., 2019 and combined with new data of this study). **82**
- Figure 4.3** : Examples of valve microstructure of female adult valves of *C. torosa*. All scales: 10 μm **83**

- Figure 4.4** : ITRAX-XRF (Ca, Sr/Ca and Ca/Fe) measurements (XRF data from Berndt et al., 2019), valve length and thickness of *C. torosa* (this study). Red lines are mean XRF values for the ostracod sampling ranges. Remark: There are different scales between the ITRAX-XRF record and subsampled mean values..... **85**
- Figure 4.5** : The valve length-salinity relationship with data of former studies in grey (data from Van Harten, 1975 and Boomer et al., 2017). The trend line y excludes our whole dataset and the trend line z includes data from the lower unit. **86**
- Figure A.1** : OSL dose-response curve constructed for the sample IKZ1-1 using sensitivity-corrected dose points..... **122**
- Figure A.2** : Precision analyses based on the Analyst program for representative samples of IKZ1-3 and KOL-1 (ten aliquots for each sample)..... **123**





A MULTI-PROXY STUDY OF THE KIZILIRMAK RIVER TERRACES AND ITS DELTA, NORTHERN TURKEY: IMPLICATIONS FOR TECTONICS, SEDIMENTATION, SEA LEVEL AND ENVIRONMENTAL CHANGES

SUMMARY

River deltas as one end feature of a river are affected by a number of factors determining their shape, presence and longevity. At present, those landforms give space for large human populations as well as agricultural farmland. Aside, plenty of species, including several threatened and rare ones, inhabit the delta's wetlands creating valuable ecosystems of international importance. Nevertheless, delta plains are highly variable environments reacting quickly to changes in sediment influx from the river as well as wave, tides and current activity. The sediment transport of a river to the delta is highly depending on external and internal environmental factors. These sediments contain data about the evolution of past climate, sea level and geodynamics on local over regional to global scales. On the other hand, several river deltas worldwide are distinctly affected by human activities such as river dams which reduce the sediment transportation downstream to the delta. Those impacts lead to artificially-induced changes in their morphology, i.e., shoreline retreats.

The lower stream of the Kızılırmak River in northern Anatolia comprises of ecologically rich wetlands on the present delta plain as well as elevated fluvial and delta terraces. The Kızılırmak River delta is located at the border between the Central Anatolian Plateau and the Black Sea. The Central Anatolian Plateau is a major feature of the Alpidic orogeny in Anatolia and uplifted slowly during Quaternary. The North Anatolian Fault Zone, forming a broad restraining bend in the central section of the Pontide Mountains, tectonically impacts the northern margin of the plateau. This northward progressing deformation is suggested to accelerate the uplift of the northern margin of the Central Anatolian Plateau until the southern coast of the Black Sea. The dating of fluvial and marine terraces has now been established to temporally constrain and reconstruct active tectonics impacting this delta during Quaternary.

On the other hand, the Black Sea is the largest semi-enclosed sea with a globally unique fauna due to its repeated disconnection from the world ocean. It was disconnected during the Last Glacial Maximum (ca. 20 ka) until it became reconnected to the Mediterranean Sea in early Holocene. Ostracod faunal assemblages are well established proxies for marine, as well as limnic, palaeoenvironmental reconstructions due to the high preservation potential of their valves in sediments. Those characteristics create the opportunity to apply quantified statistical analyses of their faunal assemblages to identify principal influencing factors. *Cyprideis torosa* (Jones) is a brackish water ostracod that lives mainly in marginal environments, but can withstand a wide variety of conditions. This species forms phenotypic adaptations of its carapace to cope with environmental changes

with up to severe hypersaline conditions. Recent studies started to use those morphological variations to create transfer functions determining palaeoenvironmental variables, i.e. salinity.

The aim of this thesis is the reconstruction of the Quaternary evolution of the lower stream and delta of the Kızılırmak River. This goal will be achieved by identifying the geodynamics at the northern margin of the Central Anatolian Plateau combined with the influence of the North Anatolian Fault Zone, which creates several fluvial terrace levels along the lower course of the Kızılırmak River; and unraveling the Holocene palaeoenvironmental evolution of the delta with its dependencies to the Anatolian climate and Black Sea sea level changes, based on ostracod faunal assemblages. In addition, we analyse how the environmental conditions modify in turn the size and shell thickness variation of *Cyprideis torosa* (Jones) as phenotypic morphological adaptations for a future improved characterization of marginal marine palaeoenvironments.

In the first part of the thesis, the interplay between coastal uplift, sea level change in the Black Sea, and incision of the Kızılırmak River in northern Turkey is analysed. These processes have created multiple co-genetic fluvial and marine terrace sequences that serve as excellent strain markers to assess the ongoing evolution of the Pontide orogenic wedge and the growth of the northern margin of the Central Anatolian Plateau. Newly acquired high-resolution topographic data and OSL ages accompanied by published information on past sea levels were used to analyse the spatiotemporal evolution of these terraces; a regional uplift model for the northward-advancing orogenic wedge Pontides was derived that supports the notion of laterally variable uplift rates along the flanks of the Pontides. The best-fit uplift model defines a constant long-term uplift rate of 0.28 ± 0.07 m/ka for the last 545 ka. This model explains the evolution of the terrace sequence in light of active tectonic processes and superposed cycles of climate-controlled sea-level change. Those new data reveal regional uplift characteristics that are comparable to the inner sectors of the Central Pontides; accordingly, the rate of uplift diminishes with increasing distance from the main strand of the restraining bend of the North Anatolian Fault Zone (NAFZ). This spatial relationship between the regional impact of the restraining bend of the NAFZ and uplift of the Pontide wedge thus suggests a strong link between the activity of the NAFZ, deformation and uplift in the Pontide orogenic wedge, and the sustained lateral growth of the Central Anatolian Plateau flank.

In the second part of the thesis, the analysis of a 14.5-m-long sediment core, drilled into the eastern delta wetlands, is presented. The palaeoenvironmental impact on the delta plain was analysed using palaeoecological ostracod assemblages accompanied by a palaeo-salinity reconstruction based on sieve pore shape variations on the ostracod *Cyprideis torosa* (Jones). This study depicts the interplay of terrestrial and marine settings forming mesohaline, shallow lagoons and deltaic lakes since ca. 7.9 ka cal BP. Lagoons with α -mesohaline to polyhaline salinities and β -mesohaline to oligohaline lake environments were identified. Reconstructed palaeo-sea level estimations depict a remarkable environmental variability. The lagoon habitats at 7.9 to 7.0 and 5.3 to 4 ka cal BP were dominated by *Cyprideis torosa*. Marine influence led to ostracod associations with *Loxoconcha* spp. and *Tyrrhenocythere amnicola* especially between 7.9 and 7.0 ka cal BP. Riverine influence in the same period, but especially at about 7.7 ka cal BP, caused dominating *Amnicythere* spp. Assemblages dominated by *Cyprideis torosa* and *Candona neglecta* characterise short phases of a mesohaline deltaic lake environments at about 7.7 and 7.0 ka cal BP as well as after

4 ka cal BP. With a subsequent salinity decrease, *C. neglecta* and (later on) *Pseudocandona marchica* became dominant with an interruption by another short-term lagoonal phase that might be associated with a ‘megadrought’ between 3.7 and 3.0 ka cal BP.

In the final part of the thesis, the valve size of adult and penultimate ontogenetic individuals and shell thickness of *Cyprideis torosa* was measured in relation to the changes in palaeoenvironmental conditions. A good positive correlation between the size of female valves and the prevailing salinity (correlation coefficient: 0.56) can be reported, while such a correlation is lacking for ontogenetic stage A-1. The absence of large individuals is indicated to be a local effect of the Black Sea fauna. No changes of the height/length ratio of the valves were recognizable along the salinity gradient. Shells are significantly thicker under relatively stable, higher saline conditions, but thinner in highly variable and low saline deltaic lakes. Both morphological features, size and shell thickness of *C. torosa*, are thus potential tools to give palaeoenvironmental information, especially in *C. torosa*-dominated, low diversity marginal marine environments.

In overall, the study shows that the impact of the North Anatolian Fault deforms the northern margin of the Central Anatolian Plateau until the Black Sea coast in the range of the central Pontide Mountains since at least 545 ka. Hence, the southern part of the Kızılırmak Delta becomes uplifted at an accelerated rate. In addition, the Kızılırmak Delta reacts rapidly on changes in Anatolian climate and Black Sea sea levels forming an alternation of lagoonal and deltaic lake environments in its eastern part since Mid-Holocene. While sea level changes predominantly modify the environments during the early Mid-Holocene, the climate changes have a much higher impact during Late Holocene. In turn, those environmental changes leading to salinity variations correlate to phenotypic changes in the morphology of the ostracod *Cyprideis torosa* (Jones).



KIZILIRMAK NEHİR TERASLARI VE DELTASININ ÇOKLU-PROKSİ YÖNTEMİ İLE ÇALIŞMASI: TEKTONİK, SEDİMENTASYON, DENİZ SEVİYESİ VE ÇEVRESEL DEĞİŞİKLİKLER İLE İLGİLİ ÇIKARIMLAR

ÖZET

Şu anda, bu topraklar tarım alanlarının yanı sıra büyük insan nüfusuna da yer vermektedir. Bunun yanı sıra, tehdit altında ve nadir olan birçok tür, deltanın sulak alanlarında yaşar ve uluslararası öneme sahip değerli ekosistemler yaratır. Bununla birlikte, delta ovaları nehirdeki sediman akısındaki değişikliklere, dalga, gelgitlere ve mevcut aktiviteye hızla tepki veren oldukça değişken ortamlardır. Bir nehrin deltaya sediman taşınımı, iç ve dış çevresel faktörlere bağlıdır. Bu sedimanlar, geçmiş iklimin, deniz seviyesinin ve yerelden bölgesel ve küresel ölçekte jeodinamiklerin gelişimi hakkında veri içermektedir. Öte yandan, dünyadaki bazı nehir deltaları, deltaların aşağı havasında bulunan sediman taşınımını azaltan barajlar gibi insan faaliyetlerinden açıkça etkilenir. Bu etkiler, morfolojilerinde, yani kıyı şeridi çekilmelerinde yapay olarak meydana gelen değişikliklere yol açmaktadır.

Bunun yanı sıra, ostrakod gurupları, kapakçıklarının sediman içinde yüksek korunabilme potansiyeli nedeniyle, limnik palaeo-çevre rekonstrüksiyonları için iyi bir proksi konumundadırlar. Geniş dağılımları ve bollukları nedeniyle, ortamı etkileyen faktörleri tanımlamak için ostrakondlar istatistiksel analizler için çok uygundur. *Cyprideis torosa* (Jones), marjinal ortamlarda yaşayan bir acı su ostrakodu olup çevresel değişikliklere hızla uyum sağlayabilir. Son çalışmalar palaeo-çevresel değişiklikleri, yani tuzluluk düzeyini belirlemek ve transfer fonksiyonları oluşturmak için bu morfolojik varyasyonları kullanmaya başlamıştır.

Bu tezin amacı, Orta Anadolu Platosu'nun kuzey kenarında yer alan jeodinamik özellikleri belirleyen Kızılırmak deltası etrafındaki nehir terasları aracılığıyla Kızılırmak Nehri'nin Kuvaterner gelişimine ışık tutmaktır. Bunun yanı sıra, deltanın Holosen paleo-çevresel evrimi, Anadolu iklimi ve Karadeniz deniz seviyesi ile ostrakod faunasındaki değişimler gözönüne alınarak ortaya konmaya çalışılmıştır.

Ayrıca bu bölge, *Cyprideis torosa*'nın (Jones) boyutu ve kabuk kalınlığı değişimini, marjinal deniz palaeo-ortamlarının gelişmiş bir karakterizasyonu için fenotipik morfolojik vekiiller olarak test etme imkanı sunmaktadır.

Tezin birinci bölümünde, kuzeydeki kıyıların yükselmesi, Karadeniz'in deniz seviyesi değişimi ve Kızılırmak Nehri'nin kesilmesi arasındaki etkileşim incelenmiştir. Bu işlemler, Pontid orojenik kamaların devam eden evrimini ve Orta Anadolu Platosu'nun kuzey sınırının büyümesini değerlendirmek için mükemmel zorlanma belirteçleri olarak hizmet veren çoklu kogenetik fluvial ve deniz terası dizileri yaratmıştır. Yeni elde edilen yüksek çözünürlüklü topografik veriler ve geçmiş deniz seviyelerinde yayımlanan bilgilerle birlikte verilen OSL yaşları, bu terasların mekânsal-zamansal evrimini analiz etmek için kullanılmıştır; kuzeye doğru ilerleyen orojenik kama Pontidler için bölgesel bir yükselme modeli, Pontidlerin

yanları boyunca da yanal değişken yükselme oranları kavramını desteklemektedir. En uygun yükseltme modeli, son 545 ka için sabit ve uzun vadeli bir yükselme oranı olan $0,28 \pm 0,07$ m / ka'ya denk gelmektedir. Bu model, teras dizisinin aktif tektonik süreçler ve iklim kontrollü deniz seviyesindeki değişim döngüleri ışığındaki evrimini açıklar. Bu yeni veriler, Orta Pontidlerin iç sektörleriyle karşılaştırılabilir bölgesel gelişme özelliklerini ortaya koymaktadır; buna bağlı olarak, yükselme oranı, Kuzey Anadolu Fay Zonu Bölgesi'nin (NAFZ) kısıtlayıcı bükülmesinin ana şeridinden uzaklaştıkça azalmaktadır. NAFZ'nin kısıtlayıcı bükülmesinin bölgesel etkisi ile Pontid kamasının yükseltilmesi arasındaki bu mekansal ilişki, NAFZ'nun aktivitesi, Pontid orojenik kamadaki deformasyon ve yükselme ile Orta Anadolu'nun sürekli yanal büyümesi arasında güçlü bir bağlantı olduğunu ortaya koymaktadır.

Tezin ikinci bölümünde, doğu delta sulak alanlarına 14,5 m uzunluğunda bir karot incelenmiştir. Delta ovası üzerindeki paleo-çevresel etki, ostrakod *Cyprideis torosa* (Jones) üzerindeki elek gözenek şekli değişikliklerine dayanan palaeo-tuzluluk rekonstrüksiyonları eşliğinde palaeoekolojik ostrakod toplulukları kullanılarak analiz edilmiştir. Bu çalışma, mezohalin, sıg lagün ve deltaik göller oluşturan karasal ve deniz ortamlarının etkileşimini ca. 7,9 ka cal BP'dan günümüze ortaya koymaktadır. α -mesohalin ile polihalin tuzluluklarına ve β -mesohalin ve oligohalin göl ortamları tespit edilmiştir. Yeniden yapılandırılmış paleo-deniz seviyesi tahminleri dikkate değer bir çevresel değişkenlik göstermektedir. *Cyprideis torosa*'da lagün habitatları 7,9 ila 7,0 ve 5,3 ila 4 ka'lık BP'lerde baskındır. Deniz etkisi, *Loxoconcha* spp. ve *Tyrhenocythere amnicola* gibi ostrakod gruplarının özellikle 7,9 ila 7,0 ka cal BP arasında gelişimine olanak vermiştir. Aynı dönemde oluşan nehir etkisi (özellikle yaklaşık 7,7 ka cal BP'de), nedeniyle *Amnicythere* spp., *Cyprideis torosa* ve *Candona neglecta* baskın hale gelmiş ve mesohaline deltaik göl yaklaşık 7,7 ve 7,0 ka cal BP'de ve ayrıca 4 ka cal BP arasında oluşmuştur. Bir sonraki tuzluluk azalmasıyla, *C. neglecta* ve (daha sonra) *Pseudocandona marchica*, “megakuraklık” ile ilişkili olabilecek kısa vadeli bir lagün evresinin kesilmesiyle baskın hale gelmiştir.

Tezin son bölümünde, yetişkin ontogenetik bireylerin kapak boyutu ve *Cyprideis torosa*'nın kabuk kalınlığı palaeo-ortam koşullarındaki değişikliklerle ilişkili olarak ölçülmüştür. Dişi kapakçıkların büyüklüğü ile hakim tuzluluk arasında iyi bir pozitif korelasyon (korelasyon katsayısı: 0,56) bildirilirken, böyle bir korelasyon ontogenetik evre A-1 için eksiktir. Büyük bireylerin yokluğunun Karadeniz faunasının yerel bir etkisi olduğu belirtilmektedir. Tuzluluk derecesi boyunca kapakçıkların yükseklik / uzunluk oranında herhangi bir değişiklik tespit edilmemiştir. Kabuklar nispeten kararlı, daha yüksek tuzlu su koşulları altında belirgin şekilde daha kalındır, ancak oldukça değişken ve düşük tuzlu deltaik gölleride ise daha incedir. Bu nedenle, morfolojik özellikler, *C. torosa*'nın büyüklüğü ve kabuk kalınlığı, özellikle *C. torosa*'nın hakim olduğu, düşük çeşitliliğe sahip marjinal deniz ortamlarında paleo-çevre bilgisi vermek için potansiyel araçlardır.

Genel olarak, çalışma, Kuzey Anadolu Fayı'nın etkisinin Orta Anadolu Platosu'nun kuzey sınırını, en az 545 ka'dan bu yana orta Pontid Dağları aralığında Karadeniz kıyılarına kadar deforme ettiğini göstermektedir. Bu şekilde, Kızılırmak Deltası'nın güneyi, hızı artan bir oranda yükselmektedir. Buna ek olarak, Kızılırmak Deltası, Anadolu'daki iklim ile Karadeniz deniz seviyelerinde meydana gelen değişikliklere, doğu kesimindeki lagün ve deltaik göl ortamlarının Orta-Holosen'den günümüze ardalanması ile hızlı bir tepki vermektedir. Deniz seviyesi değişimleri, erken Orta Holosen'de ortamları ağırlıklı olarak değiştirirken, iklim değişikliği Geç Holosen döneminde çok daha yüksek bir etkiye sahiptir. Buna karşılık, tuzluluk

değişimlerinin eşlik ettiği bu çevresel değişiklikler, ostrakod *Cyprideis torosa*'nın (Jones) morfolojisindeki fenotipik değişikliklerle deneştirilebilmektedir.





1. INTRODUCTION

Rivers play a very important role for natural environments as well as human civilizations in several ways, for example forming valleys with arable land and trade pathways (e.g., Polanyi, 1963; Berger et al., 2016). Those large natural streams flow towards a lake, sea or ocean and are generally fed by a large number of smaller tributaries, which form the drainage basin of a river. Rivers with high sediment transport form deltas at their mouth into a water-filled basin and are strongly affected by any hydrological changes in the drainage basin and water levels (e.g., Meade, 1996; Bhattacharya, 2003). All of those factors modify the river's flow so that delta environments react sensitively to changes in precipitation patterns, base levels and tectonic movements (e.g., Vandenberghe, 2008; Burbank and Anderson, 2011). The delta sediments are thus highly valuable recorders for past regional long- and short-term changes. However, many of those environments are highly threatened worldwide, due to intense human activities and modifications. For example, large scale damming of the river's course leads to sediment load reduction and intense groundwater use exacerbates natural subsidence rates of deltas (Giosan et al., 2014).

Delta plains are located very close to the sea level and build the home to a very rich and diverse fauna and flora (Giosan et al., 2014). One class inhabiting aquatic delta environments are Ostracoda (Frenzel and Boomer, 2005). These small, mostly benthic-living crustaceans are abundant in nearly all aquatic environments worldwide and appear already since Palaeozoic (Horne et al., 2002). A delta plain, as a landform at the border between mainland and sea, is a highly variable environment with a number of influencing factors of both realms leading to delta pro- and retrogradations (shifts of the shoreline) (Bhattacharya, 2003). Accordingly, assemblages of the ostracod fauna in delta sediments can be used to reconstruct palaeo-deltaic environments with highly variable conditions (e.g., Rossi, 2009).

The study area of this thesis is the delta of the Kızılırmak River, formerly called Halys. The Kızılırmak River is the largest river of Turkey that flows in a large bend across the Central Anatolian high plateau. Subsequently, the river crosses the North

Anatolian Fault and traverses the Central Pontides. Eventually, the Kızılırmak River reaches the southern central Black Sea coast of Turkey. There, it forms a wave-dominated wide delta plain, the Kızılırmak Delta or Bafra Plain. The delta contains large Ramsar wetlands including swamps, marshes, brackish lakes and dunes, which are highly threatened by human activities and active retreat of the coastline (Samsunlu et al., 2002; Öztürk et al., 2015).

The Kızılırmak Delta is also located at the northern margin of the Central Anatolian Plateau (CAP), a main feature of Anatolia, which is enclosed by the continent-continent collision zone of Eastern Anatolia and the subduction zone with extensional tectonics in the Aegean region (Kuzucuoğlu et al., 2019). Orogenic plateaux like the CAP are prime features in tectonic collision zones (Burbank and Anderson, 2011). The CAP is a rather small plateau with an average height of about 1 km, which is bordered by the Pontide Mountains to the north and the Tauride Mountains to the south (Çiner et al., 2013). The CAP was formed by the collisional accretion of the Afyon and Kırşehir blocks as well as the Tauride carbonate platform with the Pontide magmatic arc from Eocene to Early Oligocene (e.g., Şengör and Yılmaz, 1981; Görür et al., 1998; Şengör et al., 2005; Van Hinsbergen et al., 2016). Subsequently, it experienced a significant uplift of about 1 km since Miocene (e.g., Cosentino et al., 2012; Schildgen et al., 2012, 2014; Aydar et al., 2013; Çiner et al., 2015). This section of the Alpidic orogeny transformed Anatolia from a former continental margin of Eurasia to the present intracontinental basin of Central Anatolia.

To the north of the Pontide arc, the Black Sea basin has opened as two separate extensive back-arc basins (West and East Black Sea basins) in Late Cretaceous and Early Eocene, respectively, as part of the Paratethys, which had a limited connection to the open ocean (e.g., Okay et al., 1994; Rögl, 1999). The extension of the basins ended with the collision of the Arabian Plate with Eurasia until Middle Miocene (e.g., Okay et al., 1994; Robinson et al. 1996; Cavazza et al., 2018). This collision largely isolated the eastern Paratethys from the world ocean leading to a salinity drop and high endemism of the fauna (Rögl, 1999). Then, this domain had only a limited connection to the Palaeomediterranean (southern Paratethys) until the Plio-Pleistocene transition (Van Baak et al., 2015, 2019; Palcu et al., 2018). Since Lower Pleistocene, this connection was broken until Middle Pleistocene and the Paratethys

degraded into the Black and Caspian seas (Kochegura and Zubakov, 1978; Yanko-Hombach, 2013), with a reconnection of the Black Sea to the world ocean during interglacial periods since at least 460 ka (Kochegura and Zubakov, 1978; Shmuratko, 2001). At last, it was reconnected to the world ocean over the Bosphorus and Dardanelles in Early Holocene (Filipova-Marinova, 2007) and is today the largest semi-enclosed sea of the world. The timing and duration of this reconnection is hotly debated since the last two decades (e.g., Aksu et al., 2002; Ryan et al., 2003). Research about the subsequent development of the Black Sea led to highly different reconstructions (Erginal et al., 2013).

Contemporary with the Miocene collision of the Arabian Plate with Anatolia, the activity of the North Anatolian Fault Zone (NAFZ) started between 11 and 13 Ma ago and propagated towards west (Okay et al., 1994; Şengör et al., 2005). The NAFZ is a major dextral transform fault striking from East Anatolia to the Aegean Sea, which separates the CAP's interior from its northern margin, the central section of the Pontide Mountains (Central Pontides) (Şengör et al., 2005). It impacted on the Central Pontides between 8.5 and 5 Ma ago (Hubert-Ferrari et al., 2002), where it forms a broad restraining bend (Emre et al., 2009). At this bend of the NAFZ, contraction is increased, which is suggested to lead to an accelerated uplift of the Central Pontides as an orogenic wedge (Yıldırım et al., 2011, 2013a,b). Several uplifted fluvial terraces are exposed along the Kızılırmak's course inside the Central Pontides up to the delta plain (Demir et al., 2004).

This thesis aims to unravel the Quaternary development and evolution of the Kızılırmak Delta, at the boundary between the Black Sea, which has a very unique environment, and the tectonically active Anatolian plate. It will also contribute to the development of new, very sensitive ostracod proxies for marginal marine settings.

Chapter 2 aims to reconstruct the rate of regional uplift that explains the formation and level of the Kızılırmak River's fluvial, deltaic and marine terraces and compare it with the uplift information from former studies of the CAP. To achieve this goal, the fluvial and deltaic terraces of its lower stream were dated by using optically-stimulated luminescence to reconstruct the Quaternary regional uplift at the northern margin of the CAP.

In **chapter 3**, a sediment core, which was drilled into the eastern delta wetlands, was analysed by using ostracod assemblages and morphometries. Those analyses are supported by geochemical measurements and radiocarbon dating. This study aims to reconstruct the palaeo-delta environments during Holocene. In addition, the reconstructed palaeoenvironments are intended to give insight into palaeo-sea levels and the conditions during settlement phases of İ̇kiztepe, a town located at the northernmost peak of the delta terraces, which was discontinuously inhabited since Late Chalcolithic.

Chapter 4 deals with the palaeoenvironmental changes shaping the morphology of *Cyprideis torosa* (Jones), a brackish water ostracod species that is abundant in marginal marine settings over large parts of the world (Frenzel et al., 2010). Environmental changes cause phenotypic adaptations of individuals of this species (e.g., Van Harten, 1975; Boomer et al., 2017). The size of adult individuals as well as ones in the penultimate ontogenetic stage and their shell thicknesses are measured. This study aims at a correlation of those intraspecific features to environmental factors of the Holocene eastern Kızılırmak Delta as possible proxies for palaeoenvironment reconstructions, especially in low-diverse environments.

In **chapter 5** are given conclusions and future prospects.

2. QUATERNARY UPLIFT OF THE NORTHERN MARGIN OF THE CENTRAL ANATOLIAN PLATEAU: NEW OSL DATES OF FLUVIAL AND DELTA-TERRACE DEPOSITS OF THE KIZILIRMAK RIVER, BLACK SEA COAST, TURKEY¹

2.1 Introduction

Cenozoic orogenic plateaus are premier tectonic features that are characterized by low internal relief, pronounced relief contrasts along their flanks, and high average elevation. As such, they influence the tectonic evolution of adjacent forelands, cause changes in atmospheric circulation patterns, determine the distribution of rainfall and the efficiency of weathering and erosion, and impact pathways for speciation (e.g., Ruddiman and Kutzbach, 1991; Ramstein et al., 1997; Strecker et al., 2007; Placzek et al., 2009).

The world's largest Cenozoic orogenic plateaus, such as Tibet and the Altiplano-Puna of the Central Andes, are thought to have resulted from a wide range of deep-seated processes involving lithospheric delamination, crustal shortening and thickening, and underplating (e.g., Allmendinger et al., 1997; Tapponnier et al., 2001; Garzione et al., 2017). It has also been suggested that the construction of orogenic rainfall barriers along the plateau flanks, in concert with resulting changes in surface processes, may contribute to the morphologic evolution of these areas (Métivier et al., 1998; Sobel et al., 2003). In combination, all of these aspects may influence plateau growth over time in terms of elevation as well as areal extent (e.g., Isacks, 1988; Masek et al., 1994; Allmendinger et al., 1997; Tapponnier et al., 2001; Sobel et al., 2003). However, the mechanisms that are responsible for the lateral growth of these regions and the timescales that are necessary to generate topography remain subjects of debate (e.g., Riller and Oncken, 2003; Strecker et al., 2009; Schildgen et al., 2012; Allen et al., 2013). This lack of consensus may be related in part to the lack

¹ This chapter is based on the paper “Berndt, C., et al., Quaternary uplift of the northern margin of the Central Anatolian Plateau: New OSL dates of fluvial and delta-terrace deposits of the Kızılırmak River, Black Sea coast, Turkey. *Quaternary Science Reviews*, 2018, 201: p. 446-469”

of suitable rocks for thermochronology, the limited availability of proxy indicators for changes in topography through time, and the absence of chronologically well-constrained strain markers.

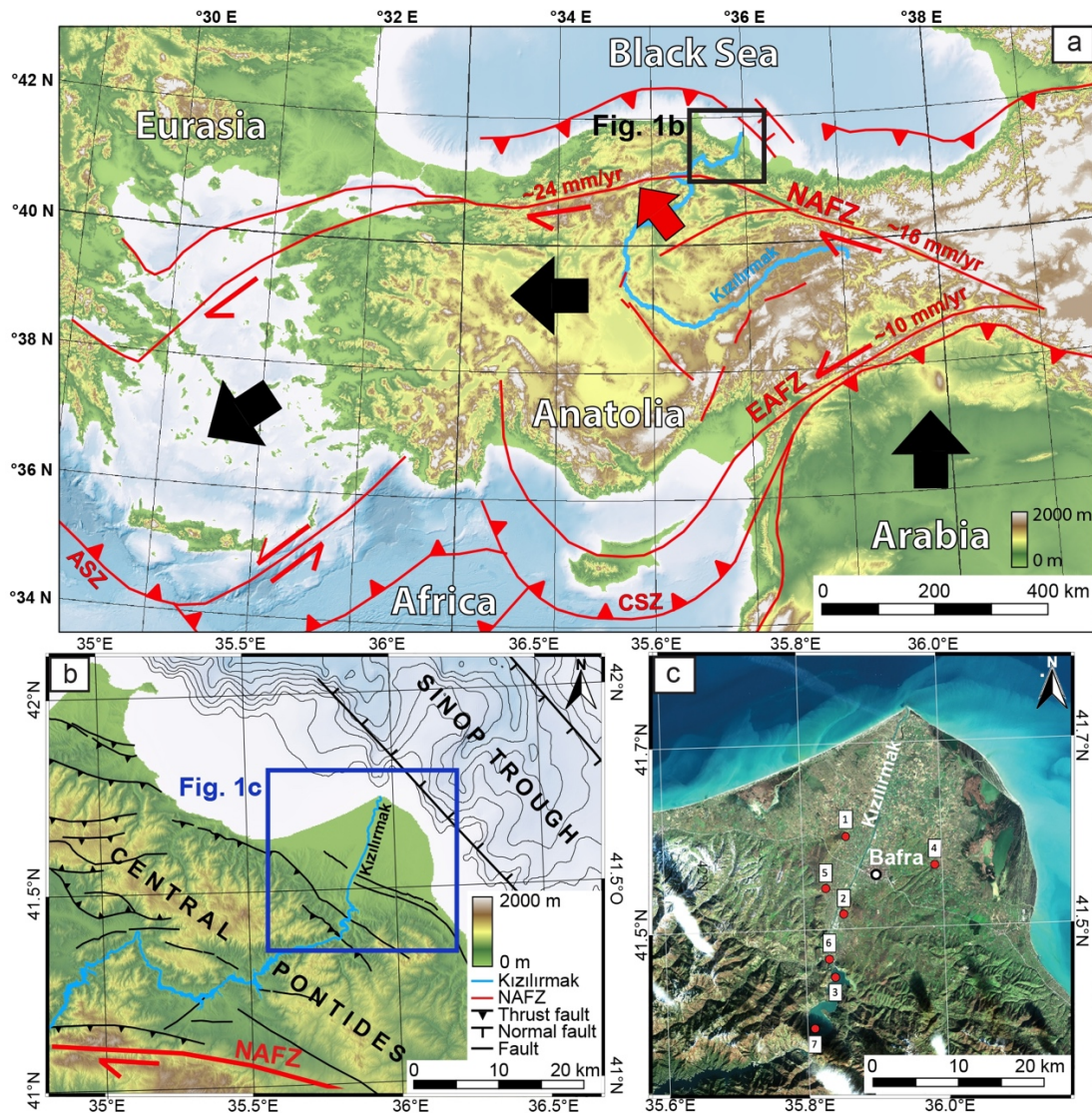


Figure 2.1 : (a) Tectonic overview of the Eastern Mediterranean region (ALOS 3D WorldDEM; modified from Robertson et al., 2012 and Emre et al., 2012); GPS-derived slip rates are taken from Tatar et al. (2012) (NAFZ) and Ozener et al. (2010) (EAFZ); black arrows denote plate motions; the red arrow marks the direction of the greatest horizontal stress (SHmax) acting upon the NAFZ and the Central Pontides (Yıldırım et al., 2011); (b) ASTER DEM of the eastern Central Pontides with main faults (Demir, 2005; Yıldırım et al., 2011; Emre et al., 2012; Yıldırım et al., 2013a; b; Espurt et al., 2014; Hippolyte et al., 2016); isobaths are shown with 200 m contours; (c) Copernicus Sentinel-2 image (2015) of the study area with sampling locations indicated by numbered red dots; 1 - İkiztepe (T3: IKZ1; T6: IKZ2), 2 - Aktekke (T1: AK2; T4: AK1), 3 - Selemelik (TX: SE1; T7: SE2; ST1: SE3), 4 - Yakıntaş (T3: YAK), 5 - Hidirellez (T6: HIR), 6 - Kızılırmak (T0: KIZ), 7 - Kolay (ST1/T6: KOL). This and all following maps are based on a UTM 32N projection of the WGS84 coordinate system; the grids depict latitude and longitude.

The Central Anatolian Plateau is the smallest and lowest Cenozoic orogenic plateau; it may represent an early-stage analog to the world's larger orogenic plateaus or the plateaus that have been inferred to have existed in the distant geological past (e.g., Schildgen et al., 2014). Flights of fluvial terraces exist at the northern and southern Anatolian plateau flanks (Yıldırım et al., 2011, 2013a; Schildgen et al., 2014), and delta deposits have been uplifted in front of the northern plateau margin (Akkan, 1970), an integral part of the growing Pontide orogenic wedge. Miocene to Pleistocene marine carbonates (Cosentino et al., 2012) and the provenance of conglomerates along the southern plateau margin (Radeff et al., 2017) allow an additional assessment to be made regarding the long-term tectonic history of the plateau's evolution. The Central Anatolian Plateau therefore presents an opportunity for studying young geological structures, tectonic landforms reflecting deformation at different scales, and the overall response of the evolving landscape with respect to plateau-building processes. Uplifted and deformed fluvial and marine terraces are key to these considerations and constitute the focus of this study.

The Central Anatolian Plateau is traversed by the Kızılırmak River, which, at a length of 1355 km, is Turkey's longest river. The Kızılırmak River is well known for its incised meanders, multiple terrace sequences, and extensive delta at the southern coast of the Black Sea (Akkan, 1970; Demir et al., 2004; Çiner et al., 2015) (Figure 2.1). The river originates in the western part of Eastern Anatolia and crosses the extensional Central Anatolian Plateau interior in the southwestward direction before changing its course toward the northeast; it then crosses the North Anatolian Fault Zone and traverses the tectonically active Pontide Mountain range of north-central Turkey before reaching the Black Sea. The river thus traverses the entire northern flank of the Central Anatolian Plateau and the Pontide orogenic wedge; the interplay between plateau-margin uplift, sea level change in the Black Sea, and incision of the Kızılırmak River has created a well-preserved staircase morphology of Quaternary fluvial terraces that may correlate with uplifted coastal terraces at the Black Sea coast (Akkan, 1970; Demir et al., 2004) and thus allow an assessment to be made regarding tectonic plateau margin processes on timescales of several 10^4 - 10^5 years.

Fluvial and marine terraces such as those that exist in the Pontide orogenic wedge are excellent strain markers. For example, Merritts and Bull (1989) and Merritts et al. (1994) used fluvial and associated marine terraces as strain markers in tectonically

active plate boundary settings. Previous morphotectonic studies carried out in northern Turkey have addressed the young tectonic evolution of the plateau margin (Keskin et al., 2011; Yıldırım et al., 2011, 2013a; b), but the spatiotemporal characteristics of deformation and uplift processes in the Central Pontide region remain largely enigmatic and poorly understood.

The Central Pontides are compressional ranges that reach elevations of up to 2000 m; they constitute an orogenic wedge between offshore structures in the Black Sea and the North Anatolian Fault Zone (NAFZ) (Yıldırım et al., 2011, 2013a; b). The dextral NAFZ is one of the most seismically active transform faults on Earth (Şengör et al., 2005). The fault has an extensive restraining bend in the transition between eastern and western Anatolia. This sector of the fault coincides with the Central Pontides (Okay and Tüysüz, 1999; Yıldırım et al., 2011, 2013b). Despite the well-known Quaternary activity of the NAFZ (e.g., Özden et al., 2008), the characteristics of activity of coastal and offshore structures beyond the bend are only known to the first order. However, faulted and uplifted river terraces in the Gökırmak Basin and coastal terraces on the Sinop Peninsula (Yıldırım et al., 2011, 2013a) unambiguously document Quaternary tectonic activity and a northward-directed migration of Pontide wedge deformation.

In light of these observations and questions particularly ones concerning plateau margin evolution, the aim of this study was to unravel the complex interplay between tectonic uplift and superposed Quaternary sea level changes in the Black Sea acting on the flanks of the Central Pontides. We present (1) new, detailed geomorphic mapping of fluvial terraces in the lower reaches of the Kızılırmak River and associated palaeo-delta levels at the Black Sea coast; (2) new OSL ages of the fluvial terraces and palaeo-delta levels, as well as their temporal relationships with Quaternary sea level changes documented at the Black Sea coast; and (3) a calculation of the incision rate of the Kızılırmak River as a proxy for regional uplift to facilitate a better understanding of the lateral and vertical growth of orogenic plateau margins.

2.2 Regional Setting

The northward-sloping Pontide orogenic wedge is located between the Central Anatolian Plateau and the Black Sea Basin where the northward-convex bend of the

NAFZ occurs (Meijers et al., 2010; Yıldırım et al., 2011) (Figure 2.1). The Pontides comprise Triassic to Paleocene island-arc rocks and Eocene flysch units related to the Alpidic orogeny (Şengör and Yılmaz, 1981; Görür, 1988; Okay and Tüysüz, 1999; Stephenson and Schellart, 2010; Tüysüz, 1999; Rangin et al., 2002; Nikishin et al., 2015).

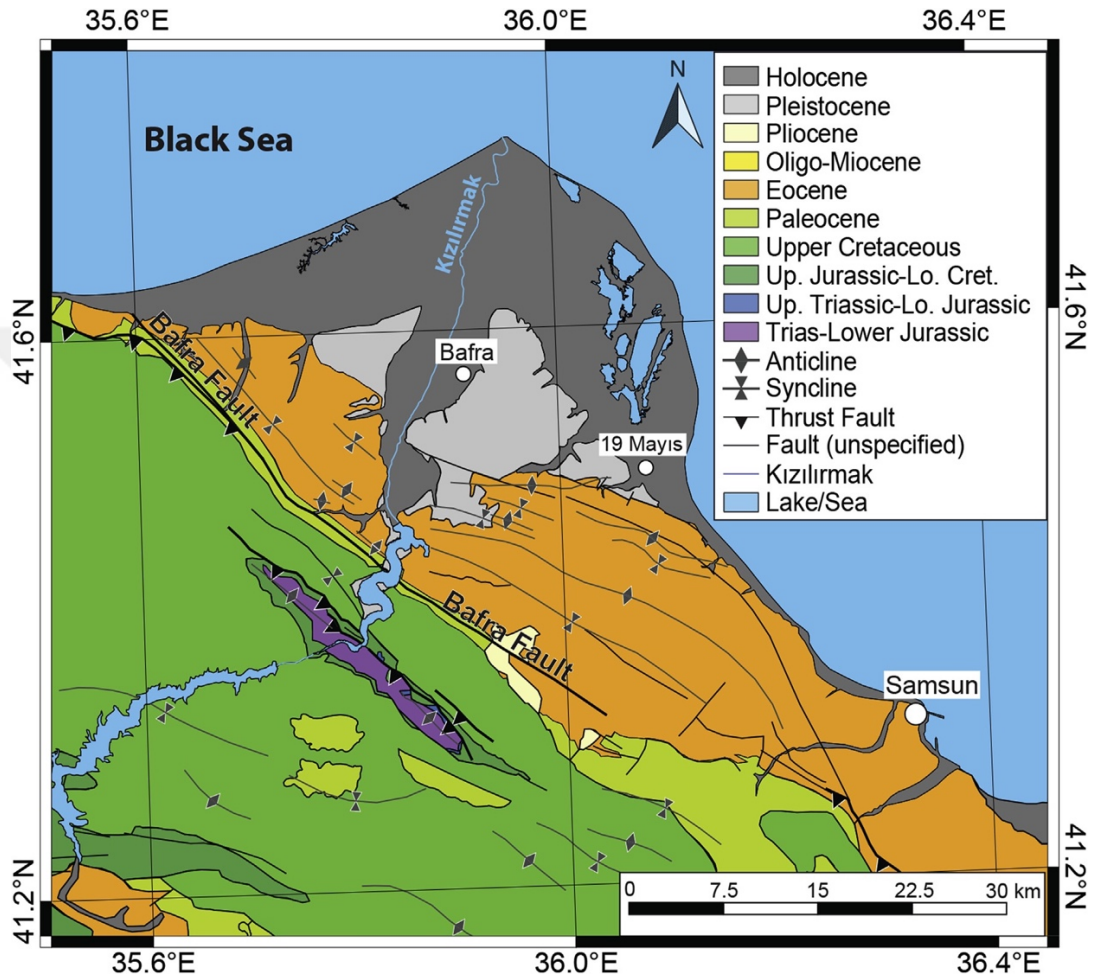


Figure 2.2 : Geologic map of the eastern Central Pontides with faults and folds (modified after Demir, 2005; Uğuz and Sevin, 2009; Emre et al., 2012). The main features are the parallel ridges in folded Cretaceous and Eocene flysch units that form the local basement of the southern terraces. Pre-Quaternary units north of the Eocene flysch are not exposed.

Beyond its confluence with the Gökırmak River, the Kızılırmak River flows through folded Mesozoic bedrock and Maastrichtian to Lower Paleocene transitional marine/continental sedimentary rocks of the Akveren Formation north of Burunca (Figure 2.2). The NW-SE-striking Baфра Fault defines the northern boundary of this formation (Figure 2.2). To the north of the fault, Eocene andesitic rocks and terrestrial northward-dipping sedimentary rocks of the Eocene Tekkeköy and Kusuri Formations represent the bedrock until ca. 6 km SW of Bafra (Demir, 2005; Uğuz

and Sevin, 2007, 2009). These Eocene units are normal-faulted, but structural reconstructions and seismic reflection profiling have shown that these old anisotropies are being inverted during the present-day tectonic regime (Robinson et al., 1996; Rangin et al., 2002).

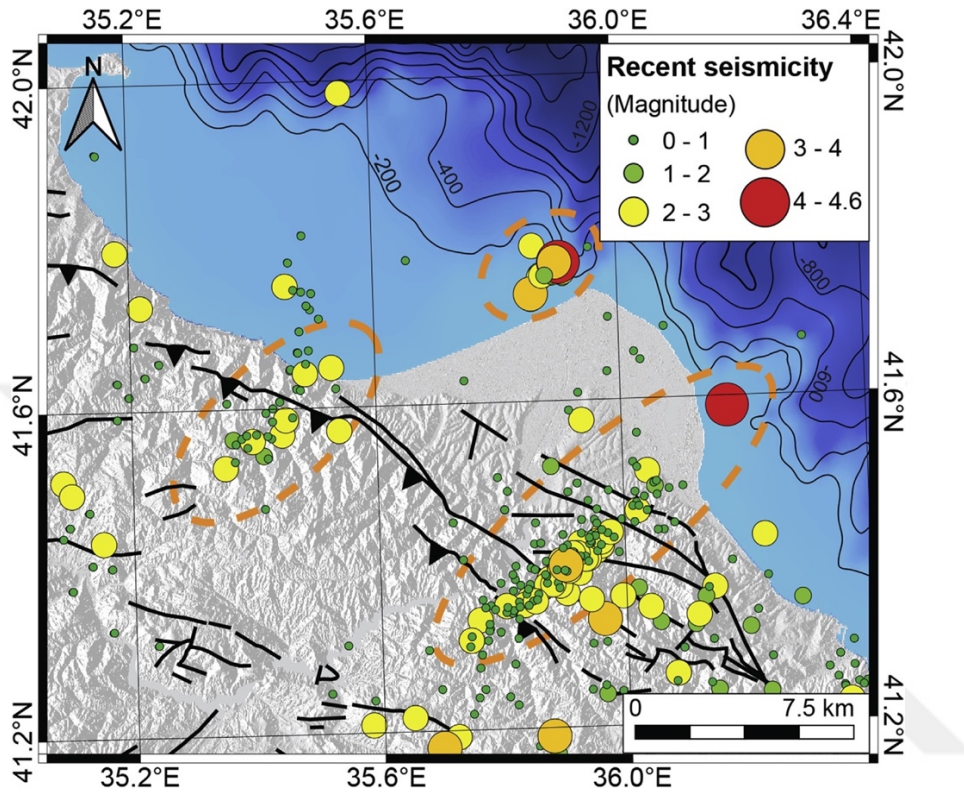


Figure 2.3 : Earthquakes between 1904 and 2017 recorded by the Kandilli Observatory and Earthquake Research Institute of Boğaziçi University (2017). The dashed circles highlight the most active seismicogenic zones; large-magnitude earthquakes occurred exclusively offshore.

The Bafra Fault is a major onshore structure in the study area, but its kinematics remains uncertain (Emre et al., 2012). The fault corresponds with a distinct lineament and coincides with the transition between the different uplifted delta deposit levels and the rugged high topography to the south. A neotectonic offshore graben, the Sinop Trough (Rangin et al., 2002), is a major structure immediately north of the Kızılırmak Delta. The bounding normal faults strike NW-SE, parallel to the Bafra Fault, and record activity until the Pliocene (Rangin et al., 2002). Rangin et al. (2002) described the Sinop Trough as an extensional step-over in an area of right-lateral shearing associated with incipient motion along the NAFZ.

The region around the Kızılırmak River gorge and delta plain is characterized by small-magnitude, low-frequency earthquakes (Kalafat and Toksöz, 2017). The only historical large-magnitude earthquakes in the region have occurred along the NAFZ (Bohnhoff et al., 2016). Earthquake magnitudes in the study region range between 2 and 4.6 (Boğaziçi University, Kandilli Observatory and Earthquake Research Institute, 2017). A prominent seismically active zone is located south of the Kızılırmak Delta on the eastern side of the Kızılırmak River and is oriented NE-SW (Figure 2.3). Here, earthquakes reach magnitudes of up to Mg. 4.4 at depths between 4 and 10 km, but deeper earthquakes with depths of ca. 22 km have also been recorded (Boğaziçi University, Kandilli Observatory and Earthquake Research Institute, 2017). Another seismically active zone that is oriented NE-SW is located at the western margin of the delta (Figure 2.3). This area has produced earthquakes with magnitudes of up to Mg. 4.2 at depths between 9 and 15 km; these hypocenters extended into the area of the southern margin of the Sinop Trough. Furthermore, widespread, isolated low-magnitude events have occurred between the Eastern Pontides in the SE and the Sinop Trough, reaching magnitudes of up to Mg. 4.6.

Landslides are common on the northern side of the Bafra Fault overlying Eocene graben fill deposits, and may have been linked with seismogenic activity; creeping landslips are common in the areas featuring exposures of Eocene rocks (Duman et al., 2011) (Figure 2.3).

The Black Sea is the largest semi-enclosed inland sea in the world. During the Quaternary, the Black Sea Basin was disconnected from the global ocean until MIS 12 (Kochegura and Zubakov, 1978; Champion et al., 1981). However, the possibility of the basin's temporal connection with the Mediterranean since 780 ka has also been proposed (e.g., Yanko-Hombach et al., 2013). With regards to transient connectivity to the World Ocean, sea level oscillations in the Black Sea are difficult to compare with globally recorded sea level changes. Although the Black Sea attained several highstands similar to present sea level and was connected to the World Ocean during interglacials over at least the last 460 ka (Kochegura and Zubakov, 1978; Champion et al., 1981), the Black Sea Basin turned into a large lake when global sea levels fell below a sill depth of ca. 32 m at the Bosphorus (Badertscher et al., 2011). The Black Sea was also repeatedly connected to the Caspian Sea since the Pliocene (e.g., Grigorovich et al., 2003; Badertscher et al., 2011); this connection has been strongly

dependent upon regional climate. In summary, during the Pleistocene, the sea level of the Black and Caspian Sea system often reacted differently than that of the World Ocean (see Svitoch et al., 2000; Panin and Popescu, 2007; Badertscher et al., 2011).

The deltas of the Kızılırmak and Yeşilirmak rivers are the largest deltas along the Turkish coast of the Black Sea (Figure 2.1). The Kızılırmak Delta is characterized by an extensive and smooth surface delimited by steep slopes of the elevated palaeo-delta levels (Akkan, 1970). Demir et al. (2004) tentatively correlated the lower elevated delta levels with MIS 5e (Karangatian stage) and the upper levels with MIS 7 or MIS 9, related to the terrace levels of the Akçay River further east (Bilgin, 1963). In addition to the varying delta levels, multiple flights of fluvial terrace levels occur along the bedrock gorge of the Kızılırmak River (Akkan, 1970).

2.3 Data and Methods

2.3.1 Geomorphic mapping and analysis

With the aid of satellite-derived elevation data, including data from ALOS (The Advanced Land Observing Satellite) World 3D, SRTM 1 (Shuttle Radar Topography Mission), and ASTER (Advanced Spaceborne Thermal Emission and Reflection), we updated the geomorphological map of Akkan (1970) using digital elevation models. Topographical maps published in 1959 (prior to the construction of the Derbent Dam) were used to determine the terrace tread elevations with respect to the position of the present-day valley floor. We additionally acquired new, high-resolution Digital Surface Models (DSM) at each sampling site (see below) to constrain the height and extent of each terrace with differential GPS measurements within the DSM area. The new GPS points were measured with a mobile Leica dGPS device, while our Sensefly eBee UAV (Unmanned Aviation Vehicle) acquired aerial images of the area with 12 MP resolution; the data have a front overlap (along track) of 75% and a side overlap (across track) of 70%. The ground-sampling distance of the derived DSM was 6-8 cm. The aerial photos were orthorectified using the dGPS points, and a point cloud was created using the SfM (Structure-from Motion) algorithm (Snively et al., 2007). The vegetation points from the surficial imagery point clouds of the DSMs were excluded using the CloudCompare CSF (cloth simulation filter) algorithm (Zhang et al., 2016; CloudCompare 2.8.0, 2016), which inverted the point cloud. Based on this data set, the remaining ground points were

connected via triangulation to form the DTM. The shoreline-angle calculation of coastal terraces was carried out using the TerraceM algorithm (Jara-Muñoz et al., 2016).

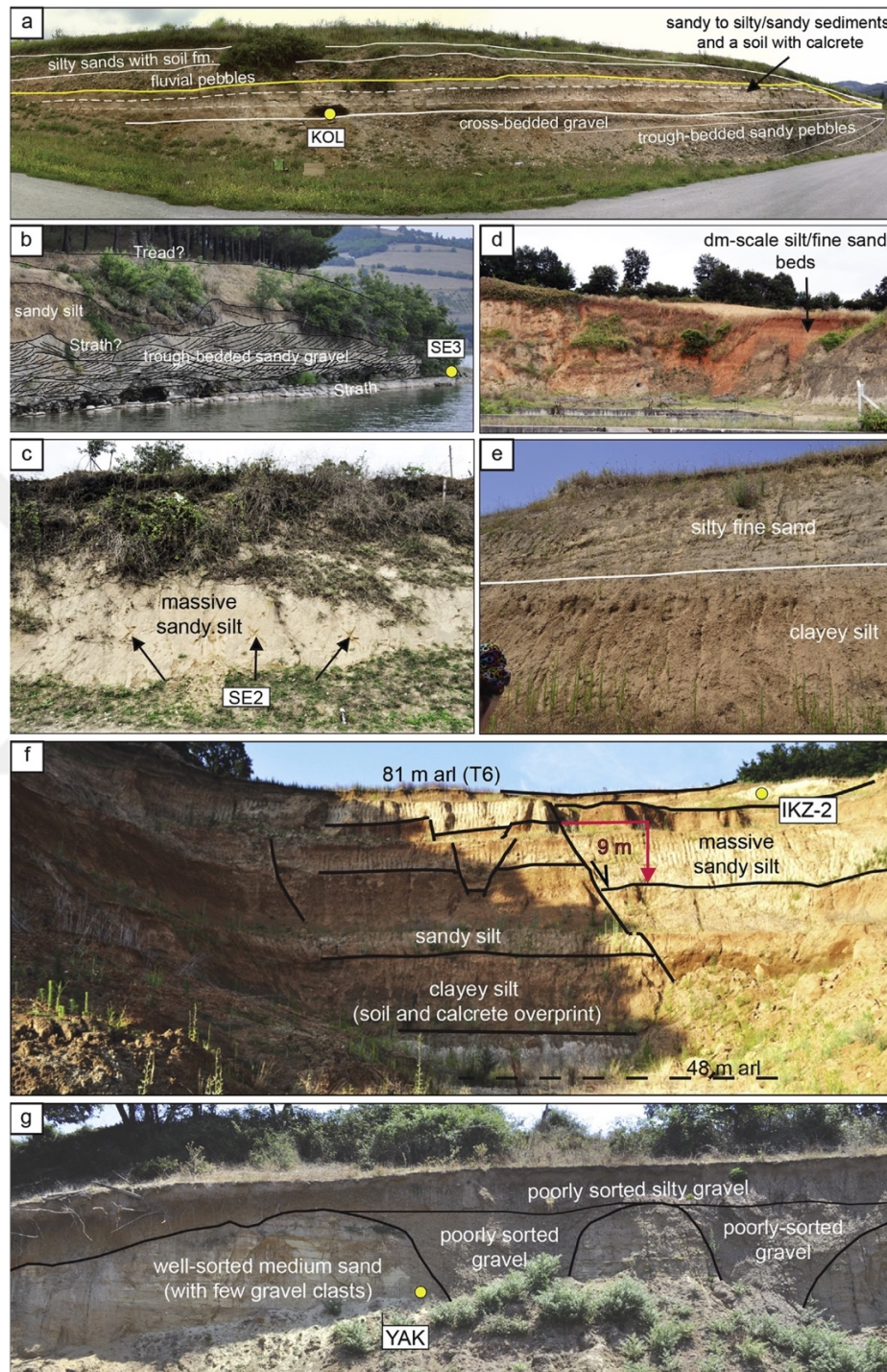


Figure 2.4 : Outcrop conditions at and close to a representative suite of sampling locations in the study area. (a) Kolay sampling site; (b) SE3 sampling site; (c) SE2 sampling site; (d) outcrop 500 m SE of the AK2 sampling site at low sun-angle conditions to highlight internal bedding; (e) outcrop approximately 100 m S of IKZ1; (f) IKZ2 sampling site and post- sedimentary normal faulting; (g) YAK sampling site.

2.3.2 OSL sampling and dating

Sediment samples for dating the elevated terraces were collected in line with two different procedures, selected depending on the cohesion of the sediments in question. First, a hole at least 40 cm in depth was dug into the outcrop wall to remove the recently irradiated surface material. As a second step, a lightproof plastic tube (6.5 cm in diameter, 4 mm thick, and 40 cm long) was driven into the sediments. During the recovery of the tube, at least 600g of the material surrounding the tube was collected to determine the environmental dose rate of the sampling location. The OSL sample tube was subsequently wrapped in black plastic bags and sealed with a cap. Unfortunately, it was not always possible to insert the tube into outcrops with very cohesive sediments; for this reason, night sampling was carried out at sampling locations IKZ1 (two out of three samples), IKZ2, AK1, HIR, KIZ, SE1, SE2, and SE3. Accordingly, holes at least 20 cm in depth were dug inside the outcrop in the absence of artificial light, and the sampling tubes and sample bags were filled with material which had been scratched from sediment deep within the deposit. Three samples were taken from each location to minimize the impact of incomplete bleaching and sediment inhomogeneity. The samples were collected at depths between 2 and 14 m below each terrace tread. The outcrop conditions of several samples are shown in Figure 2.4, and descriptions of each outcrop are provided below. Further information regarding the preparation and procedures for OSL signal measurements can be found in the Appendix A.

2.4 The Kızılırmak Fluvial Terrace Sequence

2.4.1 Geomorphology and stratigraphy of strath terraces

We identified nine fluvial terrace levels along the northern Kızılırmak River gorge (Figure 2.5). These are named T0 to T8, indicating increasing tread height and age above the current river course. The lowermost terrace, T0, is located 7-9 m above the river and contains gravels that are partly reworked. The subsequent terrace levels are T1 (16 m above the valley floor), T2 (26 m above the valley floor), T3 (42 m above the valley floor), T4 (48-49 m above the valley floor), T5 (58 m above the valley floor), T6 (82 m above the valley floor), T7 (100-104 m above the valley floor), and T8 (118-123 m above the valley floor) (Figure 2.5).

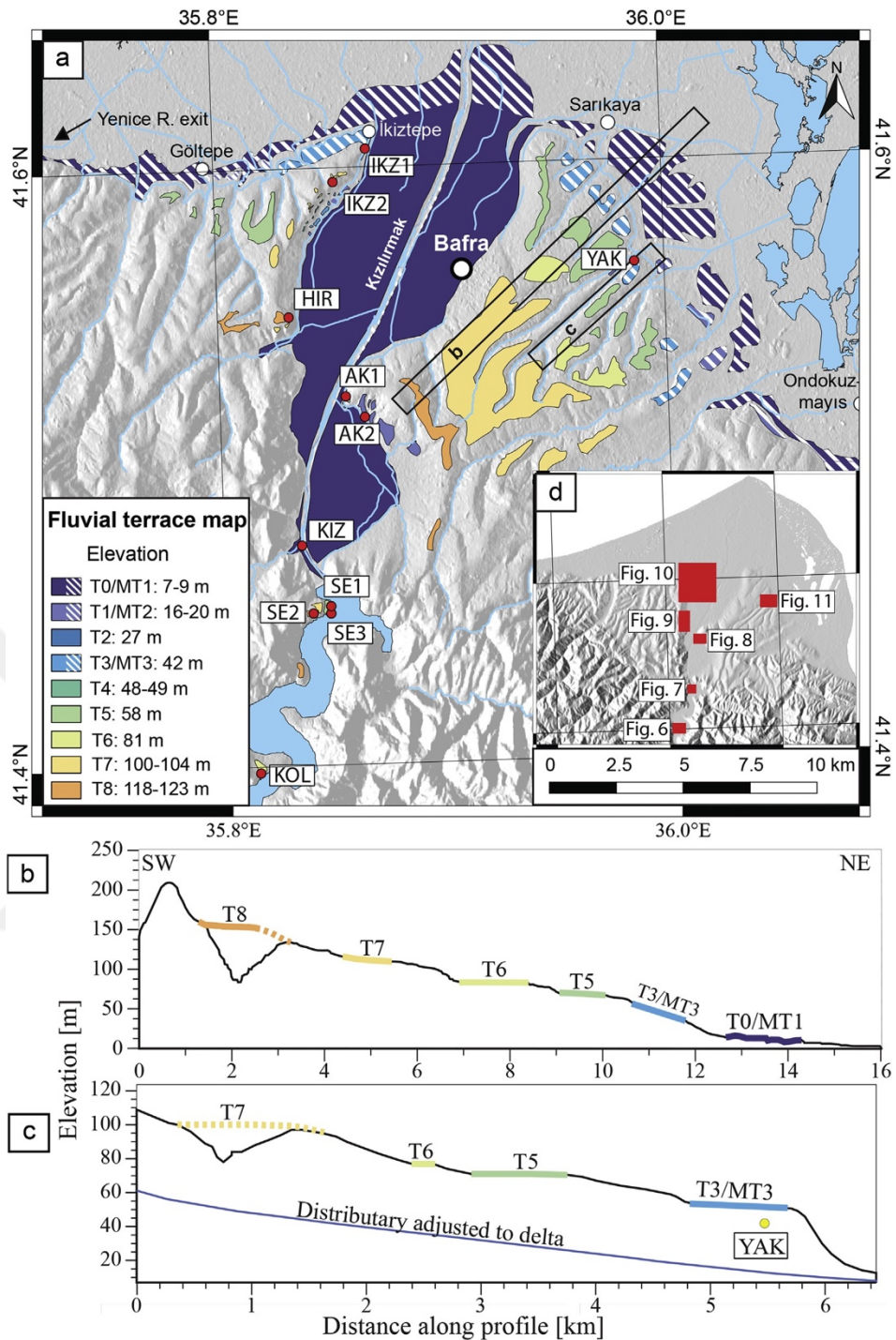


Figure 2.5 : (a) Terrace sequences at the lower sectors of the Kızılırmak River and its delta, with strath terraces inside the narrow river valley in the south, alluvial fill terraces inside river valleys, delta terraces forming the delta platform (esp. T5 and T7), and coastal terraces at the northern margins of the delta platform (hatched); (b) SW-NE oriented maximum elevation profiles across the eastern delta platform with a complete terrace sequence; (c) detailed SW-NE oriented maximum elevation profile of the Gerzeliler OSL sampling site; (d) overview of the locations of Figures 2.6-2.11.

Along the Derbent Dam, three point-bar risers exist at the western shore, and two on the eastern side (Figure 2.5a). Only the western point-bar risers contain distinctly

elevated fluvial terraces. These terraces are well preserved at the villages of Kolay and Selemelik and contain a thick alluvial sedimentary cover upon the exposed bedrock with relatively planar terrace surfaces (Figures 2.6 and 2.7).

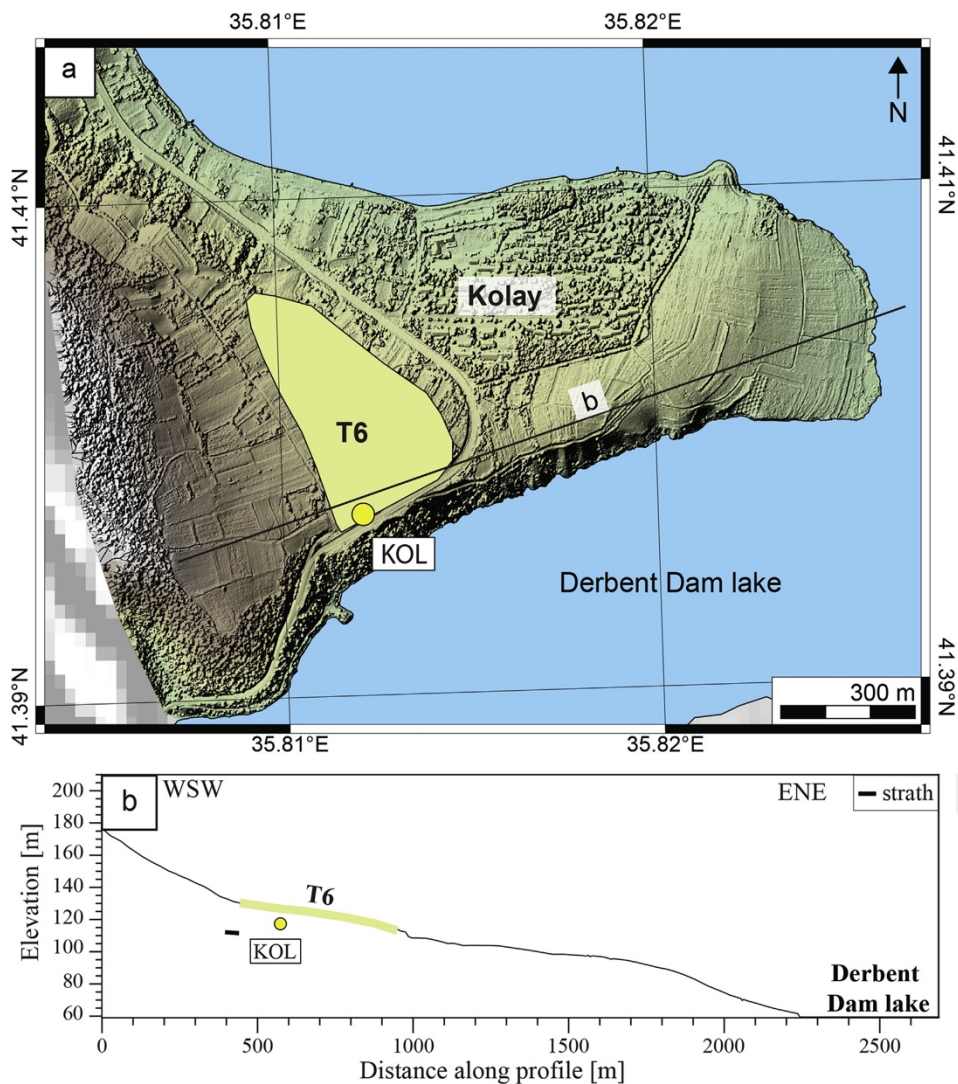


Figure 2.6 : Map (a) and topographic profile (b) across the sampling location at Kolay.

The southernmost strath terrace is located at Kolay (Figure 2.6). The original elevation of the valley floor at the time of terrace formation was ca. 40 m above sea level. We identified only one terrace with a well-preserved tread at this location. The height of the terrace tread is 82 m (T6), and the strath level is 72 m above the river valley floor (Figure 2.6b). This 10-m-thick terrace deposit consists of two sequences that are overlain by an approximately 30-cm-thick colluvium (Figure 2.4a). The lower sequence comprises gravel-to boulder-sized (up to > 40 cm in diameter) channel fill with a sandy matrix; a wide channel structure and internally variable beds can be identified. The complete layer is 5.5-m-thick. Although few lenses are

sand-rich, most of the clasts are pebble-sized. This layer is topped by a well-sorted, fining-upward sand layer composed of medium to fine sand; in the uppermost 50 cm of this layer, silt content increases and nodular calcrete formation is notable. Another 40-cm-thick, well-sorted medium sand layer overlies this sequence. This deposit is superseded by poorly sorted 80-cm-thick pebbly strata with a sandy matrix that is covered by a gravelly sand layer. This layer has an erosional unconformity where the fine-grained layers to the east have been increasingly removed. The top of the sequence is formed by silty sand to sandy-silt layer displaying evidence of pedogenesis. The pebbles of both sequences are subangular to rounded. We took OSL samples (KOL) from the sandy part of the lower sequence on top of the pebble layer (Figure 2.4a).

Downstream of Selemelik, we identified and mapped five levels of strath terraces and estimated the original valley floor height to be 32 m above sea level (Figures 2.4 and 2.7). The tread height of the lowermost level, TX, is 35 m above the river valley floor, and the strath of the terrace is lower than the reservoir level. This terrace constitutes fine-grained overbank deposits containing a massive silty fine sand layer that is at least 3 m thick. This terrace deposit was sampled (SE1).

The tread height of the second level is ca. 42 m (T3) and features a strath at 32 m above the valley floor, which is very close to the reservoir level. The sedimentary veneer of the terrace rests on mafic volcanic bedrock and shows a fining-upward sequence from sandy-gravelly conglomerate to cross-bedded sands overlain by silty overbank deposits (Figure 2.4b). The material is poorly sorted, 1.5 m thick, and contains rounded pebble-to boulder-sized clasts up to 50+ cm in diameter; the matrix is sandy gravel and carbonate-cemented. Above this, boulders are replaced by sorted pebbles, while the matrix remains sandy and the sequence grades into finer gravel and coarse sand deposits with cross-stratification. Eventually the gravel disappears, and the top of the sequence is dominated by fine sand and silt. The exposure of this unit is ca. 6 m high, but the thickness of the terrace deposit reaches ca. 10 m, with at least one more sequence on top; the tread surface is eroded. The top of the exposed lower sequence shows a step in the morphology and might represent another degraded tread. We sampled this terrace a few centimeters above the strath by collecting the sandy matrix of the conglomerate (SE3).

The third level of the terrace sequence (T5) belongs to a very degraded terrace with an exposed strath at 48 m and an estimated tread height of 58 m above the valley floor. The next-higher terrace tread level (T7) has a tread height of ca. 100 m above the river and consists of massive silty fine sands (Figure 2.4c). These sediments and the tread elevations are very similar to the terrace exposed at Burunca (between Kolay and Selemelik). We also took OSL samples (SE2) from this level at Selemelik. The highest terrace (T8) forms the basement of the upper part of Selemelik, with a tread height of ca. 123 m above the valley and a strath located ca. 115 m above the valley floor (Figure 2.7).

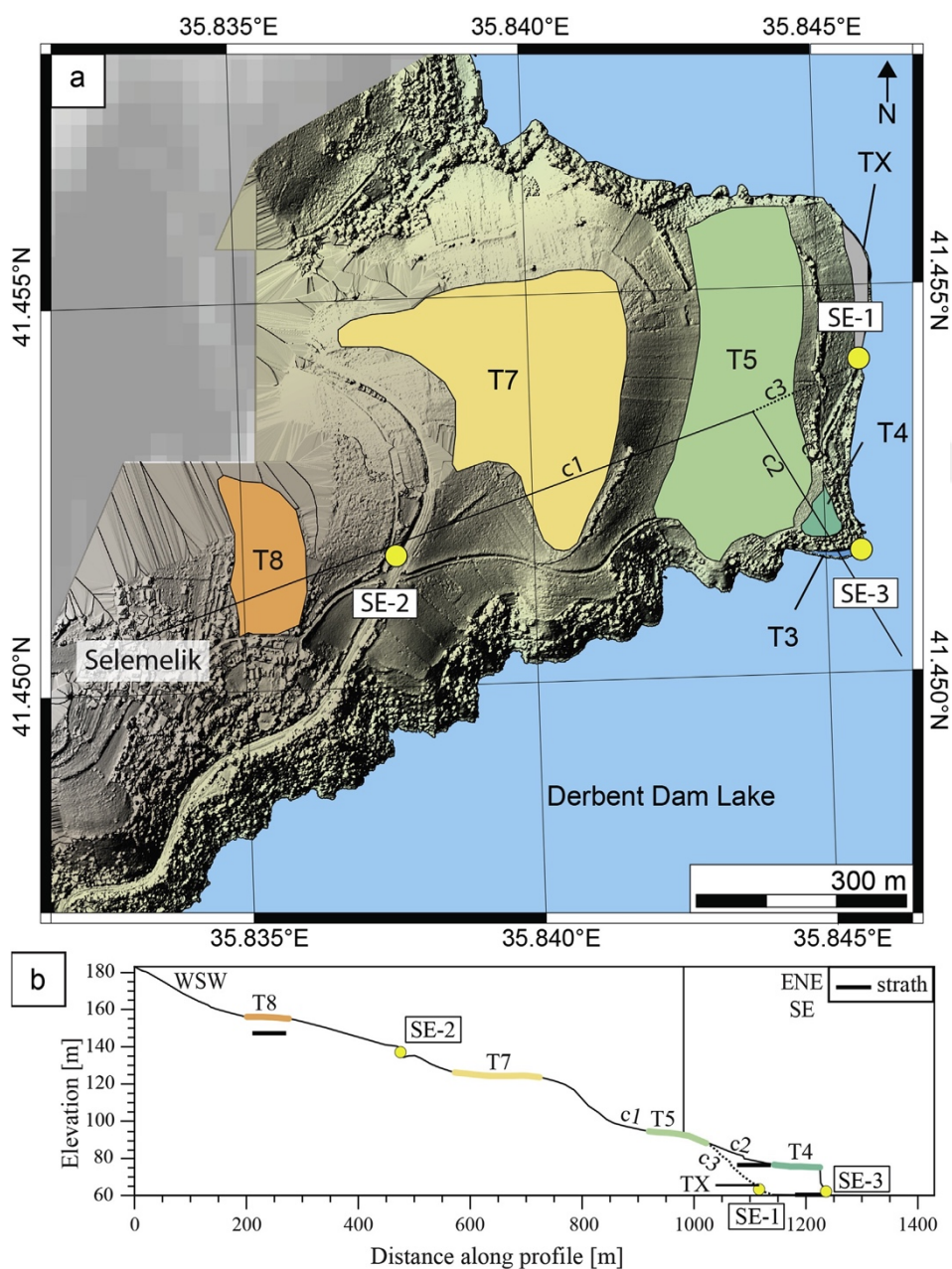


Figure 2.7 : Map (a) and topographic profile (b) of the Selemelik sampling site (c1, c2, and c3 are sections of the profile).

2.4.2 Geomorphology and stratigraphy of fill terraces

Modern delta deposits and different palaeo-delta levels are exposed where the Kızılırmak River exits its gorge and enters a large floodplain immediately north of the Derbent Dam (Figure 2.5). We mapped nine abandoned fill terrace levels along the course of the Kızılırmak River; three of these levels are adjusted to coastal terrace levels that were sculpted into the palaeo-delta levels. We evaluated these terraces regarding their overall spatial distribution (Figure 2.5). Akkan (1970) mapped two extensive palaeo-delta levels as the upper and lower levels, respectively, and tentatively assigned a Pleistocene age to them. According to Akkan, terrace T2 corresponds to the lower level, and terraces T5 and T6 correspond to the upper levels (1970). Akkan's "fossil wave-cut platform" corresponds to delta terraces T7 and T8 because of their well-developed staircase morphology and sedimentary characteristics (c.f. Figure 2.5).

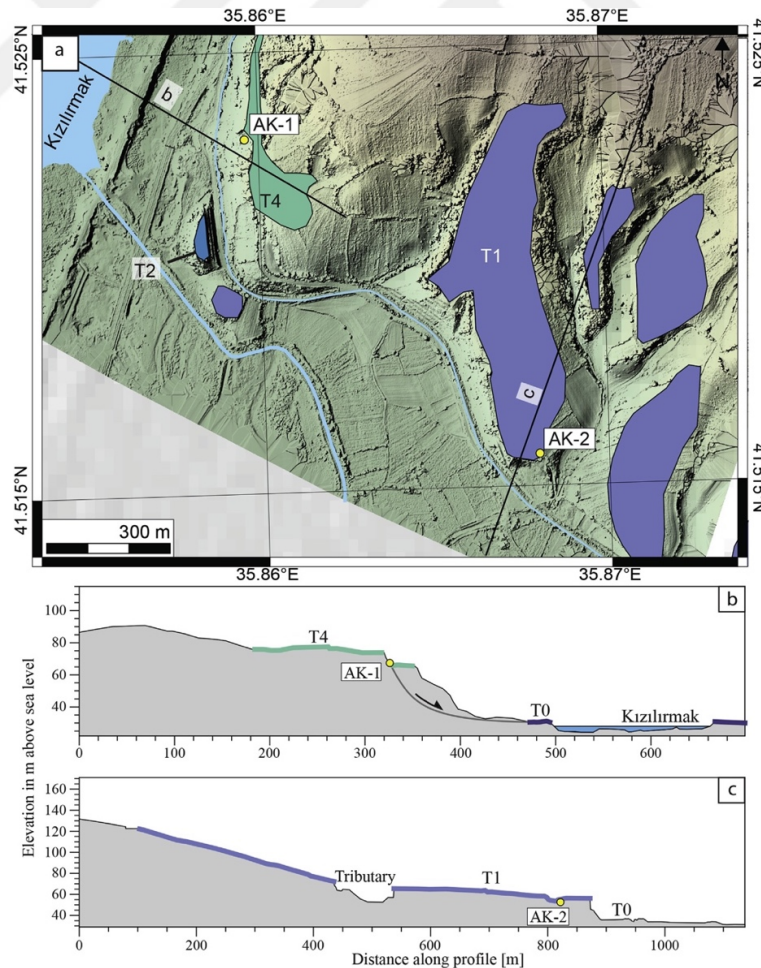


Figure 2.8 : Map (a) and topographic profiles (b, c) of the Aktekke sampling sites.

The lowermost surface corresponds to the modern floodplain (T0), located ca. 7-9 m above the present-day river course (Figure 2.5). Although the tread surface is extensively modified by anthropogenic activity, there are still some preserved unmodified areas. The height above the recent river level increases downstream from 7 m near the Derbent Dam to 9 m at the northern termination of the valley. The terrace comprises unconsolidated sandy gravel deposits. These poorly sorted sediments crop out over a long distance along the river channel. The sediments are mainly matrix-supported gravels with occasional cobbles. We took OSL samples (KIZ) from this level close to the Derbent Dam wall and used the matrix after excluding large grains. Another outcrop of this terrace deposit, located ca. 1.6 km upstream along the tributary adjacent to the Kızılırmak River at the KIZ sampling site, exposes similar deposits, with higher contents of coarser, poorly sorted gravel and cobbles. These strata are covered by an approximately 80-cm-thick layer of coarse sand to fine gravel; massive, sandy mud forms the top of the sequence. These two finer-grained layers are missing at the KIZ sampling site.

Towards the north, the first group of fill terraces is located at the eastern slope of the Kızılırmak River valley at the village of Aktekke (Figure 2.8). Two levels of the fill terraces and one strath terrace were identified at this location. The tread height of the lower fill terrace level (T1) is approximately 20 m above the confluence of a major tributary to the Kızılırmak River, located close to Aktekke and 44 m above the river. This terrace contains a stack of well-sorted silty sand layers, each ca. 50 cm thick, with no pronounced changes in composition and, consequently, rather indistinct layer boundaries (Figure 2.4d). The layers are light yellowish in color and extend from close to the tributary mouth upstream until at least the village of Doğankaya. The basement is not exposed. We sampled terrace (AK2) for OSL age determination. The next-higher level (T2) is a small strath terrace remnant located at the confluence, with a tread height of 26 m above the river. This terrace contains trough cross-bedded deposits (with a large channel structure at the base) that unconformably overlie north-dipping andesitic volcanoclastic deposits with a minimum strath height of ca. 6 m above the river. The width and the grain size of the trough cross bedding decreases towards the top. The sediments are cohesive, and deep holes occur on the tread. The third terrace level at this location (T4) has a degraded tread 49 m above the river and is at least 10 m thick. The terrace contains massive, light gray-yellowish

sandy silt, which we sampled for OSL dating (AK1). The nature of higher possible terrace levels and their deposits remains ambiguous (Figure 2.8).

The Hıdırellez terraces are located at the western slope of the valley (Figure 2.9). We identified two levels here, located 104 m (T7) and at 123 m (T8) above the river. The deposits associated with the lower level (T7) are exposed along the confluence of the Kızılırmak River and the Gökçesu River; the terrace continues northward along the Kızılırmak River, where it forms the top delta terrace. The upper terrace (T8) forms a smooth plateau at the top and extends along the northern side of the Gökçesu River valley (Figure 2.9). The terrace deposits constitute sandy conglomerates with southward-dipping pebble imbrications and an intercalated, well-sorted, 30-cm-thick sand lens. Sediments from this lens were sampled (HIR) approximately 14 m below the terrace tread. The conglomerate has a minimum thickness of 25 m. We did not observe lower terrace levels at the confluence of the Gökçesu and Kızılırmak Rivers or on the western slope of the main stem.

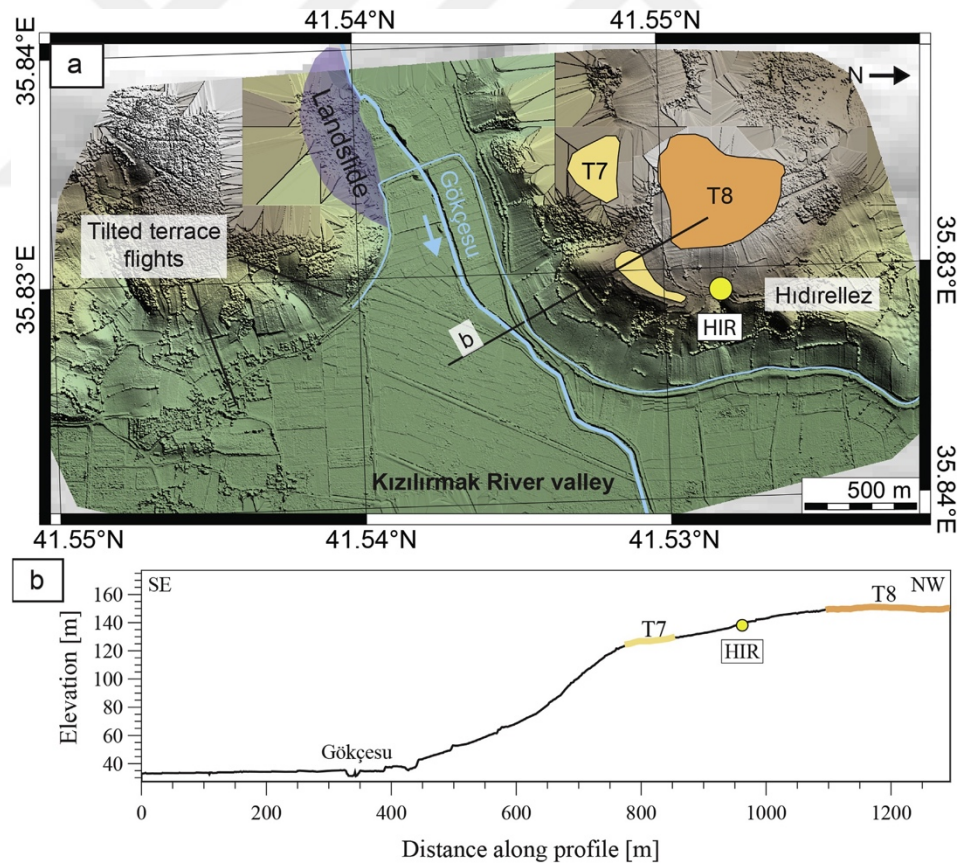


Figure 2.9 : Map (a) and topographic profile (b) of the Hıdırellez sampling site. Only the deposits of terrace levels T7 and T8 are exposed at the confluence of the Gökçesu and Kızılırmak Rivers. Since large parts of terrace T7 were covered by dense vegetation, no high-resolution DSM data could be acquired. Instead, a combination of publicly available data was used to further map this terrace.

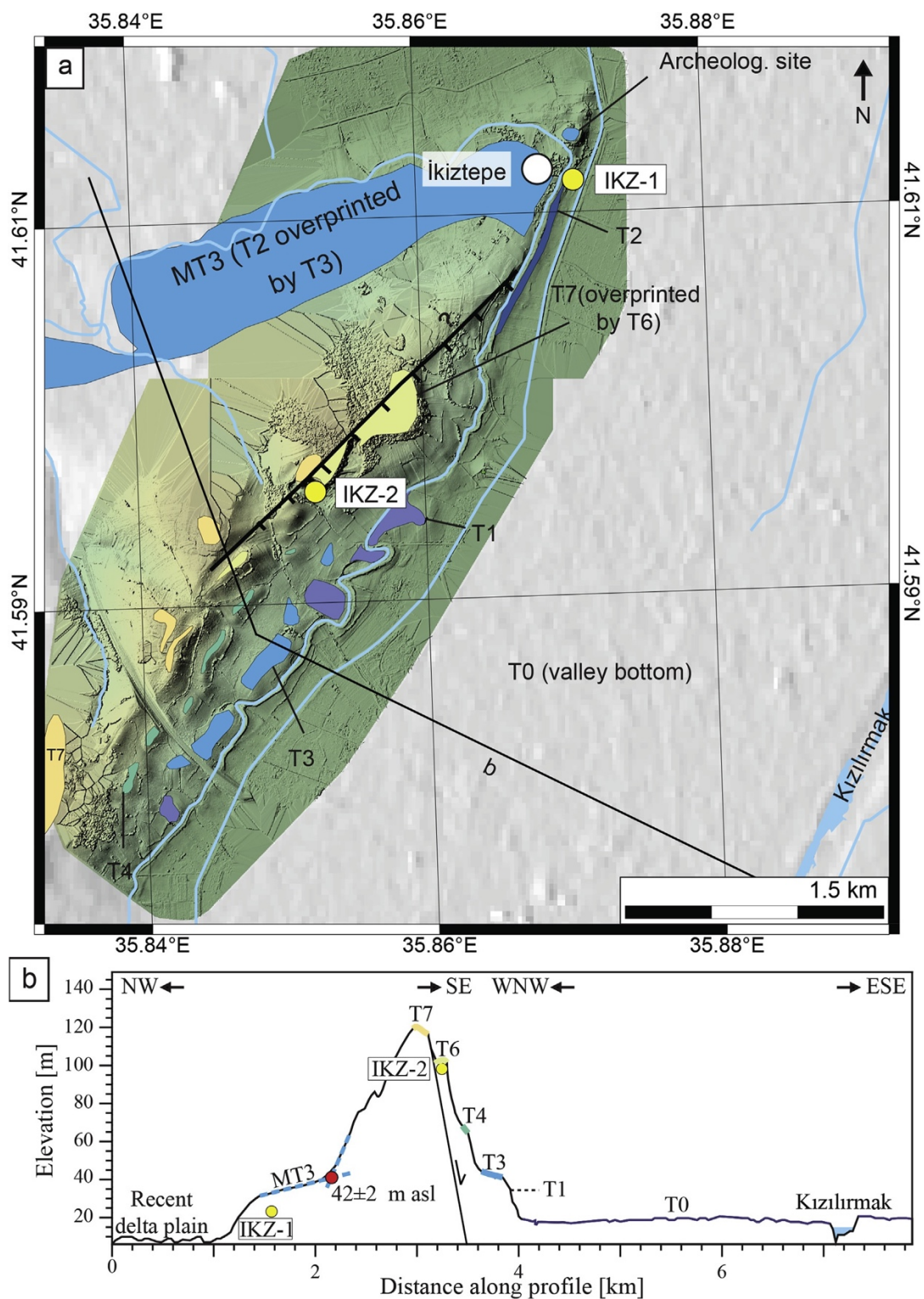


Figure 2.10 : Map (a) and topographic profile (b) of the İkiztepe sampling site. The delta terrace T7 is partly modified by the formation of terraces T6 and MT3 on both sides of the ridge. The area was affected by a SE-dipping normal fault that abuts the T6 surface. The İkiztepe archeological site is located on MT3.

The northernmost group of terraces is located south of İkiztepe, which is an important archeological site that has been repeatedly occupied since the Late

Chalcolithic (Özbal et al., 2002; Alkim et al., 2003; Welton, 2010). Four fluvial terrace levels were identified. Their tread heights were located at approximately 16 m (T1), 26.5 m (T2), and 47 m (T4) above the recent valley floor, as well as 104 m (T7) above the recent delta level (Figure 2.10). Although the higher two terrace levels are severely eroded, the lower two terrace levels are well-preserved. A landslide close to the northernmost section of the valley overprints all of the terraces in the river valley. Only T1 and T2 sediments are exposed farther north. The lowermost terrace (T1) extends along the valley in the northern and southern sections. This level is replaced by the second terrace (T2) in the central part, and a smaller terrace appears at the back of the northern section of the lowermost terrace (Figure 2.10).

Terrace T4 extends along the back of the two lower terraces, and the uppermost terrace (T7) is represented by a long ridge bordering the western side of the river valley between İkiztepe and Hidirellez (Figure 2.10). The ridge is increasingly incised northward on its main valley side, forming another tread level (T6) from Hidirellez to İkiztepe. At IKZ2, we sampled the uppermost terrace level within a sequence of four conformable sediment layers overlying sandy silt deposits that host palaeosols at the top of all layers. All of these layers have a thickness of 5-7 m; the layers are primarily light yellowish in color and change to a brownish-red color at the top, reflecting a higher clay content. Calcrete was formed at several layers of the clayey sections (Figure 2.4f).

We identified a normal fault that cuts these deposits, but the fault has no geomorphic expression at the surface (Figure 2.10). Additional small normal faults were found with a similar strike in the footwall of this structure (Figure 2.4f). The fault displacement reaches ca. 9 m close to the IKZ2 sampling site, indicating the fault's post-depositional activity. The sediments are sub-horizontal along the main valley and dip gently northward at IKZ2 (Figure 2.4f).

2.4.3 Geomorphology and stratigraphy of coastal terraces

MT1 corresponds to T0 at ca. 9 m above sea level close to İkiztepe and Gerzeliler (Figures 2.5, 2.10 and 2.11). It is mainly exposed at the distributaries draining the delta platform on the western side, and forms an extended area of a former delta lobe north of the eastern platform. Above this level, the eastern rim has a relatively straight, NW-SE oriented coastline, and hosts coastal and delta terraces of the

Kızılırmak River and its tributaries between palaeo and Ondokuzmayıs. The northern margin of the western palaeo-delta platform has a concave rim between İkiztepe and the mouth of the Yenice River (Figures 2.1c and 2.5). Furthermore, we identified two marine palaeo-cliffs with shoreline angle elevations between 16 and 20 m (MT2) and 42 m (MT3) above sea level on the northernmost limits of the palaeo-delta levels; these correspond to the depositional terrace levels T1 (MT2) and T3 (MT3), respectively.

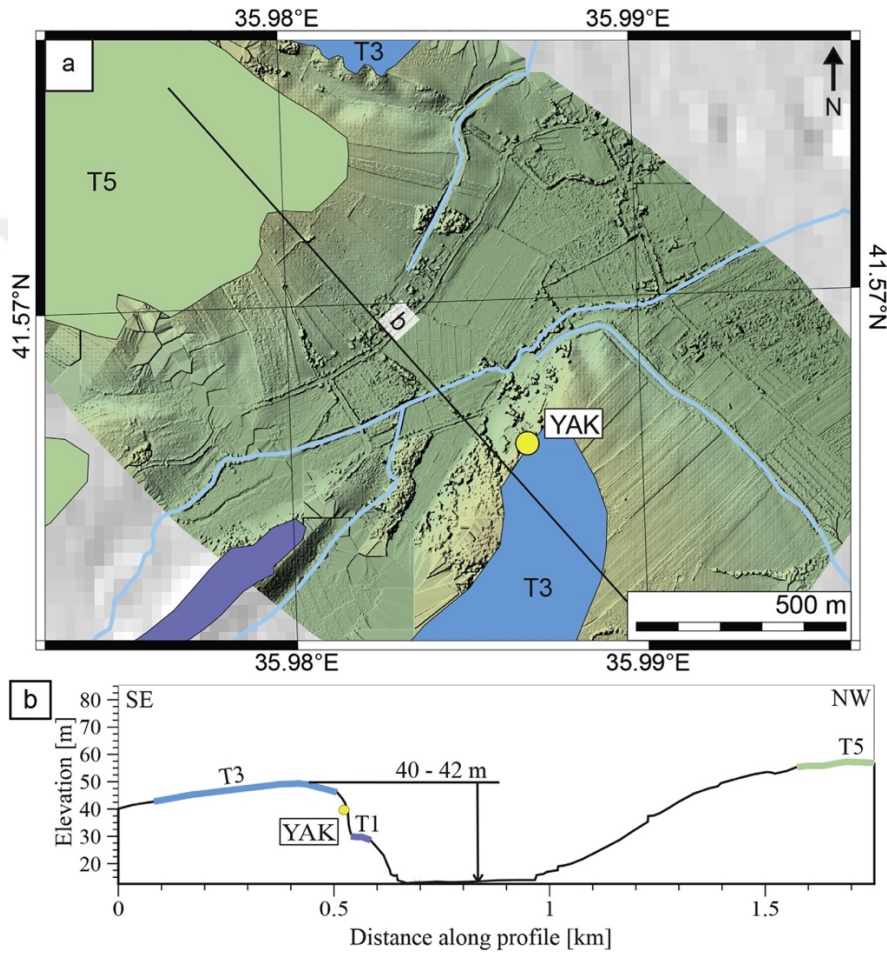


Figure 2.11 : (a) Map of the Gerzeliler sampling site at the mouths of distributaries draining the eastern Kızılırmak Delta platform; (b) profile across the Gerzeliler sampling site.

The lower coastal terrace (MT2) features preserved surfaces at İkiztepe and Gerzeliler and is located on the eastern- and westernmost convex parts of the elongated rim of the delta platform to the west of Ondokuzmayıs and the east of Göltepe (Figure 2.5). This terrace seems to be depositional (delta progradation) on the eastern side and erosional (marine terrace) to the west of the river valley. It has a tread height of approximately 16-20 m above the present-day delta in the east and

approximately 14 m above the sea level in the west, respectively. This coastal terrace spatially corresponds to the lowermost fluvial terrace inside the river valley.

The equivalent surfaces of the upper coastal terrace (MT3) are exposed again on both sides of the Kızılırmak River valley. Although the western coastal terrace forms an approximately 4-km-long and up to ~750-m-wide surface between İkiztepe and Göltepe on the western side and an elongated surface with variable width and a total length of approximately 4 km, the tread of the eastern terrace is degraded by the tributaries originating on the delta platform. The tread of this terrace forms the margin of the concave (west) and convex (east) portions of delta platform rims (Figure 2.5). The sediments at the sampling location associated with this terrace are massive, gray-yellowish, sandy-silty deposits that are at least 8 m thick at İkiztepe (IKZ1). About 150 m south of IKZ, the deposits are overlain by unconsolidated yellowish fine to medium sand (Figure 2.4e). On the eastern side of the valley, stacks of well-sorted, medium to coarse sand deposits (partly fine gravel) exhibit several decimeter-scale layers with distinct cross-stratification, interrupted by two V-shaped incised channels that contain medium-grained sorted gravel; these strata are exposed at a recently excavated outcrop close to Gerzeliler (Figure 2.4g). These deposits are eroded and covered by approximately 1-m-thick unsorted clay to coarse gravel layer. Samples for OSL geochronology (YAK) were taken from the sandbar deposits in the central part of the outcrop and ca. 1 m north of the gravel deposits (Figure 2.4g). Furthermore, four higher palaeo-delta terrace tread levels are exposed at approximately 58 m (T5), 82 m (T6), 95 m (T7), and 108 m (T8) on the eastern side of the Kızılırmak River. There is an even higher, yet very eroded, level located approximately 150 m above the present-day delta (Figure 2.5). The lower delta terrace forms the eastern valley slope from the town of Bafra northward, up to the northern margin of the palaeo-terraces. The intermediate palaeo-delta terrace forms an approximately 3-km-wide dissected strip to the southeast of Bafra, and the third delta terrace continues southward until it is deeply incised by a stream near Aktekke. The highest delta terrace extends from the area east of Aktekke southward to the Derbent Dam, mainly along the eastern valley slope (Figure 2.5).

Most of the sediments sampled for this study (SE1, SE2, IKZ1, IKZ2, AK1, and AK2) contain thick, well-sorted silty sand to sandy silt with partly increased clay contents and occasionally appearing calcrete; as such, they are inferred to be palaeo-

floodplain deposits with palaeosol development. In contrast, the other outcrops contain coarse-grained channel deposits at the bases and sandy to silty sandy flood plain deposits at the tops. KOL exhibits two of those sequences, while the covering floodplain sediments are removed at KIZ, as seen in outcrops relatively close to one another. The sediments at KIZ contain fewer pebbles inside the implied palaeo-channel deposits and feature higher matrix content as compared to the outcrops at KOL and HIR. Although the sampled sediment from the most of the channel deposits is rather loose, the sediment at SE3 is highly cemented, presumably due to its high carbonate content. Since the matrix of all channel sediments is sandy, we inferred confluence with the influx of coarse tributary sediments (pebbles to cobbles and occasionally even boulders) and sands to fine gravel from the main trunk until Hidirellez.

The YAK deposits consist of well-sorted sand with sediment structures indicating sandbars from a larger river that are subsequently incised by coarser-grained channel deposits. Both are subsequently eroded and covered by shortly transported sediments. We related the well-sorted sandy sediments at YAK to the main trunk that implies an absence of the recent blockage of the elevated terraces at the time of deposition, i.e., T5.

2.5 Results

2.5.1 OSL age determination

All of our sampling sites have low environmental radiation levels with a dose rate of ca. 0.5 Gy/ka; as a result, all of the samples were within the possible age range of OSL dating, since the growth curve is distant from saturation (Murray et al., 2008; Appendix Figure 2.1). The carbonate content of the material was generally low, with a maximum content of 18.18%, but it was high in samples IKZ2 and SE3, where it reached nearly 50%. Carbonate was absent from the sample taken from the YAK site. All of the samples provided reliable, stratigraphically meaningful ages, although a few of them yielded outliers (Table 2.1). We sampled detrital sediments with different grain sizes; incomplete bleaching may thus have influenced sediments with larger grain sizes. Furthermore, post-depositional reworking may have taken place while the uplift rates were potentially relatively low; this may have caused the river

to rework the sediments. Despite these limitations, our dates clearly document that all of the terraces were formed between the Middle and Late Pleistocene.

2.5.1.1 OSL ages of the strath terraces

Samples collected at the terrace at Kolay (KOL) yielded ages of 317.7 ± 31.6 ka, 338.1 ± 32 ka, and 355.3 ± 46.7 ka. These ages agree well with one another and result in a combined mean age of 334 ± 20 ka.

The ages of the terraces at Selemelik recorded deposition at 36.9 ± 2.4 ka, 32.0 ± 1.8 ka, and 43.2 ± 4.0 ka (SE1; TX); 402.9 ± 35.6 ka, 358.2 ± 26.6 ka, and 493.7 ± 39.1 ka (SE2; T7); and 449.8 ± 114.3 ka, 545.7 ± 79.3 ka, and 547.2 ± 39.1 ka (SE3; T3), respectively. The age determination for SE1 resulted in a pronounced spread, but the ages still fit well with one another; we thus used the mean age (36.4 ± 2.4 ka) of all three samples (Table 2.1) for our terrace age assignment. The ages of SE2 have a large spread. Here, we considered the oldest age to represent the primary depositional phase and interpreted the younger ages in the context of reworking. Due to accessibility constraints, material from SE3 was taken from the matrix-supported conglomerate; as a consequence, incomplete bleaching may have influenced the age of this sample and accounted for the two older ages. The youngest sample from SE3 has a significantly younger age with a large error, suggesting reworking. The mean age of the older samples is 547 ± 49 ka.

2.5.1.2 OSL ages of the fluvial fill terraces

Modern floodplain samples from the Kızılırmak River yielded ages between 14.4 ± 3.1 ka, 14.9 ± 2.3 ka, and 18.9 ± 6.4 ka. The third sample is considered an outlier due to its greater age and large error margin as compared to the other ages. The sediments of the dated strata were relatively coarse (gravelly). We therefore omitted the older sample from further age calculations. The corresponding mean age is 14.7 ± 1.8 ka (Table 2.1). The samples of the lower terrace (AK2; T1) were dated to 77.3 ± 5.6 ka, 71.2 ± 4.4 ka, and 59.3 ± 6.2 ka. The third age is significantly younger than the other two samples. However, the samples were taken at distances of ca. 2 m from each other within the same stratigraphic layer. Based on all three samples, the calculated mean age is 71.1 ± 3.0 ka. Nevertheless, since the two older samples are consistent, we used the mean age of these samples only; the corresponding age is 73.7 ± 3.5 ka (Table 2.1).

Tab. 2.1 : Results of the OSL signal measurements (in decreasing order by age), cosmic dose, measurements of the radioactive elements (U, Th, and K) and carbonate content used to determine the environmental dose. The OSL ages highlighted in gray are considered outliers and were not included in the mean-age calculations.

Location (Terrace)	Sample Name	Coordinates (Lat/Long)	Tread elevation	Terrace Type	Depth (below tread)	Dose (Gy)	Dose rate (Gy/ka)	Cosmic (Gy/ka)	Carbonate (%)	U (ppm)	Th (ppm)	K (%)	Measured Age (ka)	OSL Age (ka)
SE3 (T7/T3?)	SE3-1	N 41.451534	48 m	fluvial	5 m	127.05±29.06	0.28±0.03	0.14	45	0.5	1.3	0.06	449.8±114.3	547±49
	SE3-2	E 35.845594				154.14±14.55							545.7±79.3	
	SE3-3					154.56±5.34							547.2±63.3	
IKZ2 (T7/T6)	IKZ2-1	N 41.596401	104 m	marine	2.3 m	225.29±6.62	0.52±0.02	0.17	48.09	0.6	4	0.14	532.5±30.2	532±19
	IKZ2-2	E 35.852742				220.58±8.1							521.4±31.7	
	IKZ2-3					230.38±10.84							544.6±36.8	
SE2 (T7)	SE2-1	N 41.451713	100 m	fluvial	8 m	189.44±13.38	0.47±0.02	0.11	15.15	0.5	4.4	0.19	402.9±35.6	493.7±39.1
	SE2-2	E 35.837678				168.42±8.76							358.2±26.6	
	SE2-3					232.12±13.68							493.7±39.1	
YAK (T4/MT3)	YAK-1	N 41.566816	42 m	marine	14 m	143.18±13.66	0.37±0.03	0.07	0	0.6	2.7	0.07	387.9±49.1	460±36
	YAK-2	E 35.986484				166.17±13.64							450.2±52.6	
	YAK-3					172.74±11.9							468±50.5	
AK1 (T1)	AK1-1	N 41.524328	49 m	fluvial	6 m	258.84±17.13	0.55±0.03	0.13	17.57	0.5	4.3	0.11	472.8±38.9	448±27
	AK1-2	E 35.853393				229.22±17.17							418.7±40.5	
	AK1-3					238.86±10.64							436.3±33	
HIR (T8)	HIR-1	N 41.552224	118 m	fluvial	10 m	156.74±19.72	0.38±0.02	0.08	10.44	1.1	2.9	0.07	412.7±57.8	429±29
	HIR-2	E 35.830993				166.07±9.6							437.3±37	
	HIR-3					159.23±33.09							419.3±90.9	
IKZ1 (T2/MT3)	IKZ1-1	N 41.607016	42 m	marine	6.63 m	142.79±8.39	0.52±0.02	0.12	14.14	0.5	4.8	0.24	276.9±19.4	385±31
	IKZ1-2	E 35.867198				194.83±8.88							377.8±25	
	IKZ1-3					202.8±11.02							393.3±28.5	
KOL (T6)	KOL-1	N 41.398635	82 m	fluvial	2.6 m	142.7±11.83	0.45±0.02	0.18	10.9	0.5	3.6	0.11	317.7±31.6	334±20
	KOL-2	E 35.811923				151.4±11.66							338.1±32	
	KOL-3					158.86±18.96							355.3±46.7	
AK2 (T4)	AK2-1	N 41.517116	20 m	fluvial	2 m	46.81±2.11	0.61±0.03	0.18	18.18	0.5	3.9	0.15	77.3±5.6	73.7±3.5
	AK2-2	E 35.863641				43.08±1.07							71.2±4.4	
	AK2-3					36.82±3.29							59.3±6.2	
SE1 (TX)	SE1-1	N 41.453956	35 m	fluvial	2.3 m	25.72±0.99	0.7±0.04	0.17	0	0.5	4.9	0.17	36.9±2.4	36.4±2.4
	SE1-2	E 35.845699				22.33±0.48							32±1.8	
	SE1-3					30.1±2.29							43.2±4	
KIZ (T0)	KIZ-1	N 41.473631	7 m	fluvial	2 m	6.2±1.27	0.43±0.03	0.18	27.61	0.6	2.8	0.07	14.4±3.1	15.2±1.8
	KIZ-2	E 35.833854				6.45±0.89							14.9±2.3	
	KIZ-3					8.19±2.74							18.9±6.4	

The samples from the upper terrace at Aktekke (AK1) were taken at the exposed scarp of a landslide and provided ages of 472.8 ± 38.9 ka, 418.7 ± 40.5 ka, and 436.3 ± 33.0 ka. All three ages appear to be reliable, and a mean age of 448.0 ± 27.0 ka (Table 2.1) was calculated.

At Hıdırellez, we dated a sand lens that is intercalated within a matrix-supported conglomerate, indicating a rather short transport distance. The three samples yielded ages of 412.7 ± 57.8 ka, 437.3 ± 37.0 ka, and 419.3 ± 90.9 ka (HIR; T8). Although the error margin of the third sample is relatively large, the three ages are consistent with each other and result in a mean age of 429.0 ± 29.0 ka (Table 2.1).

OSL dating of samples from the coastal terrace at İkiztepe (IKZ1; MT3) resulted in ages between 276.9 ± 19.4 ka, 377.8 ± 25 ka, and 393.3 ± 28.5 ka. The dated material of the youngest sample was probably reworked, and we therefore excluded it from further age calculations. However, the older two ages are in good mutual agreement and provide a mean age of 385.0 ± 31.0 ka (Table 2.1). The delta terrace samples of IKZ2 (T7 overprinted by T6) yielded ages of 532.5 ± 30.2 ka, 521.4 ± 31.7 ka, and 544.6 ± 36.8 ka, and provide a consistent age range. We calculated a mean age of 532.0 ± 19.0 ka for this terrace (Table 2.1).

The Gerzeliler (YAK) samples yielded ages between 387.9 ± 49.1 ka, 450.2 ± 52.6 ka, and 468 ± 50.5 ka. The error ranges of all samples overlap. We therefore calculated a mean age of 460.0 ± 36.0 ka (Table 2.1).

2.6 Discussion

2.6.1 Tectonic versus climatic processes

Fluvial processes are strongly dependent on tectonic, climatic and lithologic characteristics of the underlying bedrock. These factors may force a complex response of the fluvial system and modulate aggradation and vertical incision along a river's course and ultimately result in strath and fill terraces or cut and fill terraces (e.g., Lavé and Avouac, 2001; Burbank and Anderson, 2011). Climatic factors might be very efficient forcing factors, especially with regards to the nature of runoff, slope and transport processes at different latitudes and elevations (e.g., Bull, 1991; Whipple and Tucker, 1999; Whipple et al., 1999; Blum and Törnqvist, 2000). Another impact of climatic influence on fluvial processes is determined by changing

the base level of large rivers that discharge into the oceans that are subjected to orbitally-controlled oscillations in water volume. In turn, climatically driven sea-level lowering may trigger flexural bedrock uplift as a response to water unloading. With respect to our study area Bartol and Govers (2009) calculated flexural bedrock uplift following a 1730 m drop in sea level during the Messinian Salinity Crisis (5.96-5.59 Ma); in addition, they predicted a maximum uplift of 200 m along the Black Sea coasts. Since the time frames of the sea-level falls affecting fluvial processes studied by us were much shorter (max. 20 ka) and sea-level fall amounted to a maximum of 120 m (e.g., Shmuratko, 2001; Badertscher et al., 2011), we neglect this effect in our models. Nevertheless, flights of several fluvial strath terrace and palaeo-delta levels in our study area result from long-term rock uplift that progressively elevated older straths and palaeo-delta levels to higher elevations (Maddy et al., 2001; Demir et al., 2004; Doğan, 2011; Yıldırım et al., 2011; Schildgen et al., 2012; Çiner et al., 2015).

Collectively, our results document the uplift of fluvial terraces and deltas; this constitutes unambiguous geomorphic manifestations that record lateral growth and uplift of the Pontide wedge, and thus the expansion of the northern margin of the Central Anatolian Plateau. In combination, fluvial terrace sequences, associated top-set layers of delta deposition, and co-genetic coastal terraces along the Black Sea clearly record the interplay between sea-level variations, sediment supply, and vertical crustal movements leading to the abandonment of river courses. In this context, the uplifted Kızılırmak Delta represents a first-order geomorphic feature associated with vertical tectonic motions in this region immediately to the north of the bend in the NAFZ since at least Middle Pleistocene time.

2.6.2 Timing and rate of long-term uplift

We used the elevations of the dated palaeo-delta levels and terraces as geomorphic markers to constrain uplift rates. Our geomorphic mapping and conceptual model show that the formation of each palaeo-delta level was associated with protracted sea level high- and lowstands during the Quaternary.

Overall, we identified ten terrace-formation episodes associated with sea-level changes since the Middle Pleistocene (MIS 14) (Figures 2.13 and 2.14). The first important stage of delta uplift and accompanying incision was dated to 547 ± 49 ka.

This mean age represents the deposition of a veneer of sediment on top of a strath terrace during the terminal phase of MIS 14; this sediment veneer is an older remnant that was overprinted by subsequent terrace formation processes (Figure 2.14a). However, the last depositional phase documented in this environment during the Late Pleistocene occurred during MIS 3 inside the Kızılırmak gorge; the mean age of this event is 36.4 ± 2.4 ka (Figures 2.6 and 2.13). The corresponding terrace surface is associated with floodplain sediments and was formed ca. 35 m above the present-day river level.

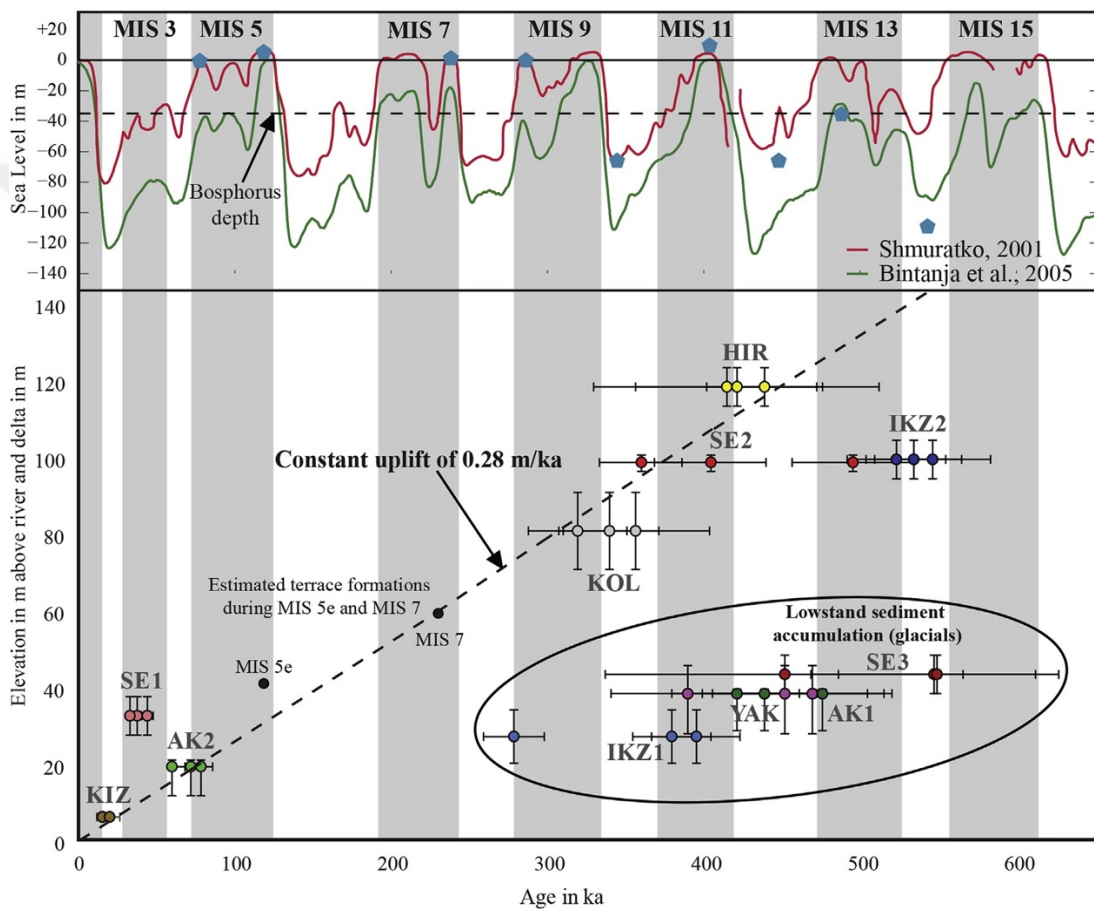


Figure 2.12 : Elevation/time plot of the OSL dating results. The inferred positions for terraces corresponding to MIS 5e and MIS 7 have been added to illustrate extrapolated terrace elevations; the lower delta platform at 58 m (T5) is assigned to MIS 7, and an extensive coastal terrace with a pronounced shoreline angle at an elevation of 42 m (MT3) is correlated with MIS 5e. The time ranges highlighted in gray correspond to odd numbers of MIS (Lisiecki and Raymo, 2005). The sea level curves emphasize differences between the reconstructions of past sea level oscillations in the Black Sea (red: Shmuratko, 2001; green: Bintanja et al., 2005; blue pentagons represent sea level estimations based on the constant uplift model).

Accordingly, we developed a conceptual model for the uplifted palaeo-delta levels based on the relative position of palaeo-sea level high- and lowstands with respect to

modern elevation of the palaeo-delta levels since MIS 13 (Figure 2.14). The palaeo-sea level estimations are based on the sea-level reconstructions by Shmuratko (2001), Bintanja et al. (2005), and Panin and Popescu (2007). Based on these reconstructions, eight out of ten delta levels should have been generated during sea level highstands. The other two delta levels at ca. 26 m and 48 m above the recent river level were generated during two lowstands of MIS 10 and MIS 12. These two terrace levels are at higher elevations now, as are the eight highstand terrace levels (Figures 2.12-2.14c and e). Such a scenario suggests that lowstand delta levels might have been exposed, provided that the uplift was greater than the elevation difference between palaeo- and subsequent sea levels. In our model, we estimated a quasi-constant uplift rate of ca. 0.28 ± 0.07 m/ka to build the overall morphology and stratigraphic sequence. The terrace levels therefore formed during glacials and interglacials; we therefore infer that tectonically controlled base level processes were the major driving forces while regional climate changes seem to have played a subordinate role.

Our uplift determination is based on a mean uplift rate starting with terrace T8, which was formed during MIS 11 (Figure 2.14). The age of terrace T6 inside the mountainous area to the south was determined to correspond to MIS 9. The OSL ages of this terrace result in a base level-independent mean uplift rate of 0.24 ± 0.03 m/ka since then. In case the terrace formation was base level-forced, the corresponding age of terrace abandonment would correspond to the end of the MIS 9 highstand at ca. 300 ka. This would imply an uplift rate of 0.27 m/ka, which corresponds well with the predictions of our uplift model. Therefore, the overall uplift rate is inferred to have been similar between MIS 11 and MIS 9.

Terrace level T1 yielded two OSL ages related to the end of MIS 5a and the beginning of MIS 3, respectively. The sea level highstand during MIS 5a existed at a position, which is comparable to the present-day level (Shmuratko, 2001). The derived uplift rates thus scatter between 0.24 and 0.38 m/ka. However, we found coastal terrace remnants corresponding to this level in the northeast and northwest of the delta terrace platform suggesting a base level-dependency and an uplift rate of 0.28m/ka since the time of abandonment.

All of these three terrace levels suggest an apparent base level-dependency. We did not date the lower major delta platform (T5), but determined the minimum

depositional age to 277 ± 19 ka and maximum depositional ages of the highest coastal terraces to 460 ± 36 ka and 385 ± 31 ka. Those ages thus suggest a maximum age of MIS 7 for T3 as well. Together, the ages of the younger and older terraces suggest similar tectonic uplift rates, which results in a MIS 7 age for T5 and a MIS 5e age for T3. Consequently, since MIS 7a or 7e (T5) average uplift rates of 0.25-0.31 m/ka dominated the coastal areas, while rates of ca. 0.29-0.33 m/ka can be assigned to the terraces that started to be abandoned after MIS 5e.

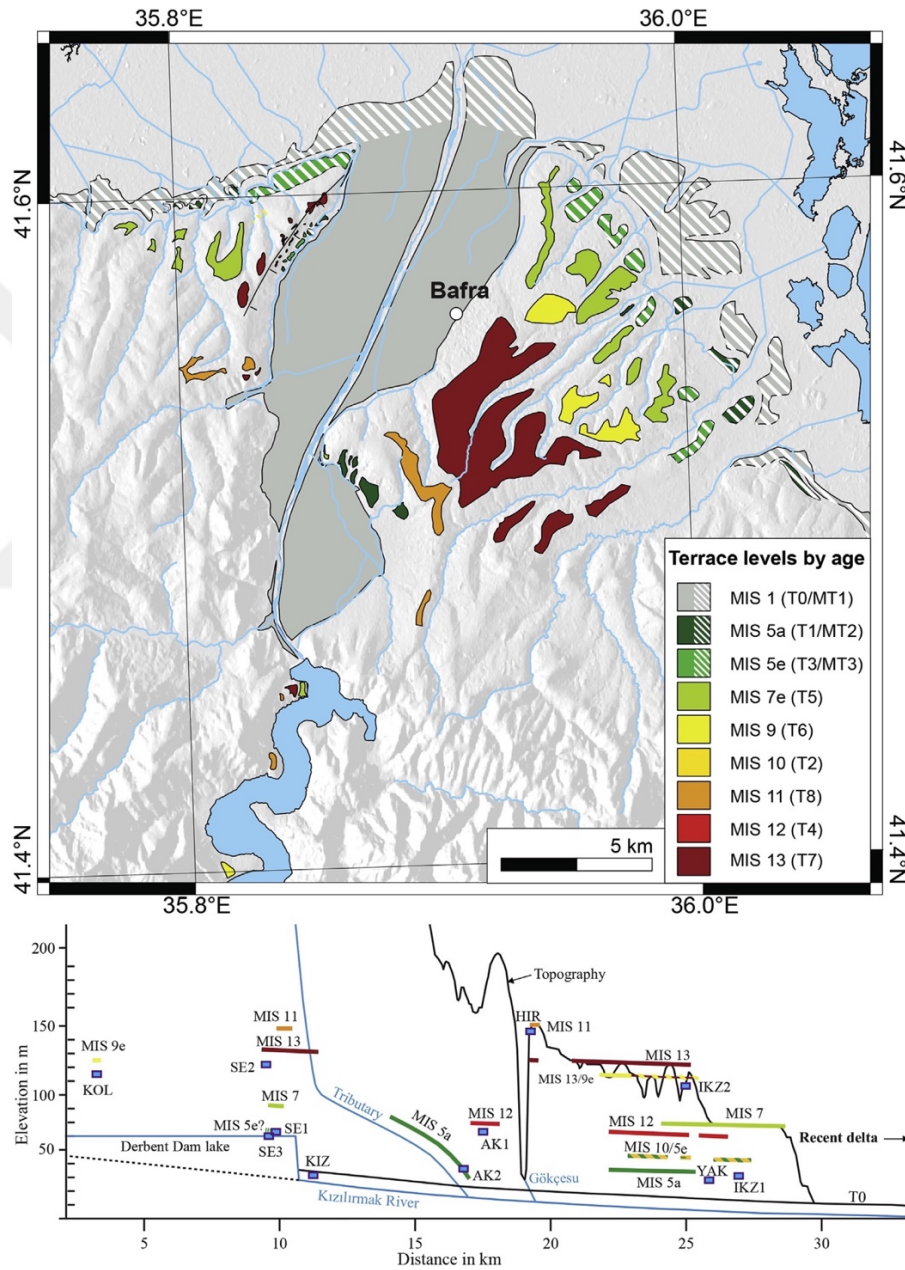


Figure 2.13 : (a) Spatial and vertical distribution of terrace flights and sampling sites along the lower reaches of the Kızılırmak River. Marine isotope stages and colors are correlated with the ages of terrace formation according to the uplift model; (b) Terrace flights with two MIS correlations document the timing of primary deposition and subsequent overprint by incision and renewed terrace formation.

Terrace T7 is older (MIS 13) than T8 (MIS 11); accordingly, the older terrace sediment appears to have constituted the substrate for T8 and thus significant erosion might have impacted T7. This implies that the original terrace tread could have been higher than at present and erosion is responsible for the large scattering of ages from this level until MIS 10. However, the ridge top elevation between İkiztepe and Hıdırellez at 100 m corresponds well with the terrace flights at Hıdırellez and Selemelik, suggesting a low impact of erosional degradation.

The dated sediment overlying the strath at Kolay results in a mean incision rate of 0.21 m/ka or ca. 0.27 m/ka since MIS 9, depending on whether the recent river is a bedrock river or alluvial river. In addition, the uplift model provides the opportunity to date indirectly the sequence of strath terrace levels at Selemelik as well. T8 and T5 exhibit as of yet undated bedrock-terrace sediment interfaces (straths) at this location - a strath elevation for T7 remains ambiguous (Figure 2.7). For the overlying sediments, our conceptual uplift model suggests a depositional age of MIS 11 and MIS 7, respectively. The sediment on top of the lowermost exposed strath (T3) at Selemelik (SE3) lies directly on basement rocks and was dated to MIS 14, which provides an overall minimum incision rate of ca. 0.06 m/ka since MIS 14, depending on whether the sub-recent river is a bedrock or alluvial river at this location. However, we interpret the date corresponding to the SE3 sediment sample in the context of an older terrace remnant that was overprinted by renewed terrace formation. Our conceptual uplift model indicates an ultimate strath formation during MIS 5e.

In line with studies by Vandenberghe (2008), we assume an end of incision, i.e., the timing of final strath formation, at the transitions between even and odd MIS. The strath terraces in the mountainous, southern part of the study area (Figures 2.6 and 2.7) thus record decreasing incision rates from 0.49 m/ka (MIS 11 to MIS 9) over 0.29 m/ka (MIS 9 to MIS 7) to 0.11 m/ka (MIS 7 to MIS 5e), followed by a possible increase to 0.25 m/ka until the present day. The discrepancy between incision and uplift rates might be a result of hydrological changes in the contributing drainage area. A distinct indication for lower incision rates compared to the regional rock uplift are knickpoints along the river course (Howard et al., 1994) and longitudinal river profiles that are significantly out-of-equilibrium. Both criteria agree well with the current characteristics of the Kızılırmak River (Yıldırım et al., 2011).

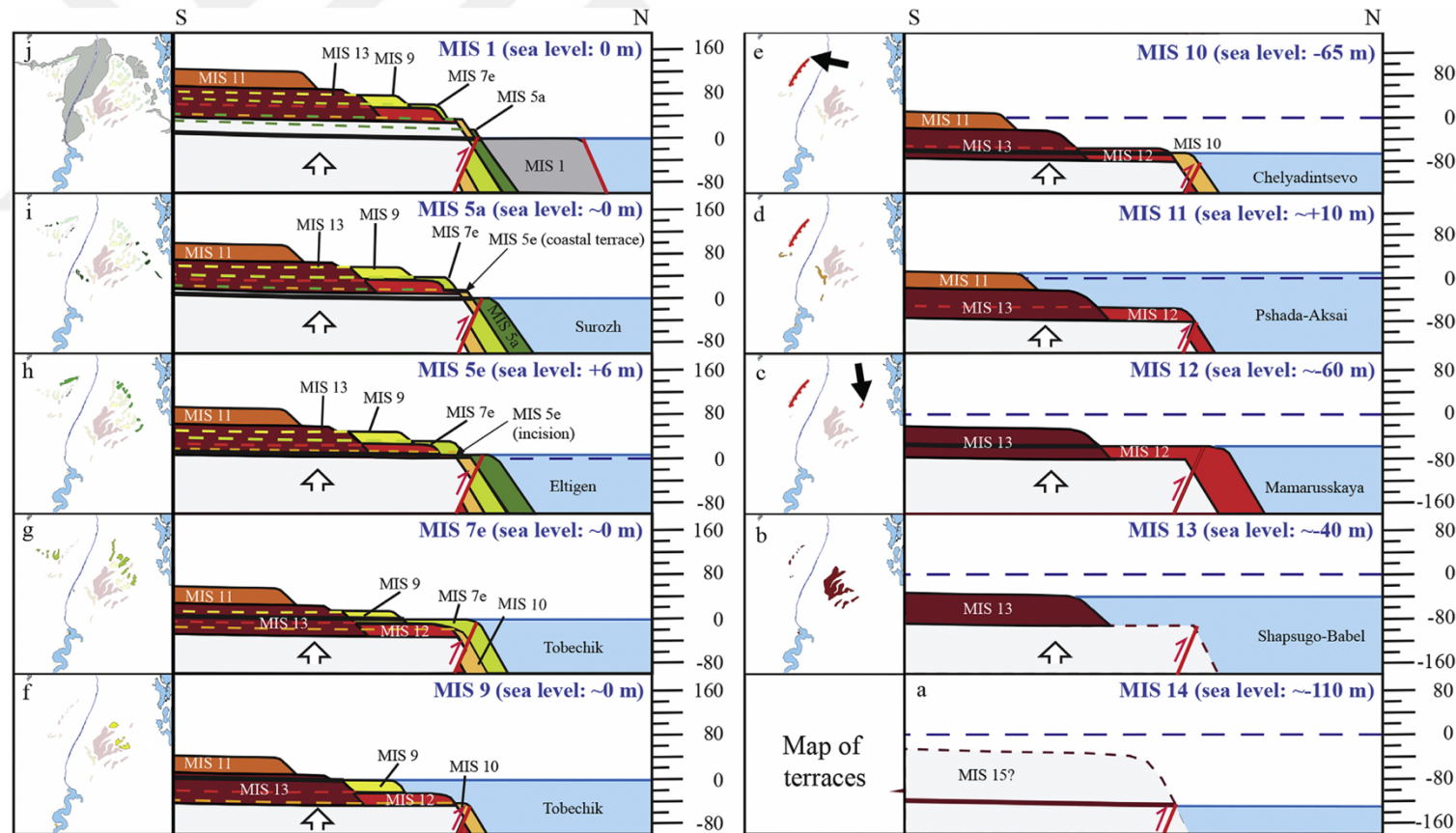


Figure 2.14 : Reconstruction of the delta terrace formation since MIS 14, with an accompanying map of the individual delta and terrace stages (a-j). Sea level stages in the Black Sea are taken from Zubakov and Borzenkova (1990); the position of the inferred reverse fault is shown according Robinson et al. (1996). Terrace formation occurs during low and high sea level stands; changes are displayed on a vertical scale. The upward-facing vertical arrow below the delta represents protracted regional uplift of the Pontide wedge. The black arrows on the maps to the left of the charts indicate small exposed terrace flights. The red lines (maps c-e) indicate prevailing active normal faulting.

Taken together, the cut-and-fill (north) and strath (south) terrace sequences agree well with the notion of a sustained constant uplift rate in relation to major sea level oscillations since MIS 11, but short-term variations since MIS 14 might have taken place as well. Especially the position of the youngest terrace levels (T1 and TX) suggests significantly higher uplift rates since MIS 3 and the Last Glacial Maximum. Interestingly, our rates are comparable with rates obtained from uplifted coastal terraces (Yıldırım et al., 2013b) and incised fluvial terraces along the central flank of the Central Pontides (Yıldırım et al., 2013a).

2.6.3 Implications for plateau margin deformation and lateral plateau growth

As the smallest Cenozoic orogenic plateau, the lateral growth of the northern margin of the Central Anatolian Plateau may provide insights about the evolution of larger plateau margins, especially in low strain settings. Our geomorphic mapping and dating efforts provide timing and rate of this growth process at the north-eastern flank of the northern margin of the Anatolian Plateau, but questions of what ultimately controls or supports this growth, still remain. In this context, the only active local onshore structure is the Bafra Fault. The kinematics of this fault is not well documented, but based on its NW-SE strike and its distinct morphologic expression it might correspond a transtensional structure that delimits the topographic boundary between delta levels in the north and rugged mountainous topography in the south. However, uplifted delta levels are also located on the hanging-wall block of this fault and with the exception of the İkiztepe terrace no deformation was observed within the delta levels.

Alternatively, offshore structures may drive the uplift of terraces in this region. The major offshore structure is the Sinop Trough, a graben delimited by NW-SE striking normal faults (Rangin et al., 2002). This trough is located immediately north of the Kızılırmak Delta and a normal fault delimits its southern sectors. Evidence for the existence of Quaternary activity along this structure is ambiguous, however, especially if flexural footwall uplift of a normal fault bounded basin is taken into account. In a normal-faulting scenario an asymmetric uplift pattern of terraces would be expected, with coeval higher terraces in the north and lower terraces in the south. We did not observe such spatial disparity in uplift patterns; the normal-fault bounded basin may thus represent a secondary structure of localized extension within the orogenic wedge, which appears to be inactive under the current tectonic stress field.

The North Anatolian Fault is a major structure that accommodates high strain along its strike, which may be responsible for contraction across the Pontides (Yıldırım et al., 2011). This contraction, however, is not equally distributed. For example, a recent study carried out in the valley of the Filyos River (western flank) at a distance of only 40 km from the NAFZ's main strand, McClain et al. (2018) reported an average local uplift rate of ca. 0.34 m/ka over the last 542 ka. At the western Sinop Peninsula (central flank), maximum uplift rates of 0.2-0.26 m/ka have been sustained since 570 ka (Yıldırım et al., 2013a). The analysis of uplifted river terraces in our study area revealed uplift rates of 0.28 m/ka. However, Keskin et al. (2011) showed that farther east in the Trabzon area, uplift rates calculated with an onset at MIS 11 decrease from 0.17 ± 0.03 m/ka to 0.07 ± 0.05 m/ka. This eastward regional decrease in uplift rates along the Black Sea coast may be explained by the distance from the NAFZ's main strand and a corresponding difference in strain accumulation along the coast. This phenomenon could thus be interpreted to be related to the change in shortening direction and amount that drive uplift and deformation in the restraining bend of the NAFZ. For example, the Trabzon region studied by Keskin et al. (2011) is rather far away from the sector constituting the restraining bend of the NAFZ (ca. 130 km). In contrast, our study area is much closer (<70 km) and is thus expected to be under a more pronounced influence of this feature. In turn, the uplifted terraces of the Sinop area (Yıldırım et al., 2013a) are 90-110 km away from the NAFZ. We therefore suggest that uplift rate and lateral growth of the Pontide wedge are closely coupled with the overall geometry of the NAFZ, and thus the lateral growth of the Central Anatolian Plateau; moreover, the uplift rate variability along the Black Sea coast appears to be determined by the distance to the restraining bend of the NAFZ (also see Yıldırım et al., 2013a,b).

2.7 Conclusions

We documented multiple sequences of uplifted Quaternary coastal, delta front, and fluvial terraces along the lower Kızılırmak River in the area of the northern flank of the Anatolian Plateau. We used detailed field observations, stratigraphy, remote sensing, and OSL dating to quantify our observations. Based on these studies, we derived a new terrace chronology that spans the ultimate 545 ka (MIS 14); this helps to constrain sea level changes in the Black Sea. Uplift has been relatively uniform

along the Kızılırmak valley in a N-S direction, with a sustained rate of 0.28 ± 0.07 m/ka. We explained the uplift of the Kızılırmak Delta and the corresponding fluvial terraces along the main stem within the context of the advancing Pontide orogenic wedge. Our study supports the notion that uplift rates along the southern Black Sea coast decrease eastward and diminish away from the Central Pontides, where pronounced shortening is parallel to regional GPS trajectories in the restraining bend area of the North Anatolian Fault Zone. Structurally, the uplifting sector along the Black Sea coast thus corresponds to the northward-growing Pontide orogenic wedge, a positive flower structure related to a restraining bend of the North Anatolian Fault Zone that constitutes part of the northern margin of the Anatolian Plateau.



3. HOLOCENE MARGINAL MARINE OSTRACOD SUCCESSIONS FROM THE KIZILIRMAK RIVER DELTA; IMPLICATIONS FOR DEPOSITIONAL ENVIRONMENTS AND SEA-LEVEL CHANGES AT THE SOUTHERN BLACK SEA COAST²

3.1 Introduction

The quantitative analysis of ostracod associations is an often used and powerful tool for reconstructing the development of a large variety of aquatic palaeoenvironments (e.g., Holmes, 1992; Smith and Horne, 2002; Frenzel and Boomer, 2005; Rossi, 2009; Boomer et al., 2010; Dabkowski et al., 2016; Kihn et al., 2017). It has been previously shown that, besides specific assemblage compositions characteristic for the prevailing habitat, some ostracod species respond to the physicochemical conditions of the ambient water such as salinity (Rosenfeld and Vesper, 1977; Boomer and Eisenhauer, 2002; Frenzel and Boomer, 2005; Fürstenberg et al., 2015), substrate (Zhai et al., 2010) and water chemistry (Ramos et al., 2015) by phenotypic variation. While the genotypic patterns may cause morphological variation in other species (e.g., Yin et al., 1999), the phenotypic variability of the brackish water species *Cyprideis torosa* (Jones, 1850) has been proven under both natural and laboratory conditions (e.g., Engel et al., 2012; Frenzel et al., 2016; Berndt et al., 2019).

Deltaic systems are located at the border between marine and terrestrial settings, where a river with high sediment load enters a water-filled basin, and their elevation is strictly controlled by the water level of the basin and the sediment load of the river (Posamentier and Morris, 2000). The ecology of a delta plain is dependent on the hydrological (sediment and water supply and marine currents) and climatic conditions (Reineck and Singh, 1980). Due to high sedimentation rates, delta systems

² This chapter is based on the paper “Berndt, C., et al., Holocene marginal marine ostracod successions from the Kızılırmak River delta; Implications for depositional environments and sea-level changes at the Southern Black Sea coast. *Sedimentary Geology*, 2019, 382: p. 103-121”

react rapidly to changing conditions and keep even pace with relatively fast sea-level changes (Posamentier and Morris, 2000).

Among others, paralic swamps and marshes associated with lakes and floodplain muds are common features of the subaerial delta and their deposits can be interpreted as delta topset deposits slightly at or above prevailing sea level (Reineck and Singh, 1980). These deposits and their microfauna can be used as good indicators for relative palaeo-sea levels (Brückner et al., 2010).

The Black Sea is a restricted brackish water basin that exchanges water with the world's oceans only via the Bosphorus (ca. 35 m sill depth) – Marmara Sea – Dardanelles (ca. 85 m water depth) seaway and formed, along with the Caspian Sea, the Ponto-Caspian meltwater trap during the Late Glacial period (e.g., Bahr et al., 2005; Eriş et al., 2007). The Black Sea has been decoupled from the world's oceans during glacial periods, but has been partially connected with the Caspian Sea, and became reconnected with the world's oceans during transitions to interglacial periods when global sea levels rose to the level of the Bosphorus sill (e.g., Shmuratko, 2001; Badertscher et al., 2011). Due to these changes and the periodic decoupling from the world's oceans as well as the Caspian Sea, the ecology of the Black Sea is globally unique and the rapid ecological changes taking place during reconnection were drastic, especially because of salinity differences along the fresh to mesohaline Caspian Sea – meso- to polyhaline Black Sea – normal marine to hyperhaline Mediterranean Sea corridor (e.g., Mudie et al., 2002; Yanko-Hombach, 2007).

While most research in the shallow marine Black Sea is concentrated on the western and northern basins, little is known about the ecological impact of hydrological reconnection and subsequent development of the eastern Turkish Black Sea coast. Its response to the rapidly changing environmental conditions during the Holocene is studied here on the basis of ostracod successions and their morphological responses, thus giving insights into the local sea level and context for the region's archaeological history.

3.2 Regional Setting

The Black Sea is the world's largest semi-enclosed, microtidal inland sea with an area of 423,000 km² and a maximum depth of 2212 m (Zaitsev and Mamaev, 1997).

The Kızılırmak Delta is located on the Black Sea coast of Turkey between Sinop and Samsun bays within the province of Samsun (Figure 3.1a). The wave-dominated delta plain comprises an area of 50,000 ha with wetlands covering 15,000 ha (Demirkalp et al., 2010). Of these, 11,000 ha are a Ramsar site as wetlands of international ecological importance. Those delta wetlands were added to the tentative list of UNESCO World Heritage Sites in 2016 (<http://whc.unesco.org/en/tentativelists/6125/>).

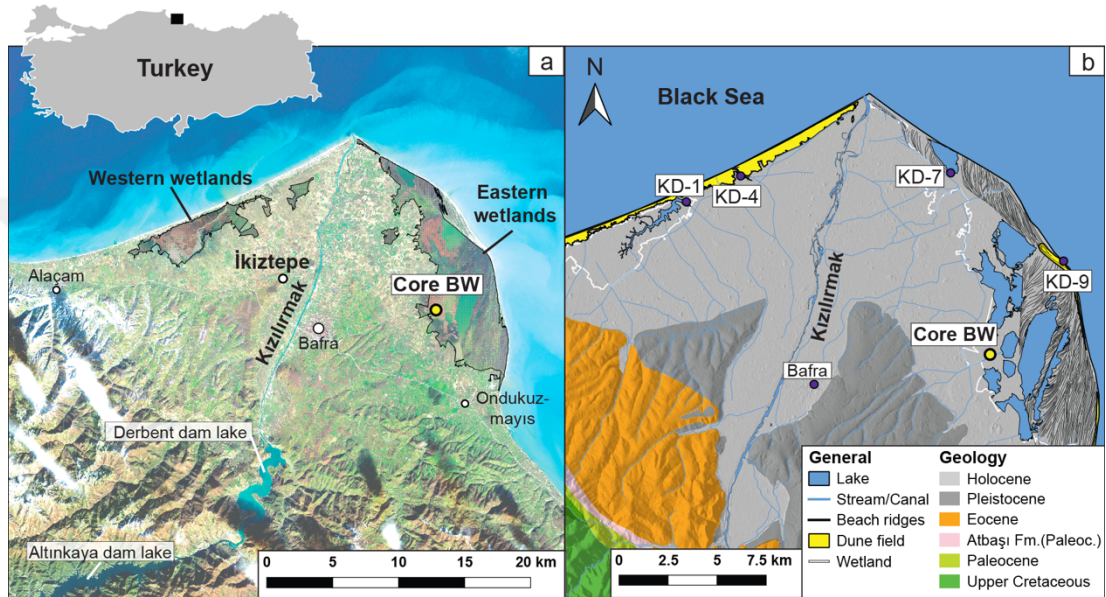


Figure 3.1 : (a) Overview of the Kızılırmak Delta and its location in Turkey; Area of the delta wetlands and the sediment core location (BW). (b) Geology, geomorphology and sampling sites. Holocene: Recent delta plain, Pleistocene: elevated riverine, deltaic and marine terraces of former delta plains, Eocene: volcanoclastics. Atbaşı Fm.: volcanics, Paleocene: volcanics, Upper Cretaceous: volcanics and carbonates. Recent samples: KD-1: Karaboğaz Lake, KD-4: Sahilkent estuary, KD-7: Liman Lake, KD-9: NE-delta beach.

The Kızılırmak River is the longest river in Turkey with a length of 1355 km, a discharge of 5.9 km³/yr (average flow: 185 m³/s) and a drainage area of 78,646 km² (Yılmaz, 2005). It flows across the Anatolian Plateau in a large bend, converges with the Devrez and Delice rivers, and crosses the North Anatolian Fault Zone (Ketin, 1948; Şengör, 1979; Şengör et al., 2005). The Kızılırmak River reaches the Black Sea after traversing the Central Pontide Mountains, where it converges with the Gökırmak River, and finally discharges into the southern central Black Sea.

Large parts of the former delta plains have been uplifted during the Quaternary (Akkan, 1970; Demir et al., 2004; Berndt et al., 2018) so the river channel drains

between the older delta terraces (Figure 3.1b). The recent Kızılırmak Delta forms an alluvial fan on top of Neogene (Pontian) marine sediments (Robinson et al., 1996; Tunoğlu, 2001) along the southern shoulder of the spreading Sinop Trough (Haşimoğlu et al., 2016) as the south-eastern extension of the Western Black Sea basin (Okay et al., 1991).

The local climate of the Kızılırmak Delta is dominated by the Black Sea and thus it shows a maritime climate of the temperate climate zone 'C1' to 'C2' (Şensoy et al., 2008; Köse et al., 2014). Air humidity is relatively high at >70% throughout most of the year (Arslan et al., 2007). Nevertheless, the climate of the delta plain is semi-arid to semi-humid and thus drier than the adjacent coastal regions of Sinop and Samsun, which are semi-humid to humid with relatively cool summers and mild winters (Şensoy et al., 2008; Köse et al., 2014). The region south of the delta plain is semi-arid (Şensoy et al., 2008).

3.2.1 Regional Black Sea oceanography

The regional Black Sea surface water temperatures range from 9°C in February to 23°C in September (Özsoy and Ünlüata, 1997). The tides of the Black Sea are small at 3–9 cm (Defant, 1961) so that seasonal variations of the wind pattern have a dominating influence with a difference of 19 cm between low (October/November) and high levels (May/June) (Alpar et al., 2000). The sea has a surface salinity of ca. 18‰ (Hay et al., 1991) that rises to 22.3‰ between 50 and 150 m water depth with an oxygenated zone above 60–200 m water depth (Murray et al., 1991; Oğuz et al., 1992; Purcell et al., 2001). The surface salinity is lower close to deltas due to freshwater run-off.

The strong cyclonic rim circulation of the Black Sea surface water currents with an eastward current along its southern margin dominates the coastal regions (Özsoy and Ünlüata, 1997), which splits into minor anticyclonic eddies due to the rapidly changing morphology at the Turkish Black Sea coast. Of those, the mushroom-like, but variably shaped, Kızılırmak eddy develops in front of the Kızılırmak Delta (Oğuz et al., 1992; Korotaev et al., 2003). The Kızılırmak eddy creates a nearshore, anticyclonic spiral-eddy chain that acts between the Sinop Peninsula, Kızılırmak and Yeşilirmak deltas (Karimova, 2011). These currents influence the shape of the Kızılırmak River delta and modify the deposition of the river sediments. This

western sea current with eastward transport creates a concave, erosive coastline in the western delta (Alpar, 2009). The sediment is deposited at the eastern delta plain producing a convex coastline and a large area of beach ridge formation (Alpar, 2009; Erginal and Öztürk, 2010).

3.2.2 Ecological conditions of the eastern delta plain

The recent wetland lakes of the Kızılırmak Delta plain are remnants of a large deltaic lake that extended southwards until the elevated delta terraces (Butler, 1907; Turoğlu, 2010). Landsat images depict a seasonal reconnection of the remnant lakes today. Studies on the recent ecology of the wetland lakes have concentrated mainly on zooplankton (Saygı et al., 2011; Can and Taş, 2012; Ustaoglu et al., 2012; Gündüz et al., 2013) and measured the ecological characteristics of the lakes (Demirkalp et al., 2004, 2006, 2010; Saygı et al., 2011; Ustaoglu et al., 2012) (Figure 3.2). According to these studies, the salinity of most of the lakes is changing from fresh to brackish conditions depending on precipitation. While Çernek Lake is mixo-mesohaline, the lakes to the south are mixo-oligohaline according to the classification of brackish waters (Remane and Schlieper, 1971).

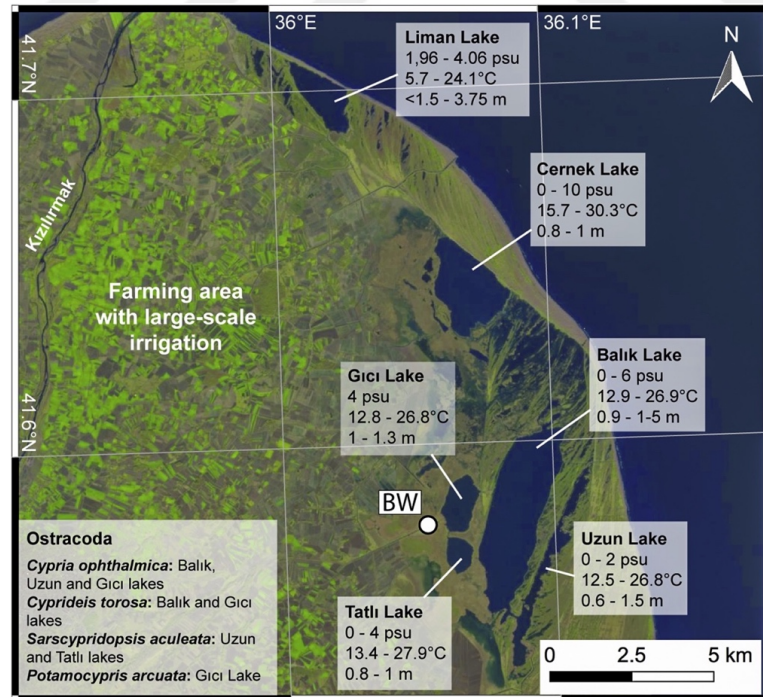


Figure 3.2 : Ecological conditions (salinity, temperature and water depth; pH for all lakes ca. 8.1 to 9–10) of the Recent delta lakes and the recent occurrence of ostracods (collected in 1995 and 1996; Ustaoglu et al., 2012). Satellite image by Sentinel-2 30.11.2017 [modified]. White dot indicates the location of the sediment core BW (this study).

All southern lakes are between 1.0 and 1.5 m deep and have a water temperature of ca. 12 to 27°C, and are all interconnected (Figure 3.2). The water temperature range is similar to the northern lakes (5.7–24.1°C; Ustaoglu et al., 2012). Çernek Lake reaches >30°C (Ustaoglu et al., 2012). The largest lake, Balık Lake with an area of 1300 ha, reaches up to 6‰ salinity (α -oligohaline). The other surrounding lakes change only from freshwater to β -oligohaline conditions (Figure 3.2). Only Liman Lake has a permanent connection to the sea and shows lower salinity fluctuations between 2 and 4‰, i.e., brackish with mixo-oligohaline conditions, with no continuous stratification and well-oxygenated water (Demirkalp et al., 2010).

3.3 Methodology

We obtained a 14.5 m-long sediment core (BW) at 41°34'40"N and 36°02'51"E at about 1 m above sea level, from the wetland ca. 10 km ENE of Bafra (Samsun) and ca. 800 m W of the Gıçı Lake using rotary drilling (diameter: 76 mm). The coring process comprised taking 4 m-long cored units to minimize the disturbance of the sediments. The drilling was carried out in October 2015 and the sediment core was preserved in plastic boxes. The original final depth of the drilling process was 32 m. The sediment core contains partly highly compressed sediments with a recovery of about 50%.

Subsamples (5 and 10 cm-long) were taken with gaps of 10 or 30 cm, and subsequently sieved with a mesh size stack of 125, 200 and 500 μ m. We took a total of 31 sediment samples between 1.3 and 14.5 m depth (depth reference points below surface level are represented by the centre of the sample; Table 3.1). The samples containing high amounts of adhesive material were dispersed in hydrogen peroxide and washed with tap water.

In addition, we sampled different recent environments across the deltaic plain including two restricted estuaries at the western part of the delta plain at Karaboğaz Lake (KD-1; 41°40'29.22"N, 35°48'44.80" E) and near Sahilkent (KD-3; 41°41'27.72"N, 35°51'18.95"E). On the eastern plain, we sampled Liman Lake (KD-7; 41°41'9.19"N, 36°1'12.40"E) and its northeast beach (KD-9; 41°38'18.37"N, 36°6'3.97"E) (Figure 3.1b, Table 3.1). All recent surface samples were taken at water depths of ca. 15 to 20 cm with a small shovel with an estimated sample size of at least 100 mL sediment volume.

Table 3.1 : Samples of sediment core BW with mean core depth in m and recent samples (KD).

Samples of sediment core BW with depth in m below surface level			
BW-1M	1.4	BW-8M	8.28
BW-2M	1.7	BW-9M	8.38
BW-2C	2.46	BW-9B	8.63
BW-2A	2.58	BW-9A	8.95
BW-2B	3.15	BW-9C	9.22
BW-3M	3.51	BW-10M	9.42
BW-3B	3.68	BW-10B	9.75
BW-3A	4.07	BW-10A	9.99
BW-4M	4.49	BW-10C	10.33
BW-4A	4.99	BW-11M	10.67
BW-5M	5.5	BW-11B	10.87
BW-5A	5.93	BW-11A	10.98
BW-6M	6.37	BW-11C	11.2
BW-6A	7.06	BW-12M	11.4
BW-7M	7.67	BW-12A	12.05
BW-7A	8.03	BW-12B	14.5
KD-1	Karaboğaz Lake	KD-7	Liman Lake
KD-4	Sahilkent estuary	KD-9	NE-Delta beach

All samples were dried at 60°C in an oven. The sediment volume of several samples was high, especially in the lower part of the core, so that the samples were split and picked in order to collect a minimum of 100 individual ostracod valves per sample.

Ostracods were identified with support of SEM images and reference to several publications regarding the ostracod fauna of the Black Sea or in Europe, mostly Schornikov (1972), Meisch (2000) and Dykan (2016). The ecological preferences for each species were taken from Frenzel et al. (2010), Bony et al. (2015) and Dykan (2016).

Diversity indices were determined and principal components analysis (PCA) was employed by using PAST (Hammer et al., 2001) while cluster analysis was employed using the *CONISS* method of the R-Package Rioja (Grimm, 1987; Juggins, 2012) based on relative abundances of species.

The sieve pore shape analysis (SPA) on valves of *Cyprideis torosa* was executed with the aid of a polarized microscope by counting round and non-round sieve pores, following the methodology successfully used in previous studies (e.g., Frenzel et al., 2011, 2016). For radiocarbon dating, we selected six cleaned, larger shells of *Cerastoderma edule* (Linnaeus, 1758) and three samples of peat from evenly

distributed intervals of the core. One wood piece was dated to validate the reservoir effect correction. The calibrations of all our samples were done by BETA Analytic Inc. using High Probability Density Range (HPD) method connected with Marine13 and IntCal13 (Reimer et al., 2013). We used the Venice System (Symposium on the Classification of Brackish Waters, 1958) for salinity classification.

In addition, the upper 12.3 m of the sediment core were continuously subsampled by using U-channels. The elemental content of the subsampled sediment was measured by using ITRAX X-ray fluorescence (XRF)-core scanner at Eastern Mediterranean Centre for Oceanography and Limnology of Istanbul Technical University (ITU-EMCOL) with 2.5 mm intervals. For a comparison of the elemental content with the ostracod samples, mean values of the sediment range related to the ostracod samples were calculated (Figure 3.3).

3.4 Results

3.4.1 Sediment core description

The whole sediment core profile shows a fine-bedded and laminated alternation of detrital sediments that are sedimentologically classified into four major units (Figure 3.3).

Unit A (14.5 to 8.23 m depth) shows a general fining-upward sequence from grey sand to darker grey, and slightly brownish sandy silt. The light grey lower unit (A-1) (14.5 to 11.4 m depth) contains high amounts of fine to coarse sand (mainly fine to medium sand). The darker grey unit above shows increasing contents of mud until 9.65 m. A 3-cm-thick greenish layer appears at 9.78 to 9.75 m depth. A 5 cm-thick black mud layer tops this part. Above this layer, another fining-up sequence continues with light grey fine sandy silt (few thin middle sandy layers) with occasional broken shells and few gravel grains that turn into dark greyish silt with decreasing sand content. The top of the unit is represented by a 10-cm thick black mud layer (8.23 to 8.33 m depth) with very high organic content (peat).

Unit B (8.23 to 3.75 m depth) follows-up discontinuously with medium dark grey sandy silt in its lower part. In this unit, the grey tones become generally darker with the darkest sediment between 6.5 and 5.7 m depth. The silty fine sand deposits of the unit are relatively continuous with slight changes in its fine to very fine sand content.

At 6.2 and 6.3 m depth are two shell break layers. The upper part until the top of this unit (3.75 m depth) turns into a roughly dm-scale alternation of very light, greenish grey and very dark, slightly violet, fine sandy silts. The layers contain shell break and whole shells of *Cerastoderma edule* (Linné) until 4 m depth. Another layer containing big shells appears 10–20 cm below the top of the unit (3.9 to 4 m depth).

In unit C (3.75 to 0.93 m depth) the mean grain size of the sediment decreases while the clay content remains high and the sand content almost disappears. A shell break layer appears at the basis of the unit. The colour is reddish-brown grey within the lower 40 cm and turns sharply into a light brownish medium grey. A sharp change to dark grey alternates with very dark to medium dark grey mud until the top of the unit. One lighter unit is visible between 2.1 and 2.5 m depth and contains five discontinuities. A thinner unit between 1.5 and 1.7 m depth contains black mud and large amount of plant remains. Dots and patches of iron oxide are observed regularly.

Within the lowermost 20 cm of the uppermost unit D (above 0.93 m depth) the dark grey mud turns alternatingly into unstructured medium greyish brown silty sand with a thin layer of dark mud (0.85 to 0.88 m depth) and a dark brown coarse sand layer between 0.78 and 0.75 m depth. Two discontinuities were observed at 0.26 and 0.72 m depth, respectively.

3.4.2 Elemental content

The content of several chemical elements in the sediment core BW was determined for the upper 12.3 m of the sediment column. In this study, we implement the contents of Ca, Sr/Ca and Fe/Ca as shown in Figure 3.3. While the Ca content is highly variable, the Fe content continuously increases causing a Ca/Fe ratio variation similar to this of Ca but at a relatively low level. The two peat layers at 9.65 to 9.6 m depth and 8.33 to 8.23 m depth correspond to very low Ca contents. Very high Ca peaks in unit B correspond with shell-rich layers and/or larger embedded shells. The Ca content shows three separated sections of very low values in unit C, which become more extensive towards the top of the unit. The Sr/Ca ratio is very low throughout unit A. The lower half of unit B is characterized by relatively stable intermediate Sr/Ca ratios ending in high values at around 6 m depth. Above, the variability of Sr/Ca increases continuously until only an alternation of very low and very high values remains throughout unit C.

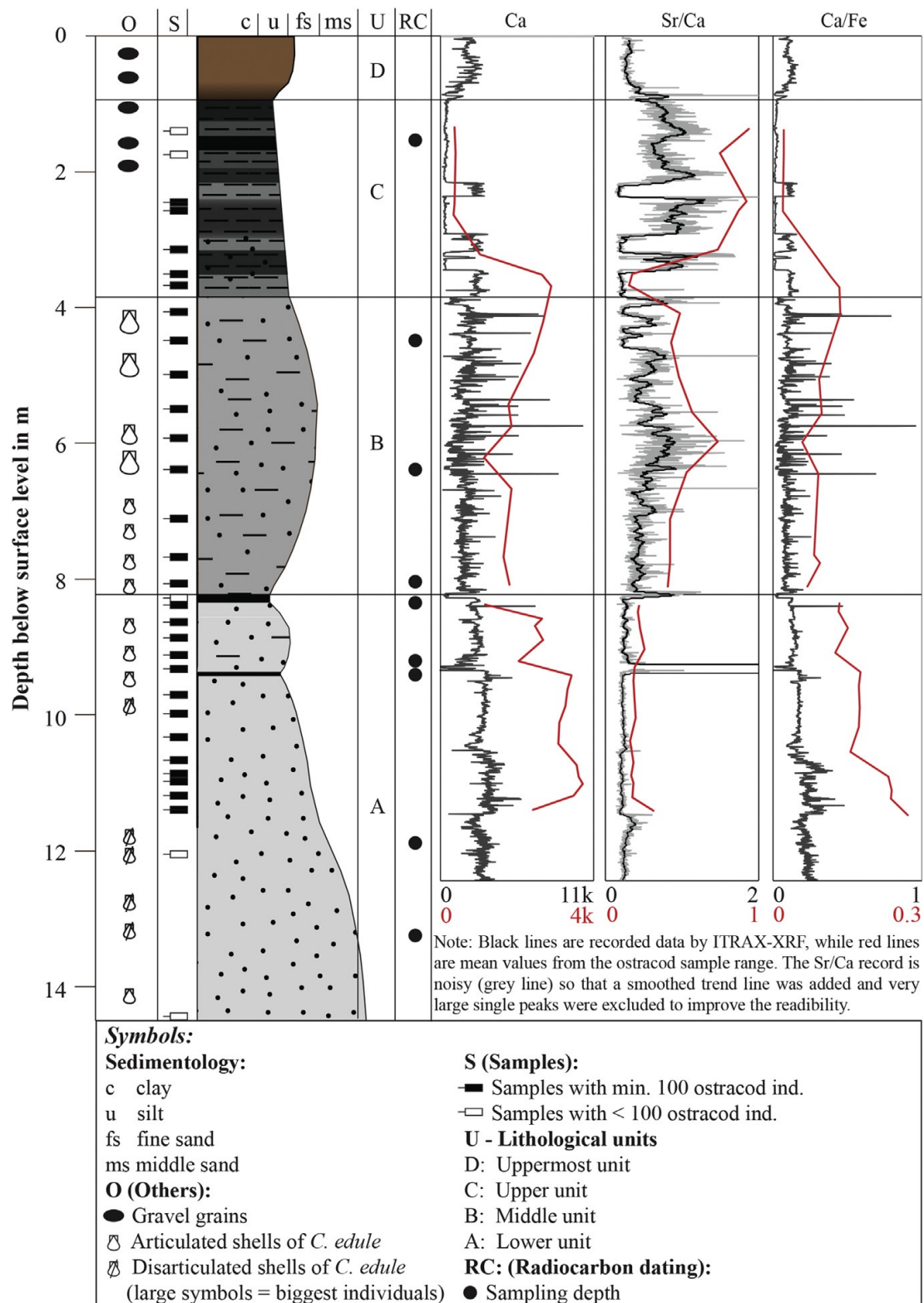


Figure 3.3 : Lithological profile with grain size classes, samples of the sediment core BW and marked radiocarbon samples and ITRAX-XRF measurements of Ca, Sr/Ca and Ca/Fe.

3.4.3 Radiocarbon dating

Six single valves of the bivalve *Cerastoderma edule*, two peat samples and a piece of wood were radiocarbon dated, including $\delta^{18}\text{O}$ and $\delta^{13}\text{C}$ values, from nine locations of the sediment core (Table 3.2, Figure 3.4). The two samples RC-2 (wood piece, taken directly from the sediment core) with a conventional age of 6820 ± 30 yrs BP and RC-2A (shell of *C. edule*) with a conventional age of 7210 ± 30 yrs BP were taken from 24 cm vertical distance to each other for determining the local reservoir effect. With reference to the depth-age curve (Figure 3.4) an age difference, i.e., reservoir effect, of 417 yrs can be estimated. This is very similar to the surface water marine reservoir effect of 415 ± 90 ^{14}C yrs BP in the Black Sea (Siani et al., 2000; Reimer et al., 2013). We therefore applied a reservoir effect of 415 yrs to all dated aquatic samples and calibrated the resulting conventional ages. Accordingly, the two lowermost dated samples of shells yield overlapping ages of 7800 ± 155 yrs cal BP and 7880 ± 145 yrs cal BP and a shell from the top of the middle unit was dated to 4085 ± 220 yrs cal BP. The only dated sample from the upper unit gave an exceeding ^{14}C content indicating a sub-recent age (after 1950s) with some probability that the plant material was formed since the 18th century.

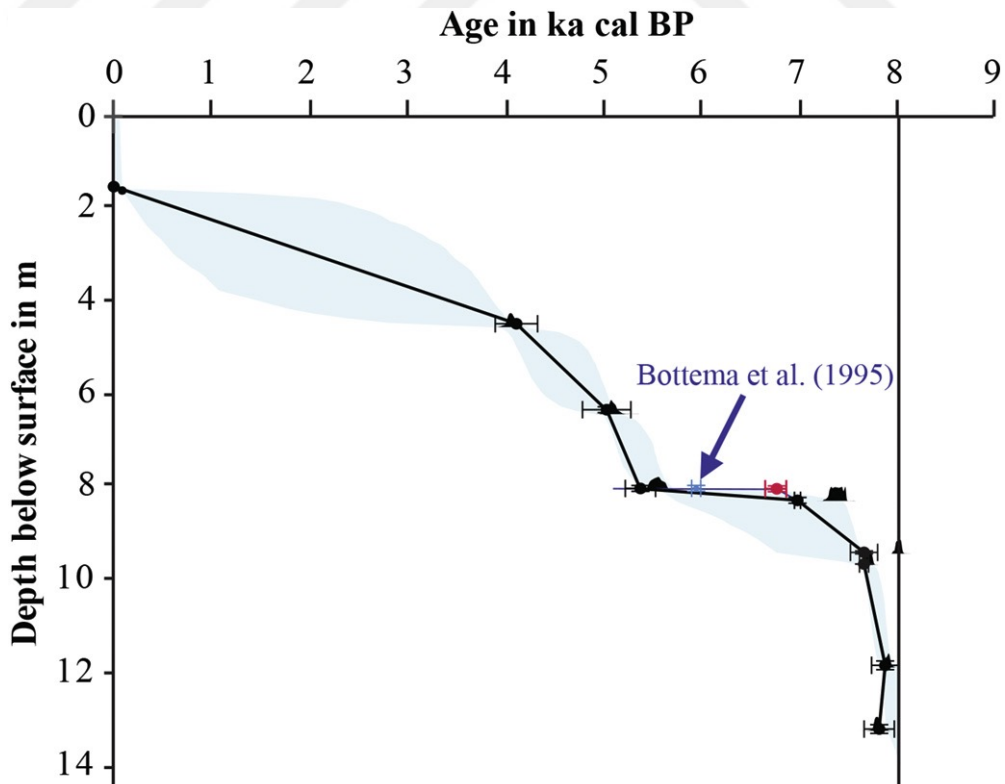


Figure 3.4 : Calibrated radiocarbon ages according to the depth with added conventional (blue) and calibrated (red) date of Bottema et al. (1995).

Table 3.2 : Radiocarbon dating results (Beta Analytics, USA).

Sample	Sample origin	Lab. code [BETA-]	Depth [m]	Material	Age [cal BP]	Age (conv.) [BP]	d ¹⁸ O [‰]	d ¹³ C [‰]
RC-8	Core	436513	1.54	peat	sub-recent (max. 18 th century)	112.1 ± 0.03 pMC	n. d.	-26
RC-5	BW-4M	436511	4.49	shell	4085 ± 220	4090 ± 30	-2	-0.2
RC-4	BW-6M	436510	6.37	shell	5035 ± 245	4770 ± 30	-1	-1.4
BW-7A	BW-7A	465361	8.03	shell	5353 ± 156	5080 ± 40	-2.6	-2.6
RC-3	BW-8M	436509	8.28	peat	6975 ± 30	6110 ± 30	n. d.	-28.4
RC-2A	BW-10	436514	9.42	shell	7648 ± 143	7210 ± 30	-3.2	-0.4
RC-2	Core	436508	9.66	wood	7650 ± 40	6820 ± 30	n. d.	-26.5
RC-1	Core	436507	11.88	shell	7880 ± 145	7470 ± 30	-2.4	0
RC-0	Core	436506	13.25	shell	7800 ± 155	7380 ± 40	-4.5	1.5

3.4.4 Ostracoda

The 27 ostracod-bearing core samples contain 35 species belonging to 18 genera. Five of these species were found in the sample of the recent Liman Lake as well. Table 3.3 shows a taxonomic list of all ostracod taxa encountered. A representative panel of the most important ostracods in this study is shown in Figure 3.5. Out of these species, *Cyprideis torosa*, *Candona neglecta* (mostly juveniles), *Pseudocandona? marchica* (mostly juveniles), *Heterocypris salina*, *Amnicythere longa* and *Amnicythere quinquetuberculata* are the most abundant and dominate the faunal assemblages.

3.4.4.1 Ostracods from the samples of the recent delta plain

Only one sample (KD-7) from Liman Lake contained some valves of ostracods. While all other recent samples were sand-rich, the substrate of KD-7 was composed of mud. This sample contained valves of *P. marchica*, *Candona* sp., *I. bradyi*, *H. salina* and *C. torosa* with only a few individuals, and therefore has no statistical significance.

3.4.4.2 Faunal associations of the sediment core

The ostracod associations along the sediment core BW change rapidly upwards as shown in Figure 3.6. The lower unit contains two different parts. The lower part until 9.71 m depth is characterized by changes between nearly monospecific *C. torosa*-dominated faunas with minor constituents of *L. rhomboidea* and *Candona* sp. and more diverse samples. The more diverse samples contain either higher contents of *Amnicythere* spp. (i.e., *A. longa* and *A. quinquetuberculata*) or high contents of

Candona sp., *H. salina* and *Pseudocandona* sp. accompanied by other limnic species (Figure 3.6).

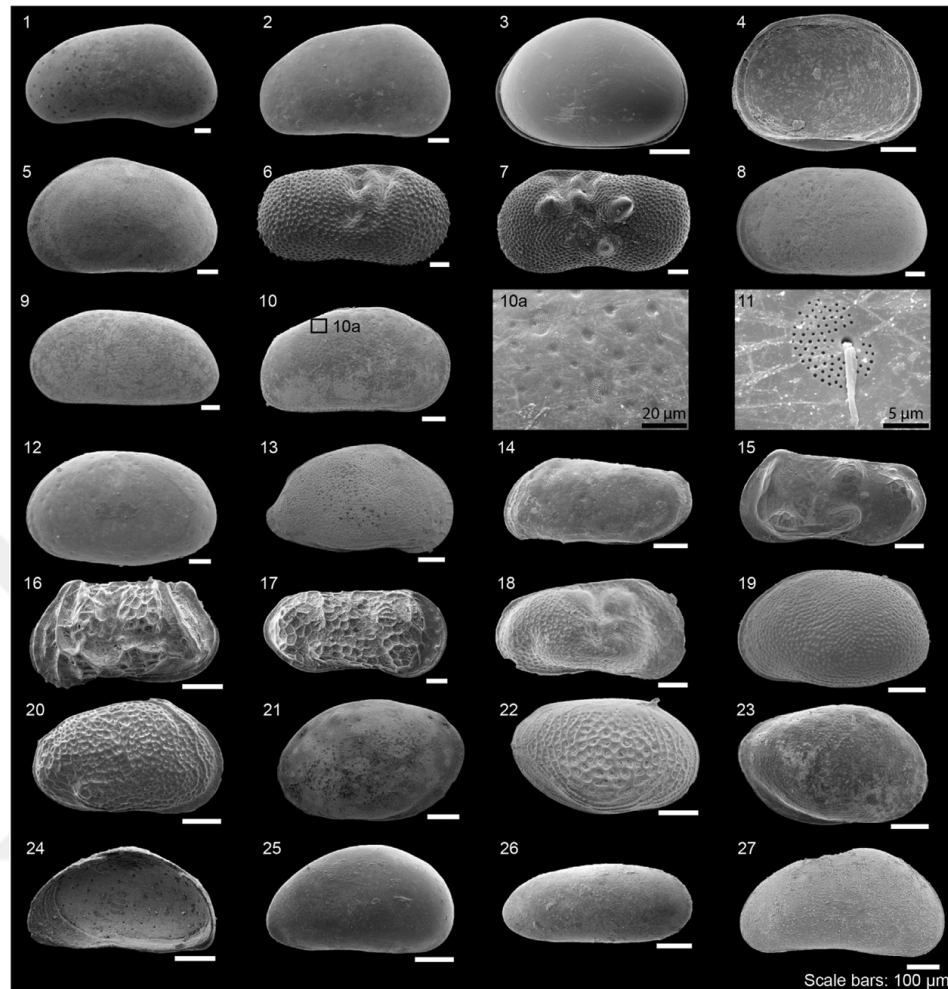


Figure 3.5 : (Scale bars: 100 µm) (1) *Candona neglecta* Sars, 1887, male LV, exterior. (2) *Pseudocandona marchica* (Hartwig, 1899), adult LV, exterior. (3) *Cyclocypris ovum* (Jurine, 1820), adult carapace from left. (4) *Physocypris kraepelini* G. W. Müller, 1903, adult LV, interior. (5) *Heterocypris salina* (Brady, 1868), adult LV, exterior. (6) *Ilyocypris bradyi* Sars, 1890, adult RV, exterior. (7) *Ilyocypris gibba* (Ramdohr, 1808), adult LV, exterior. (8) *Cyprideis torosa* (Jones, 1850), female LV, exterior. (9) *C. torosa*, male LV, exterior. (10) *C. ?torosa*, instar A-1, RV, exterior. (10a) ornamentation. (11) *C. torosa*, adult RV, sieve pore. (12) *Cyprideis pontica* Krstic, 1968, female LV, exterior. (13) *Tyrrhenocythere amnicola* (Sars, 1888), adult RV, exterior. (14) *Amnicythere longa* (Negadaev, 1955), adult LV, exterior. (15) *Amnicythere quinquetuberculata* (Schweyer, 1949), adult LV, exterior. (16) *Euxinocythere bacuana* (Livental, 1929), adult LV, exterior. (17) *Euxinocythere crebra* (Suzin, 1959), adult RV, exterior. (18) *Limnocythere inopinata* (Baird, 1843), juvenile RV, exterior. (19) *Metacypris cordata* Brady and Robertson, 1870, adult LV, exterior. (20) *Cytheromorpha fuscata* (Brady, 1869), female RV, exterior. (21) *Loxoconcha bulgarica* Caraion, 1960, adult LV, exterior. (22) *Loxoconcha gibboides* Livental, 1949, adult RV, exterior. (23) *Loxoconcha rhomboidea* Fischer, 1855, adult RV, exterior. (24) *Xestoleberis aurantia* (Baird, 1838), adult RV, interior. (25) *Xestoleberis cornelii* Caraion, 1963, adult LV, exterior; (26) *Darwinula* sp., juvenile LV, exterior. (27) gen. et sp. inc., exterior.

Table 3.3 : Ostracod taxa of sediment core BW. The systematic follows Brandão et al. (2018).

Suborder Cypridocopina Jones, 1901	Genus <i>Tyrrhenocythere</i> Ruggieri, 1955
Superfamily Cypridoidea Baird, 1845	<i>T. amnicola</i> (Sars, 1888)
Family Candonidae Kaufmann, 1900	Family Leptocytheridae Hanai, 1957
Genus <i>Candona</i> Baird, 1845	Genus <i>Amnicythere</i> Devoto, 1965
<i>C. neglecta</i> Sars, 1887	<i>A. longa</i> (Negadaev, 1955)
Subfamily Candoninae Kaufmann, 1900	<i>A. quinquetuberculata</i> (Schweyer, 1949)
Genus <i>Pseudocandona</i> Kaufmann, 1900	Genus <i>Euxinocythere</i> Stancheva, 1968
<i>P. marchica</i> (Hartwig, 1899)	<i>E. bacuana</i> (Livental, 1929)
Subfamily Cyclocypridinae Kaufmann, 1900	<i>E. crebra</i> (Suzin, 1959)
Genus <i>Cyclocypris</i> Brady and Norman, 1889	Family Limnocytheridae Klie, 1938
<i>C. ovum</i> (Jurine, 1820)	Genus <i>Limnocythere</i> Brady, 1867
Genus <i>Physocypris</i> Vávra, 1897	<i>L. inopinata</i> Baird, 1843
<i>P. kraepelini</i> G. W. Müller, 1903	Subfamily Timiriaseviinae
	Mandelstam, 1960
Family Cyprididae Baird, 1845	Genus <i>Metacypris</i> Brady and
	Robertson, 1870
Genus <i>Cypria</i> Sinroth, 1910	<i>M. cordata</i> Brady and Robertson, 1870
<i>C. ?candonaeformis</i> (Schweyer, 1949)	Family Loxoconchidae Sars, 1925
Genus <i>Heterocypris</i> Claus, 1893	Genus <i>Cytheromorpha</i> Hirschmann, 1909
<i>H. salina</i> (Brady, 1868)	<i>C. fuscata</i> (Brady, 1869)
Genus <i>Ilyocypris</i> Brady and Norman, 1889	Genus <i>Loxoconcha</i> Sars, 1866
<i>I. bradyi</i> Sars, 1890	<i>L. bulgarica</i> Caraion, 1960
<i>I. gibba</i> (Ramdohr, 1808)	<i>L. gibboides</i> Livental, 1949
Subfamily Cypridopsinae Kaufmann, 1900	<i>L. rhomboidea</i> (Fischer, 1855)
Genus <i>Potamocypris</i> Brady, 1870	Family Paradoxostomatidae Brady and
	Norman, 1889
<i>P. fallax</i> Fox, 1967	Genus <i>Paradoxostoma</i> Fischer, 1855
<i>P. pallida</i> Alm, 1914	<i>P. guttatum</i> Schornikov, 1965
Genus <i>Sarscypridopsis</i> McKenzie, 1977	Family Xestoleberididae Sars, 1866
<i>S. aculeata</i> (Costa, 1847)	Genus <i>Xestoleberis</i> Sars, 1866
Suborder Cytherocopina Baird, 1850	<i>X. aurantia</i> (Baird, 1838)
Superfamily Cytheroidea Baird, 1850	<i>X. cornelii</i> Caraion, 1963
Family Cytherideidae Sars, 1925	<i>X. decipiens</i> G. W. Müller, 1894
Genus <i>Cyprideis</i> (Jones, 1857)	Suborder Darwinulacopina Brandao, 2010
<i>C. acervumis</i> Dykan, 2016	Superfamily Darwinuloidea Brady and
	Norman, 1889
<i>C. pontica</i> Krstic, 1968	Family Darwinulidae Brady and
	Robertson, 1885
<i>C. torosa</i> (Jones, 1850)	Genus <i>Darwinula</i> Brady and
	Robertson, 1885
Family Hemicytheridae Puri, 1953	<i>Darwinula</i> sp.

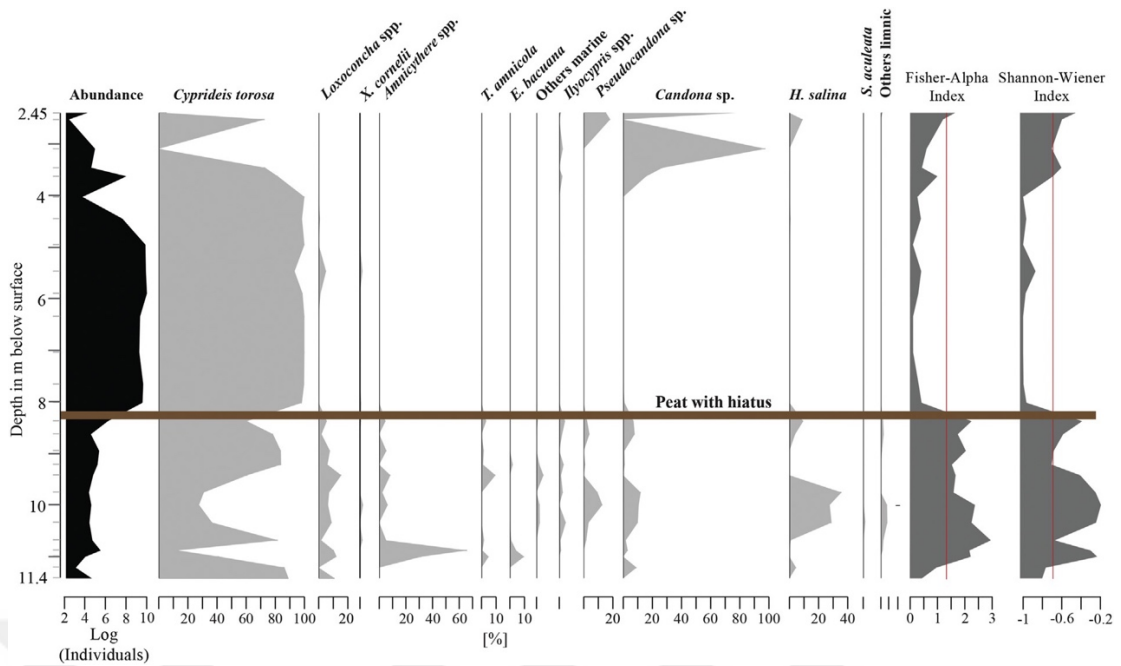


Figure 3.6 : Abundance (valves/100 g), principal ostracod-associations and diversity of Ostracoda along the sediment core. Red lines indicate the overall mean and grey bars the major peat level between 8.23 and 8.33 m below surface.

The transition to the upper part is sharp with a dominance of *C. torosa* along with the highest values of *Loxoconcha* (here: *L. rhomboidea*). *C. torosa* increases in relative abundance after the transition and *Loxoconcha* spp. (predominantly *L. gibboides*) remain as primary minor constituents (Figure 3.6). Subsequently, *C. torosa* is replaced gradually by *H. salina* and *Candona* sp. In addition, *Pseudocandona* sp. and *Ilyocypris* spp. appear in the highest samples of the lower unit along with the marine species *T. amnicola* and *Amnicythere* spp. (Figure 3.6).

The middle unit from 8.03 to 4.07 m depth is largely dominated by *C. torosa* with only scarce appearances of other species (*X. cornelii* and *L. bulgarica*) (Figure 3.6).

The upper unit starts with two transitional samples at 3.68 m and 3.51 m depth with a marked increase in *Candona* sp. that leads to a monospecific assemblage at 3.15 m depth. The low abundance assemblage changes to a dominance of *C. torosa* at 2.58 m depth accompanied by minor constituents of *H. salina* and *Pseudocandona* sp. The topmost ostracod-bearing sample (2.45 m depth) is dominated by *Candona* sp. accompanied by some *Pseudocandona* sp. (Figure 3.6).

Throughout the sediment core, the preservation of specimens is generally good with traces of dissolution in parts of the lower unit and some broken valves observed in the lower part of the middle and upper units. Sample BW-6M (6.37 m depth, middle

unit) shows a clear dominance of adult and instar A-1 specimens while all other samples show a dominant number of juvenile individuals. We did not sample the unit above 0.93 m depth because of soil formation and anthropogenic reworking.

3.4.4.3 Abundances and diversity

The abundance of ostracods in the lower unit is relatively low with ca. 100 valves/mL sediment, while the samples from ca. 8.03 m to 4.07 m depth (middle unit) show high abundances (11,591 to 22,545 valves/100 mL sediment). The ostracod-bearing samples of the upper part of the profile (above 4.07 m depth) show variable abundances (Figure 3.6). Ostracods are too low in number in two samples for statistical applications, and are absent in three other samples.

The Fischer's alpha diversity increases significantly within the lower unit from 0.42 to 2.95 in the lower part and decreases with relatively large variations to 1.6 until the top of the unit. The samples of the middle unit are mostly monospecific and highly fluctuating in diversity in the upper unit (Figure 3.6).

3.4.4.4 Cluster analysis

For the purpose of sub-zonation of the sediment core according to the environmental changes indicated by ostracod associations, a constrained cluster analysis was executed. Eight clusters were identified that correspond well to the lithological units A–C (Figure 3.7). The lower unit contains the clusters 1 to 3 and the middle unit coincides with cluster 4. Clusters 3 and 5 appear as transitional clusters between the main units. We classify cluster 3 as part of the lower unit because of the low abundance and appearance of lower diversity of ostracods, and cluster 5 as part of the upper unit based on the first appearance of *Candona* sp. in significant numbers and lower total abundances. The uppermost three clusters (6–8) contain only one sample each due to significant differences in ostracod contents.

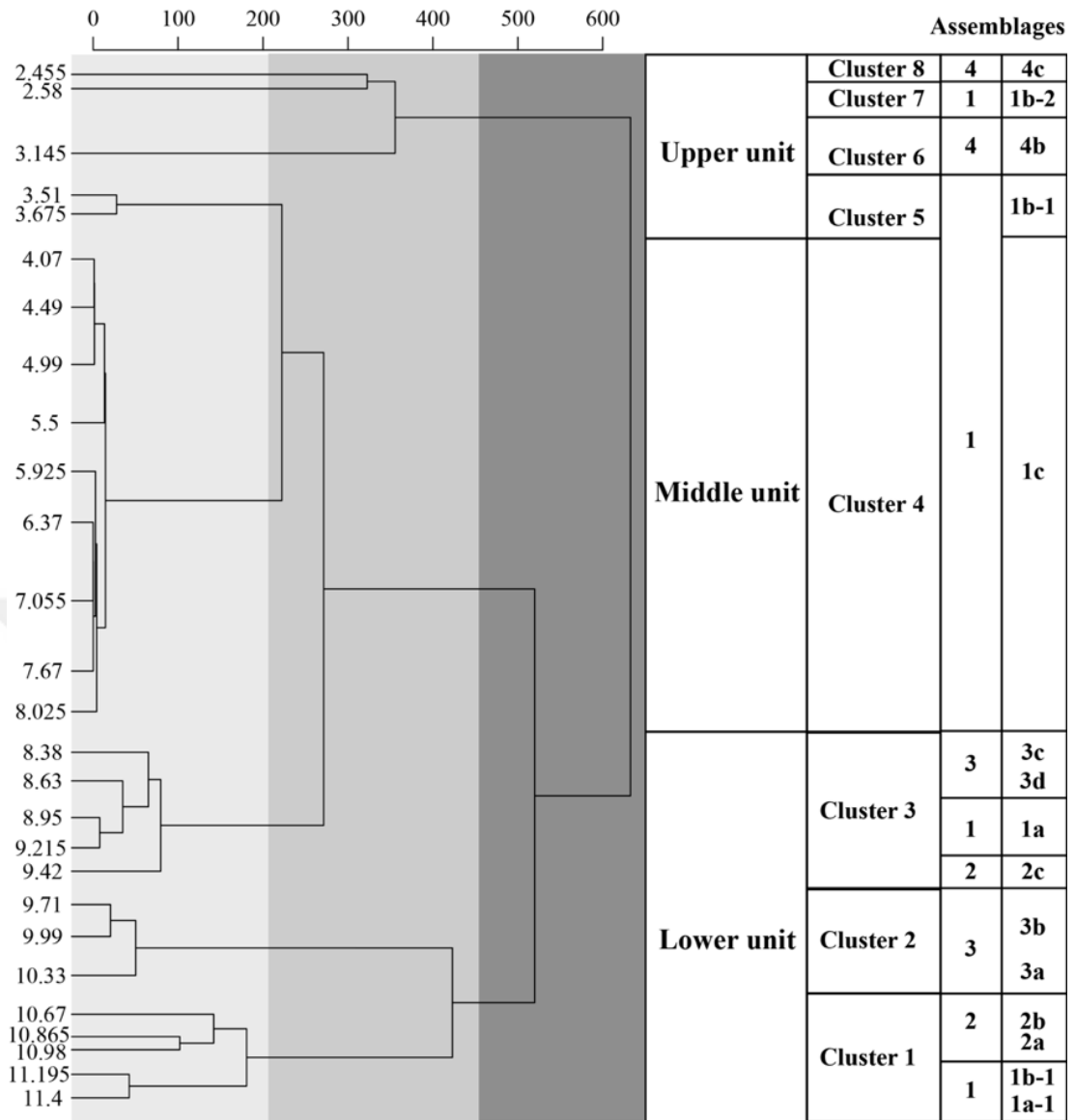


Figure 3.7 : Cluster analysis (Method: *Coniss*) with ostracod units, cluster, assemblage and sub-assemblage classification.

3.4.4.5 Principal component analysis and assemblages

For the principal component analysis, we used the percentages of the taxa. At first, we excluded the highly correlating (>0.90 and <-0.90) taxa. *Amnicythere longa* correlates highly with *E. bacuana*. Furthermore, *E. relictata* and *X. cf. decipiens* were removed due to the high correlation with *C. candonaeformis* and *M. cordata*.

Two significant principal components impacting the environments have been identified (Figure 3.8). The first component (PC 1) explains 74% of the variance. The scores of this component correlate strongly positive with *C. torosa* (and the ecological group of opportunists) with ca. 98%, and negatively with *Candona* sp. (Figure 3.8c). The lower unit shows a varying impact of this component. Several

samples of the lower unit correlate with the scores of PC 1 in a positive way and the samples in between are strongly negatively correlated. The negative loading decreases throughout the lower unit from -48 to -7 (Figure 3.9). All samples of the middle unit are strongly positively correlated to the scores of this component, but turn strongly negative at the transition to the upper unit, and those scores vary significantly between the upper three samples (Figure 3.9).

The second component (PC 2) is an environmental parameter that is represented mainly by *Candona* sp. juv., but also *H. salina* (Figure 3.9). This component explains 16% of the variance and its scores alternate between decreasing negative impact and no significant influence in the lower unit. It has a consistently small positive impact on the samples of the middle unit and largely mirrors the impact of PC 1 beginning with the transition to the upper unit (Figure 3.9). The scores of this component negatively correlate by 77% to the marine ecological species group.

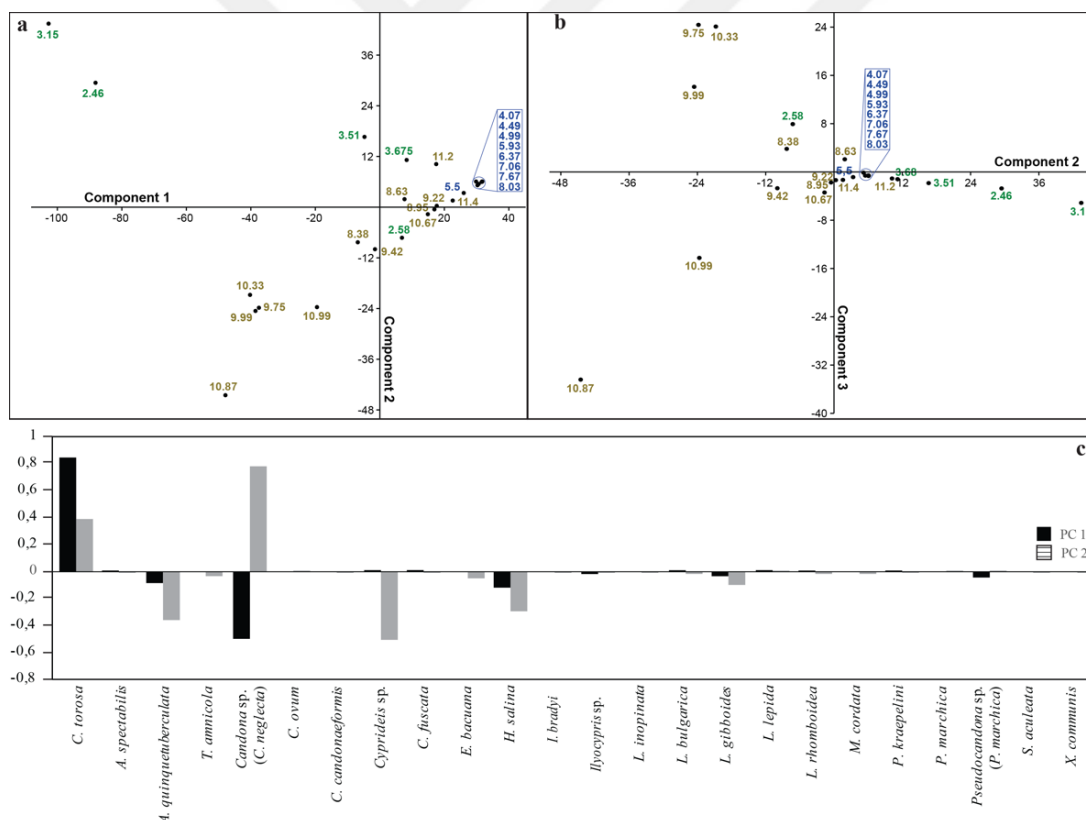


Figure 3.8 : Principal components that account for 90% of the variance [%] (PC 1: 74%, PC 2: 16%) representing main influencing factors (components). Sample names are given by their depth and colours refer to the units (brown: lower unit, blue: middle unit and green: upper unit). (a) Components 1 and 2, (b) Components 2 and 3.

Table 3.4 : Categorization of the four main assemblage types and their sub-assemblages.

Sub-assemblages	Associated taxa
1a	<i>C. torosa</i> dominating; <i>Loxoconcha</i> spp., <i>Amnicythere</i> spp. and <i>T. amnicola</i> (partly only <i>L. rhomboidea</i> as minor constituent)
1b	<i>C. torosa</i> dominating; abundant <i>Candona</i> sp. juv., <i>Pseudocandona</i> sp. and <i>H. salina</i> (plus <i>I. ?bradyi</i> and other rare low salinity species) with variable amounts
1c	Nearly monospecific and high abundance of <i>C. torosa</i> ; rarely <i>X. cornelii</i> and <i>Loxoconcha</i> spp. (mainly <i>L. bulgarica</i>)
2a	Equal ratio between <i>C. torosa</i> and the total of all other taxa; relatively high content of <i>E. bacuana</i> , <i>Loxoconcha</i> spp. and <i>T. amnicola</i> ; ratio between <i>A. quinquetuberculata</i> and <i>A. longa</i> is 1:2
2b	Dominance of <i>Amnicythere</i> spp. and high relative abundance of <i>L. gibboides</i> ; ratio between <i>A. quinquetuberculata</i> and <i>A. longa</i> is about 1:3; limnic species are rare (<i>Candona</i> sp., <i>Ilyocypris</i> sp. and <i>M. cordata</i>)
2c	High proportion of <i>L. rhomboidea</i> , <i>T. amnicola</i> and <i>C. fuscata</i>
3a	<i>H. salina</i> and lower but relatively high amounts of <i>Candona</i> sp. and low amount of <i>Pseudocandona</i> sp. with small content of <i>Amnicythere</i> spp. and <i>Loxoconcha</i> spp.
3b	Like assemblage 3a, but with an equal amount of and <i>Pseudocandona</i> sp. with <i>Candona</i> sp.
3c	Like assemblage 3a, but higher (>60%) amount of <i>C. torosa</i>
3d	Like assemblage 3c, but a low amount of marine species
4a	Only <i>Candona</i> sp. (<i>C. torosa</i> is absent)
4b	Strongly dominated by <i>Candona</i> sp., lower content of <i>Pseudocandona</i> sp. and a low amount of <i>C. torosa</i>

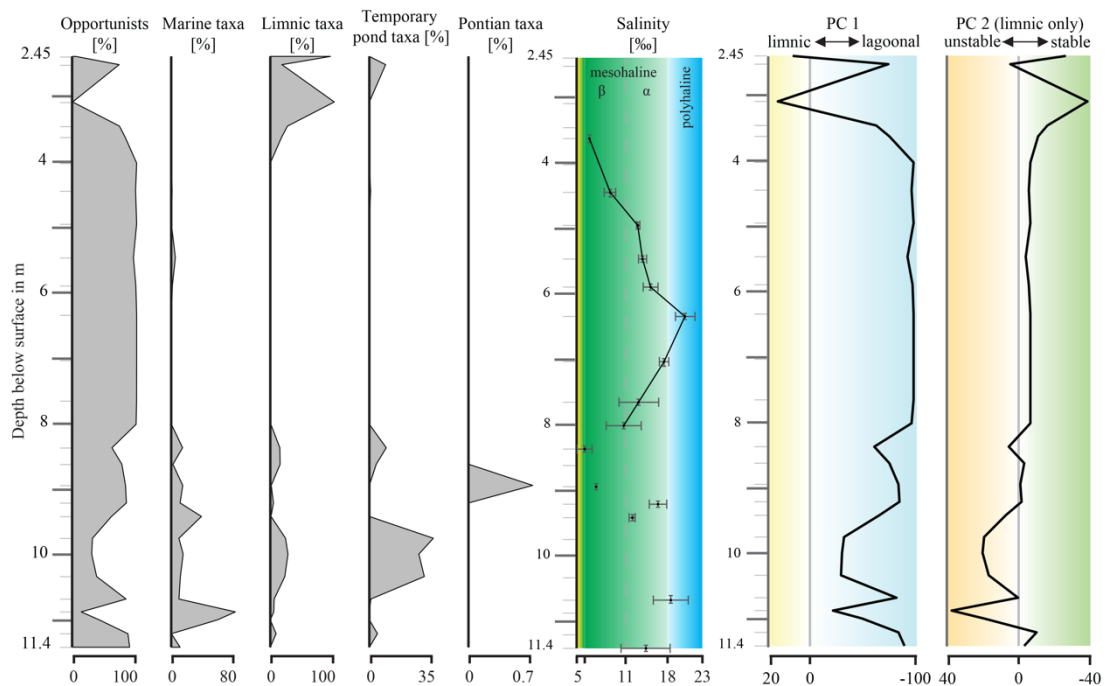


Figure 3.9 : Distribution of the ecological groups, salinity (based on sieve pore-analysis) and principal components along the sediment core. Thin scale lines indicate sample depths.

The sediment core contains four main ostracod assemblages, which indicate distinctly different environments with short and long-term changes (Table 3.4). The assemblages of the sediment core are distinct and can be explained by the combination of the two formerly named environmental factors by 85% in total. In addition, 15 sub-assemblages were identified within the eight clusters based on dominant and primary minor constituents (cf., Figures 3.7–3.9, Table 3.4).

3.4.5 Morphological analysis

Due to the ubiquity of the holeuryhaline species *C. torosa* throughout most of the section, we applied sieve pore analysis to reconstruct palaeo-salinity. The salinity was reconstructed by using the revised transfer function of Frenzel et al. (2016) based on usually at least ten adult valves so that the reconstructed salinity displays the mean value for the sample. The complete profile shows predominant mesohaline conditions (5 to 18‰) but varies significantly within its range and approaches the threshold to oligohaline (ca. 6‰) and polyhaline (ca. 20‰) conditions (Figure 3.9). Not enough adult and well-preserved specimens were recovered for the sieve pore analysis in most samples of the lower unit, and only five samples contained a useful number of specimens. The valves of which a definite assignment was not possible were excluded. Most of the shells are smooth and nodding appears only very rarely.

Salinity is well constrained along the middle unit until the base of the upper unit (Figure 3.9). The base of the middle unit (BW-7A) shows a salinity of $11.7 \pm 2.5\text{‰}$ that increases constantly to $20.5 \pm 1.4\text{‰}$ in BW-6M. In the next higher sample, the salinity is slightly lower with $15.6 \pm 1.1\text{‰}$ and the reconstructed salinity decreases continuously to $6.9 \pm 1.1\text{‰}$ at the basis of the upper unit (BW-3B).

3.5 Discussion

3.5.1 Environmental control on the ostracod assemblages and sediment chemistry

Most of the assemblages are dominated by *C. torosa*, which is a brackish water species and mostly found in shallow marine and lagoonal settings, although it can survive in a wide range from freshwater to hyperhaline environments (Vesper, 1972; Almogi-Labin et al., 1992; Handl et al., 1999; Meisch, 2000; Berndt et al., 2019). The dominance of this species varies negatively with the occurrence of limnic and

marine specialists (Figure 3.9) reflecting marginal marine conditions with a varying degree of confinement.

The first assemblage is characterized by a high amount of *C. torosa* indicating a shallow brackish water habitat (e.g., Frenzel et al., 2010). High abundances of this species are often associated with stressed and very shallow lagoon environments at shallow water depths (3–5 m) (Gofman, 1966). This assemblage is highly correlative with PC 1 and thus is considered as the dominating factor. The minor constituents are mostly marine taxa (especially *Loxoconcha* spp. and *Amnicythere* spp.) indicating a connection to the open sea. A predominance of limnic species (i.e., *Candona* sp.) and species indicative of confined stressed, low-salinity environments like *H. salina* (Smith and Horne, 2002) indicate closed lagoons or coastal lakes (Meisch, 2000), which are largely influenced by freshwater influx (Figure 3.9). The appearance of only one regularly associated species indicates environment instability so that no other species succeeded under the prevailing conditions. The positive correlation of PC 1 with both (open marine and limnic) environment types points to stress by strong salinity variation and temporary oxygen deficiency under restricted conditions (Figure 3.8). The component correlates inversely strongest with Assemblage 1b (Table 3.4) indicating the ecological instability of the lagoon (cf., Figures 3.8, 3.9).

The second principal component correlates well with the appearance of the limnic species *Candona* sp. and thus assemblages 3 and 4; partly also with *C. torosa* (opportunist) with positive loadings. It correlates negatively with the endemic shallow marine, but delta-related (oligo- to β -mesohaline) species *A. quinquetuberculata* (Opreanu, 2008; Chekhovskaya et al., 2014; Dykan, 2016) and the coastal marine species *L. gibboides* (Dykan, 2016) of assemblage 2 (Figures 3.8, 3.9). Additionally, it also shows negative loadings for *H. salina* as an indicator for a restricted or possibly even temporary lake. Specimens of *Candona* and *Pseudocandona* are identifiable in most cases only at a genus level due to a problematic assignment of juvenile specimens. However, it is very likely that these specimens are mostly or completely juveniles of *C. neglecta* and *P. marchica* of which adults were rarely found. These species occur often concurrently within the core and their ecological preferences (lower oxygenated, fresh to mesohaline coastal pond) largely overlap (Meisch, 2000; Frenzel et al., 2010). *A. quinquetuberculata* is related to sandy substrates (Opreanu, 2008), which means a relatively high current

activity due to a proximity and/or wave actions close to the river mouth. Based on the inverse relationship, we interpret decreasing salinity to be represented by component 2. The lower section is reflecting restricted, relatively small water bodies (pond/lake). Larger freshwater bodies promote the dominance of *C. neglecta* in the upper unit.

All reconstructed salinities range between oligo- and polyhaline while the Black Sea surface salinity is reconstructed to about 13–15‰ from 8 to 6 ka cal BP with a subsequent increase to about 17–19‰ between 6 and 4 ka cal BP after which it remained relatively stable until today (Mertens et al., 2012). Salinity values for the lower unit of the sediment core are reconstructed only at certain points, but show the same range as the middle unit with well-constrained salinity development until the upper unit. Near-polyhaline conditions are reached between 7.9 and 7.7 ka cal BP indicating slightly hyperhaline conditions shortly after a river-dominated phase with significantly lower salinity. At this time, the lagoon environment had a salinity similar to the open sea shortly after onset of the lagoonal phase. This indicates a relatively open environment that is supported by the dominance of *Loxococoncha* spp. The salinity falls to oligohaline values until 7 ka cal BP indicating delta progradation with increasing freshwater influx. Low lagoonal salinities with larger errors are found in the lowermost part of the middle unit implying a variable but significant freshwater influence during salinization of the Black Sea. The Black Sea salinization seems to have impacted the lagoonal environment with a steady increase in salinity until 5 ka cal BP although the lagoon reached even slightly hyperhaline conditions due to its restriction from the open sea and a negative water balance under a more arid climate. Subsequently, salinity fell due to increasing freshwater impact following a continuously proceeding separation from the sea, accompanied by higher impacts of riverine and meteoric water impact leading to oligohaline conditions like in today's delta lakes.

The content of calcium (Ca) the ratios Sr/Ca and Ca/Fe, are commonly applied to give insight into the extent of biogenic carbonate sedimentation and the detrital influx (Ca and Ca/Fe) as well as an authigenic carbonate precipitation (Sr/Ca) (Rothwell and Croudace, 2015). There is a high Ca content nearly throughout the sediment core indicating a high influence of sea water and authigenic carbonate production. Only the upper unit shows very low values alternating with two short

peaks of higher Ca values, indicating a lack of marine influence except in two short periods. The Ca content of the lower unit is slightly higher than the one of the middle unit that might be related to lower Ca-bearing detrital influx. The low Ca/Fe ratios throughout the sediment core indicate a strong detrital input. However, the co-variability of Ca/Fe with Ca means that the detrital and detritus input is rather constant, while the influx of seawater seems to be the primary factor. An overall increasing Fe content is likely caused by changes in the source of the detritus, which might be climate-related. The Sr/Ca ratio is very low in the lower unit. This could be caused by a lower temperature and salinity, reducing authigenic carbonate precipitation in the lower unit. In the central part of the middle unit, high values of Sr/Ca are recorded which seems to be caused by higher degrees of confinement leading to increased evaporation. Subsequently, the variability of Sr/Ca increasing in frequency and amplitude indicates an alternately higher temporal freshwater impact due to separation from the sea influence and increasing evaporation rates due to progressive hydrological isolation.

The major environmental control on sediment core BW is the restriction from the open sea with its strong currents and thus the mixing between freshwater (fluvial, meteoric and groundwater) and brackish seawaters. The influence of both water types is often concurrent and changes with the level of confinement of environmental and climatic conditions. The prevailing salinity is mainly reconstructed by sieve pore analysis, and oligohaline conditions can be confirmed by the appearance of the freshwater species *P. marchica* (Meisch, 2000) and a dominance of limnic species, i.e., in the lower and upper units.

We dated shells of *C. edule* and peat levels in our study. Datings of paralic peats are often-used sea level indicators (e.g., Brückner et al., 2010). Peat levels since ca. 6 ka cal BP are located close to recent sea level position and older levels cover a range of tens of meters but do not reach the present level thus reflecting a transgressive trend (compare Figure 7 of Brückner et al., 2010).

Kwiecien et al. (2008) showed that the Mid- to Late Holocene reservoir effects of Black Sea surface waters have remained about 400 ^{14}C yrs since ~ 8300 ^{14}C yrs BP. This time range covers the total time range of our studied core section and re-samples our reservoir effect estimate of about 415 ^{14}C yr. The $\delta^{13}\text{C}$ of *C. edule* is in a typical range for a marine organism with carbonate shell (Bradley, 2015). The $\delta^{18}\text{O}$

ratio in a marine environment is negative correlated to temperature changes, but also highly dependent on a changing precipitation-evaporation ratio and salinity (Hoefs, 2009). The increasing ratio thus indicates a significant increase in evaporation caused by a drier regional climate while global temperatures increase during the Holocene (Bradley, 2015). Another important factor for both ratios is the influx of river waters, which is more pronounced in the lower unit that brings nutrients, but also low- $\delta^{18}\text{O}$ and $\delta^{13}\text{C}$ -modified river waters, to the river mouth (Bradley, 2015). This implies that higher $\delta^{13}\text{C}$ and $\delta^{18}\text{O}$ values are highly affected by terrestrial impact, but lagoons also contain local vegetation as a carbon source as well (Keith and Parker, 1965). The riverine input can cause significant hard water effects so that the radiocarbon used to form the shells, especially in the lower unit, might be old. This could partly explain the apparent long-lasting hiatus from 7 to 5.3 ka cal BP although the dating of wood and peat at the end of both regression cycles contradicts a large impact of hard water effects.

3.5.2 Holocene environments compared to recent delta lakes

In comparison with today's wetland lakes of the delta plain, we observe some similarities between the past and recent conditions. Most of the recent lakes of the eastern delta wetlands show seasonal salinity and temperature variations (Ustaoğlu et al., 2012). The low-salinity environments of the past correspond well to the measured recent wetland lake salinities, which are seasonally highly variable (Figure 3.2).

Only KD-7 from Liman Lake contained ostracod valves and shows similar species (*C. neglecta*, *P. marchica*, *S. aculeata*, *I. bradyi* and *C. torosa*) to the final stages of both regression cycles of the lower and upper units, so that these stages are indicated to have been similar to today's Liman Lake (Figure 3.2). This lake shows relatively constant oligohaline conditions (Figure 3.2). *Ilyocypris bradyi* with an ecological range from freshwater to oligohaline salinities (Meisch, 2000; Chekhovskaya et al., 2014) appears only in the lower unit of the sediment core under highly unstable conditions. *Cyprideis torosa* is very abundant nearly throughout the unit, *S. aculeata* was found only in one sample within an inferred restricted pond environment of the lowermost part of the core (BW-10C). This matches well with ecological preferences of both species (Meisch, 2000) and with recent conditions (Figure 3.2).

(Near-)oligohaline conditions also prevailed in each of the remnant ponds of each succession in the lower part of the core. *Candona? candonaeformis* coexists with *Pseudocandona* sp. indicating the habitat being (at least temporally) oligohaline (Frenzel et al., 2010; Dykan, 2016) during both the lower unit and the upper part of the upper unit. We infer a similar setting to recent times for the lower and upper parts of the core (final stages of each regressive cycle), but to a smaller extent, similar to the Uzun and Tatlı lakes, and proximity to the seashore like Liman Lake. The recent wetland lakes around the sediment core location mostly reach only freshwater to oligohaline conditions so we can compare them to the near-final stage of the environments at the top of both core units before swamp formation. The marine assemblages show α -mesohaline to polyhaline salinities that were significantly higher than in any recent wetland lake.

3.5.3 Processes forming the lagoons of the Kızılırmak Delta

The primary factors for creating lagoonal and restricted lake environments during interglacials, such as the Holocene, are the hydrography of the Kızılırmak River, i.e., its watershed and local conditions, as well as oceanographic current patterns of the Southern Black Sea. Ridges of previous beaches of a prograding shoreline are primary features at the eastern delta plain which show two orthogonal aligned patterns (Erginal and Öztürk, 2010). The northward-migrated beach ridges are cut by the eastward-migrated ones in the northern part originating close to the Kızılırmak River. These landforms confirm a wave-domination of the delta during the Holocene at least since sea level reached a level close to its present elevation about five thousand years ago. The juvenation pattern of the ridges indicates that the Kızılırmak River resulted in a mouth bar forming the E-W-directed beach ridges. This mouth bar originates north of the elevated delta terrace platform (Berndt et al., 2018) that might have reduced river influence on the lagoon and increased the restriction of the lagoon environment. This suggests that nearshore water current eddies restricted the delta growth with a retreating and erosive western and prograding and depositional eastern shore resulting in a concavo-convex pattern of the delta margins. A similar shoreline pattern is seen in the Quaternary delta terraces south of the recent delta plain (Berndt et al., 2018), thus regional sea current patterns seem to have remained relatively stable (at least during Middle to Late Pleistocene highstand conditions). In addition,

historic maps show a large lagoon on the eastern delta plain enclosed by a similar spit-like structure (Butler, 1907).

Today's semi-arid Central Anatolian Plateau as the watershed of the Kızılırmak River experienced precipitation values during the Last Glacial Maximum (LGM) similar to today although its lakes reached their maximum water levels and higher than at present (Van Zeist et al., 1975; Kuzucuoğlu and Roberts, 1997; Sarıkaya et al., 2009). This discrepancy is explained by low evaporation, but higher catchment runoff by snow-glacier melting (Kuzucuoğlu and Roberts, 1997). It also caused active down-cutting of the Kızılırmak River while the vegetation cover composed of cold steppe, woody steppe and coniferous forest prevented sediment influx so that the water discharge was high with a low sediment supply (Doğan, 2010; Çiner et al., 2015). On the other hand, increased intra-basinal aggradation took place during warmer and drier conditions on the post-LGM plateau (Doğan, 2010). This process stored sediment on the plateau instead of transporting it to the delta. Generally, sediment transport is highest during transitional phases (cold to warm and warm to cold) and lower during high and low precipitation periods due to buffering by vegetation and stream power effects (e.g., Langbein and Schumm, 1958; Vandenberghe, 2008; Doğan, 2010). However, the Mediterranean regional climate was wetter during glacial periods and drier during interglacials (Leeder et al., 1998). This indicates primary sediment transport to the delta took place with moderate precipitation and temperatures (drier/warmer than Late Glacial and wetter/cooler than the warm semi-arid Late Holocene) in the Central Anatolian Plateau. Following this scenario, it is apparent that regionally moderately cooler phases, in a warm and wet period like the Holocene, increase the sediment influx and thus delta progradation.

The drilling location was selected in the northwest of the Pleistocene delta terraces (Akkan, 1970; Berndt et al., 2018) so that it is likely that most of the direct riverine influx came from the streams draining down the Pontide Mountains and Kızılırmak Delta terraces rather than the main trunk of the Kızılırmak River. However, deflection of the main river waters into the Black Sea and mixing with the sea water towards the east is likely due to the appearance of *A. quinquetuberculata* and *A. longa* (Bony et al., 2015; Dykan, 2016).

Consequently, the balance between sediment supply from the Kızılırmak River, possibly also from the Yeşilirmak River to the east, and modification of the depositional centre through Black Sea currents helped to retain the sediment bars which enclose the lagoon of the Kızılırmak Delta. This process, together with transgression leading to erosion and re-deposition by sea currents, was essential for the palaeogeographic development of the Kızılırmak Delta.

3.5.4 Holocene environmental development of the eastern Kızılırmak Delta plain

The lower unit is highly impacted by riverine detrital influx. The two restriction phases of the lower unit (lithological unit A) evolving from a lagoon to pond environment with frequent connection to the sea took place between ca. 7.9 and 7.65 ka cal BP, and from 7.65 to 6.8 ka cal BP. Salinity seems to have been close to the α -meso- to polyhaline range at this time with a dominance of *C. torosa* during open phases and oligo-mesohaline during restricted phases. Nevertheless, marine taxa (i.e., *Loxococoncha* spp. and *Amnicythere* sp.) appear in low amounts throughout the whole lower unit and indicate at least a temporary connection to the sea during limnic phases. Until the top of the lower unit, the environment returned to relatively wide-open lagoonal conditions with a connection to the open sea, although subsequent restriction and final desiccation took place gradually. The limnic phases were suppressed or shorter, but became more distinct towards the top. The final phase of the lower core unit is represented by an ostracod-free peat layer (BW-8M) that we interpret as a sub- or anoxic pond remnant after continuous restriction at 6975 ± 30 cal BP.

This peat layer (8.23–8.33 m depth) was similarly identified at 8.14–7.6 m below the Tatlı Lake level by Bottema et al. (1995). It is significantly thicker in their profile compared to our sediment core, which indicates longer-lasting deposition under lagoonal and sub(an-)oxic conditions or a wetter area with higher production of organic material. Bottema et al. (1995) dated the peat at 7.98–8.06 m to 5945 ± 45 ^{14}C BP (conventional age) and identified this boundary as a significant hydrological change with a vanishing riverine influx. We calibrated their peat age to 6779 ± 108 cal yr BP, which corresponds approximately with our own calibrated age (6975 ± 30 cal yr BP). An increasingly higher mud content indicates a decreasing sedimentation rate in the lower unit at this stage. The ostracod abundance of the higher succession

is about twice to three times high compared to the lower parts. The inferred mean sedimentation rate is ca. 1.0–1.6 mm/yr, which seems to decelerate through this regressive period. The delta plain was most likely exposed and/or became eroded between 6.8 ka cal BP and 5.3 ka cal BP.

The middle unit (lithological unit B) does not have a faunal transition accompanied by largely broken mollusc and ostracod shells, which is typical for a rapid transgressive or erosive environment (Swift, 1968). The transgression started to impact shortly before 5.3 ka cal BP and salinity increased suddenly by ca. 6‰ (Figure 3.9). This unit shows a stable lagoonal environment largely dominated by *C. torosa* and lasting until a few centuries after 4 ka cal BP. There are no indications of open marine conditions as observed at the base of the marine succession in the lower core (assemblage 1a in clusters 1 and 3), thus a barrier must have been already present. Increased carbonate precipitation at this time clearly shows an immediate and continuous marine water influence. Salinity increases from low α -mesohaline to low polyhaline up to the central part of the core (Figure 3.9). Although salinity increases to low polyhaline and decreases subsequently to near-oligohaline conditions, there is no faunal change. This might indicate that the restriction of the lagoon through the barrier remained, and that the water of the restricted basin became more saline through increased evaporation, which caused a significant increase in authigenic carbonate inside the sediment, and later less saline but more variable conditions due to higher freshwater influx and decoupling from the sea. This salinity variation in a stable habitat indicates that salinity does not solely define the faunal distribution, but rather the complete setting and the complex interplay of different variables (especially restriction) at least within the oligo-mesohaline range.

The upper unit (lithological unit C) shows the development from 4 ka cal BP to recent with a major faunal change from a near monospecific occurrence of *C. torosa* to a dominance of limnic species accompanied by an absence of sea water influence and sandy detritus. After a transitional period with a co-existence of *Candona* sp. and *C. torosa* (Assemblage 4) combined with highly variable sea water influence and frequent changes in evaporation representing confinement and transformation into a brackish lake, *Candona* sp. replaces all marine species (Assemblage 4a) and evaporation rates reach their maximum while marine influence is not recognisable. This indicates that the contact to the open sea was blocked. The lake experienced two

short-term seawater incursions introducing unstable lagoonal phases based on the dominant appearance of *C. torosa* and *H. salina* found in the older phase of the intrusion, causing further restriction and return to an oligohaline lake.

Subsequently, the habitat's pH and oxygen content are indicated to lower significantly so that ostracods were absent and/or dissolved post-depositionally, with high organic mud and plant detritus content that desiccated to a peat layer. This peat layer was deposited very recently so that the sediment above is classified as sub-recent. Dissolution of valves might also cause their absence in low-salinity habitats. In contrast to the low-salinity parts of the lower core, the upper part shows an absence of marine influence within the reconstructed limnic units. The inferred mean sedimentation rate until the top of the upper unit is the lowest over the whole profile with ca. 1 mm/yr.

3.5.5 Relative water depth estimation

Local vertical accommodation space is controlled by Black Sea sea level, while sediment influx is controlled by the Kızılırmak River's sediment load, which is largely a result of climate (i.e., precipitation) in the hinterland (Central Anatolia). During the Holocene, vertical accommodation space is created due to global sea-level rise. On the other hand, delta progradation acts regressively as a result of a surplus of sediment influx filling the created subaquatic space (e.g., Bard et al., 1996; Allen, 2000; Bhattacharya, 2003; Behre, 2003; Seeliger et al., 2017). Additionally, erosion and re-deposition take place through longshore sea currents (spit formation) restricting the size of the wave-dominated delta (Bhattacharya, 2003).

The analysed section of the sediment core BW covers the Mid- to Late Holocene as the transitional time between the wet and fast transgressional Early to Mid-Holocene to the Late Holocene recent dry period of the Anatolian Plateau with relative sea level stability. Based on habitat changes inferred from our sediment core, the relative sea-level can be calculated semi-quantitatively. A depiction of local water depth estimations is given in Figure 3.10. The exact sediment depth information remains questionable. The recovery of about 50% is relatively low, but is rather related to drilling-induced sediment compaction than to missing sediment. The compaction rate is relatively similar throughout the upper 8.3 m of the core, but reaches variable values in the lower unit due to highly porous sediment. Herein, we use core-meters

(distance along the sediment core from top) as depth although the depth of deposition might be originally different because those correspond best to results of previous sea-level studies (e.g., Seeliger et al., 2017) in combination to our radiocarbon dating. We thus interpret no loss in sediment recovery but drilling-induced compaction of the cored delta sediment.

Local water depth during the lagoonal phases is inferred to be between 0 and 5 m due to the appearance of *L. bulgarica* and *A. longa* (Bony et al., 2015; Dykan, 2016) accompanied with a dominance of shallow-marine water taxa (*C. torosa*, *T. amnicola* and *Loxoconcha* spp.) throughout the core (Figure 3.9). Environments of the regression cycle between 7.8/7.9 and 7.65 ka cal BP are quickly changing between limnic (*C. neglecta*, *H. salina*, *Ilyocypris* spp., *M. cordata* and *P. marchica*) with only shallow to very shallow marine species (i.e., *Amnicythere* spp., *Loxoconcha* spp. and the dominating species *C. torosa*) (Frenzel et al., 2010; Dykan, 2016) so we estimate a shallow water depth (<3 m) and more likely a water depth of <1 m.

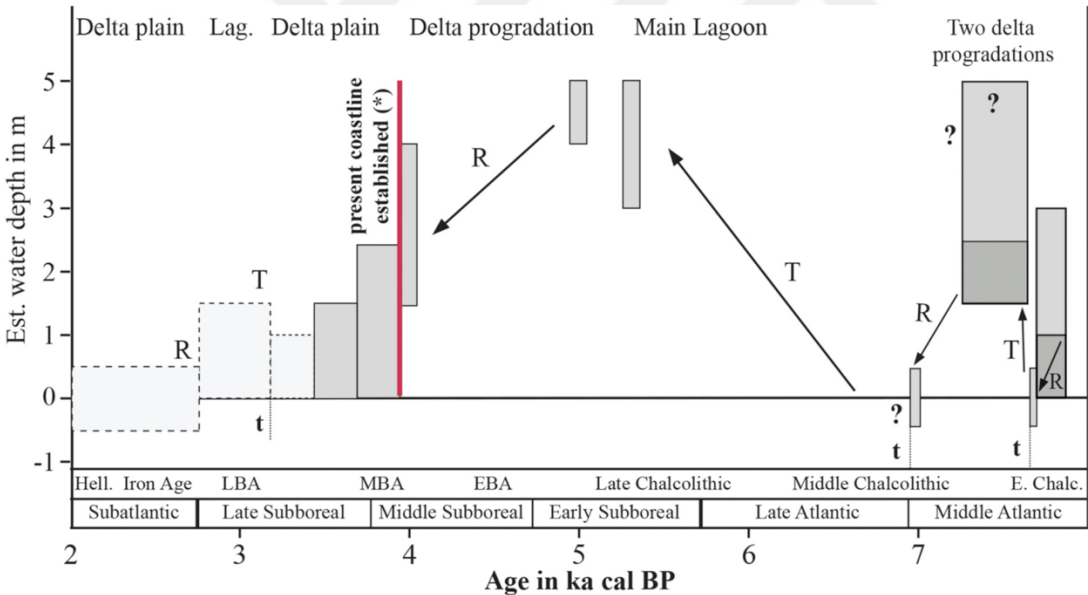


Figure 3.10 : Water depth range estimations based on the ostracod fauna (*Tyuleneva et al., 2014; R – regression, T – transgression, t – possible terrestrialization). Dark grey ranges before 7 ka cal BP are ranges of higher probability of the surrounding rectangle and light grey rectangles with dashed margins indirectly dated.

Information about water depth throughout most of the middle unit is limited because of the mostly monospecific dominance of the shallow-marine *C. torosa* with a general depth range of 0 to maximum 30 m (Dykan, 2016). However, high population densities occur only in water depths between 3 and 5 m (Dykan, 2016) so

we infer the depth of the lagoon during the Mid Holocene to be within this range. In several parts of the lower and upper units, marine species co-occur with limnic species (Figure 3.9), thus rapid changes between marine-lagoonal and limnic conditions, and even shallower (<3 m) water depths are implied (Figure 3.10). The recent lakes (except Liman Lake) have a maximum water depth between 1.0 and 1.5 m with a level at about sea level (Figure 3.2). This seems to be a good water depth approximation also for the palaeo-wetland lakes.

Higher amounts of limnic taxa indicate the predominance of limnic conditions during a regressive phase in alternation with marine waters. The final phase of such a regressive period is the deposition of peat that takes place very close to the lake and sea level within swampy wetlands of the delta plain.

3.5.6 Holocene sea level and climate of the Black Sea region

3.5.6.1 Middle Holocene wet period and rapid rising sea levels

The timing and style of the Early Holocene Black Sea reconnection to the Mediterranean Sea - and thus to the world ocean - is highly disputed (e.g., Görür et al., 2001; Aksu et al., 2002; Ryan et al., 2003; Bahr et al., 2008; Eriş et al., 2011; Ivanova et al., 2015), but it is commonly agreed that the Black Sea was connected to the Mediterranean Sea within the last 7.9 ka (Filipova-Marinova, 2007). The base of the herein studied sediment core shows development since this re-connection.

Climatic shifts might have caused variations in the Holocene transgression of the Black Sea and modified the sediment influx of the Kızılırmak River. The regional climate ameliorated since the Late Glacial until ca. 8.8 ka cal BP (Filipova-Marinova, 2007). Mixed oak forests replaced the herb communities of the circum-Pontian region gradually around the Black Sea since Boreal (ca. 9.6 to 8.2 ka cal BP) (Filipova-Marinova, 2007). Nevertheless, Late Glacial and Holocene climate records of Anatolia are only regionally valid and show significant disagreements. By comparing the dated samples showing direct sea-level indicators (peat and limnic/marine-mixed fauna) with recent independent sea level, our sea-level estimation is partly correlative but especially local regressions and transgressions depict a distinct regional control (Figure 3.11).

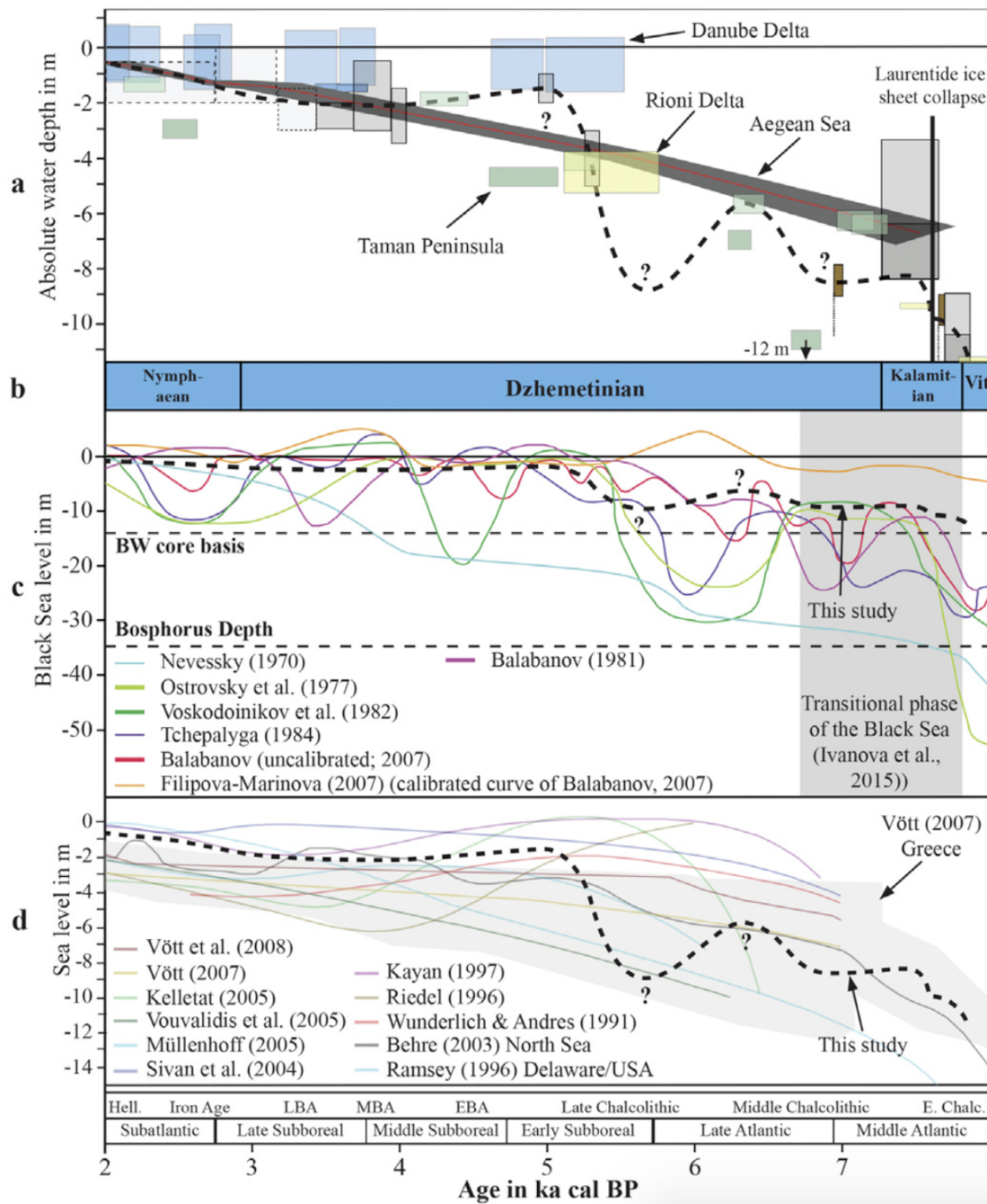


Figure 3.11 : Sea level variability between 8 and 2 ka cal BP. (a) Reconstruction of the absolute Black Sea level (this study; c. f. Figure 3.10) and comparison to the Mediterranean Sea (Seeliger et al., 2017) and the sea level indications (peat) for the Danube Delta (blue: Giosan et al., 2006), Taman Peninsula (light green: Brückner et al., 2010 and dark green: Bolikhovskaya et al., 2018) and Rioni River delta (grey: non-peat estimations and brown: peat levels; yellow: Laermanns et al., 2018). (b) Timeframe of Yanko-Hombach (2007). (c) Black Sea level reconstructions (data from Erginal et al., 2013). (d) Sea level curves from the Mediterranean Sea, North Sea and Northern Atlantic (USA) (compilation of Ramsey and Baxter, 1996; Behre, 2003, Brückner et al., 2010 and references therein). Grey shade indicates the total range of sea level curves of Greece (Vött, 2007).

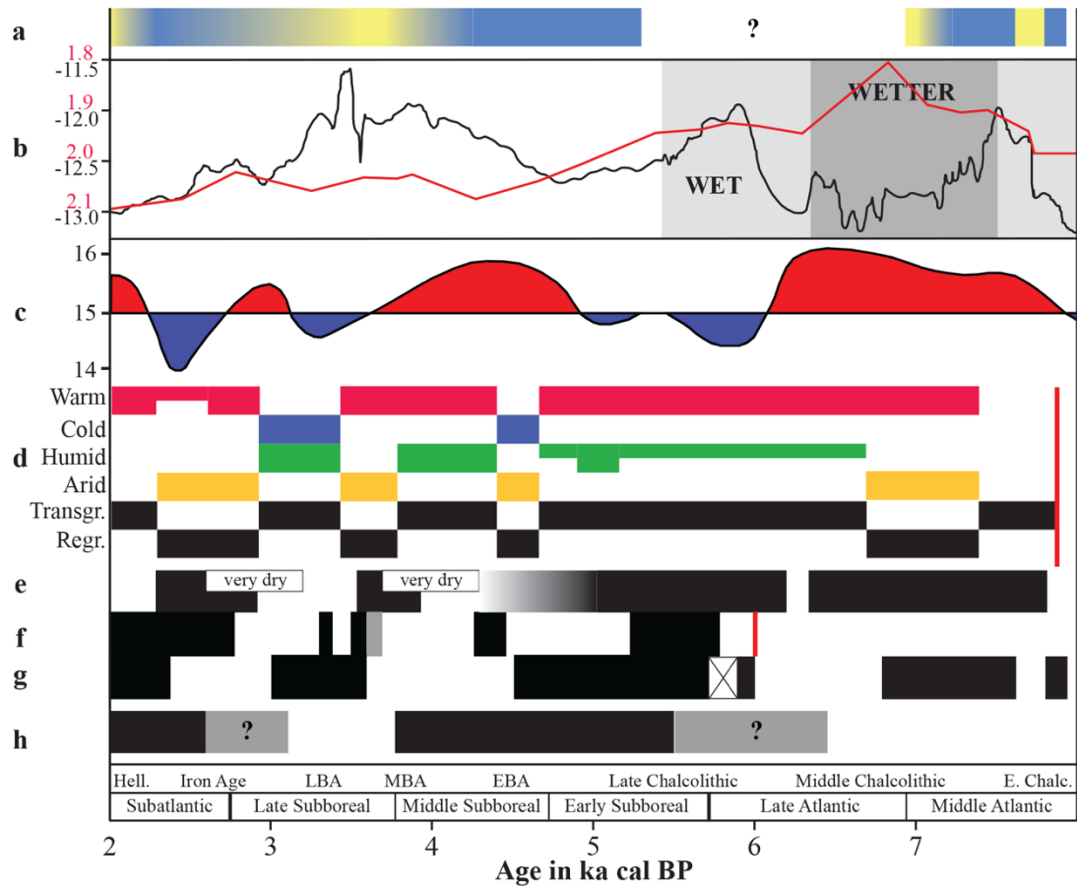


Figure 3.12 : (a) Holocene environments of the Kızılırmak Delta (2 to 8 ka cal BP) (this study; marine: blue and limnic: yellow). (b) Stalagmite $\delta^{13}C$ of Sofular Cave (black) and $^{238}U/^{234}U$ (red) (SW Black Sea coast; data from Göktürk et al., 2011). (c) Simplified climate oscillations of the Holocene of Europe (Schönwiese, 1995). (d) Climate and sea level variation of Taman Peninsula (NE Black Sea coast; modified from Bolikhovskaya et al., 2018). (e–g) Wet (black) and very dry phases of the lakes Eski Acıgöl and Nar Gölü (e; Central Anatolia; Turner et al., 2008; Berger et al., 2016), Tecer Lake (f; Northern Anatolia; Kuzucuoğlu et al., 2011) and Western Anatolian lakes (g; based on Akçer Ön, 2011 and Ocakoğlu et al., 2013). (h) Occupation phases of İkittepe (based on Alkim et al., 1988; Alkim et al., 2003 and Welton, 2010). The red vertical barrens in (d) and (f) refer to the basis of the related record.

The sediments of the lower unit of the core were deposited under wet and warm conditions prevailing during the Atlantic period (8.8 to 5.8 ka cal BP) supporting mixed oak forests even in higher elevations in Europe and Anatolia (Schönwiese, 1995; Wick et al., 2003; Filipova-Marinova, 2007; Çağatay et al., 2014) (Figure 3.12). Within this period, the time between 7.9 and 6.5 ka cal BP is recorded as the wettest phase of Central Anatolia during the Holocene (Göktürk, 2011; Kuzucuoğlu, 2015; Berger et al., 2016) (Figure 3.12). The wet climate even prevailed until 5.4 ka cal BP in Anatolia (Göktürk, 2011; Küçükuysal and Yavuz, 2017), which is

supported further by glacier advances in Anatolia until the middle Atlantic (e.g., Sarıkaya and Çiner, 2015, 2017, and references therein). The precipitation in eastern Anatolia even increased until 6.2 ka cal BP (Landmann et al., 1996). On the other hand, the climate in northwest Anatolia became drier already between 7.3 and 6 ka cal BP (Ocakoglu et al., 2013).

The sea level rose from 11.4 to 9.6 m below the recent surface level from ca. 7.9 to 7.65 ka cal BP. Nonetheless, the delta plain was fast prograding (Figure 3.11) due to high discharge with high sedimentary influx under wet conditions (Figures 3.11, 3.12). Subsequently, the site flooded very rapidly at ca. 7.65 ka cal BP by a sea level rise of at least 1.4 m. The sea level implications agree well with Herrle et al. (2018), who connect this rise of sea level to Laurentide ice sheet collapse (Törnqvist and Hijma, 2012). Subsequently, sea level remained constant or a slight regression occurred until 7 ka cal BP with a final sea level position at ca. 8.3 m below recent surface level (Figures 3.10, 3.11). The flooded plain returned to a swamp due to lagoon silting up. At our core site, a peat formed atop 8.33 m sediment depth, which is ca. 20 cm deeper than in Bottema et al. (1995). This difference in depth of the peat levels might be due to preceding accumulation of organic matter of a more marginal swamp area. An earlier terrestrialization of our location might have led to erosion and thus could have created a small topographic difference between both drilling sites.

Subsequently, the study site was exposed for up to 1700 years (7 to 5.3 ka cal BP). A millennium of sea-level stability or fall could accelerate delta progradation even without hydrological changes within the watershed. However, this phase is accompanied by increasingly drier conditions in Anatolia (Figure 3.12) so that the terrestrialization seems to be primarily associated with a delta progradation or (slight) sea-level fall (Figure 3.11). A regression is also indicated by a peat studied by Bolikhovskaya et al. (2018) at Taman Peninsula (NE Black Sea), while Brückner et al. (2010) found a slightly younger peat at -5.6 m depth, which implies a transgression above the peat level until 6.3 ka cal BP. This transgression might account for peat erosion, but storm surges cannot be excluded. A hard water effect might explain partly the apparent long-lasting hiatus, but the ages and sea level estimations of the lower unit correspond well with a major transgression identified by Herrle et al. (2018) and the top-level peat age of the lower unit is similar to the

one of Bottema et al. (1995). Future studies of the Kızılırmak Delta might answer the question about the origin of the 1700 year-long hiatus and the previous delta development since the last glacial.

3.5.6.2 From the Middle Holocene climatic optimum to the semiarid Late Holocene

The sea reached a near-recent level at 5 ka cal BP that coincides well with the sea-level estimations of Giosan et al. (2006) from the Danube Delta (Figure 3.11). However, this is significantly earlier than reconstructed by Seeliger et al. (2017) (Figure 3.11). The subsequent sea level highstand from 5 to 4 ka cal BP is represented by a lagoon in our study area under warmer than present and relatively wet conditions of the Holocene Climate Optimum (6.2 to 4 ka cal BP) in Anatolia (Schönwiese, 1995) (Figure 3.12).

The overall climate of Anatolia in this period oscillates towards drier conditions and the Black Sea region beginning at 6.4 ka cal BP (Landmann et al., 1996; Kremenetski et al., 1999; Roberts et al., 2001, 2011; Wick et al., 2003; Eastwood et al., 2007; Fulton et al., 2012; Küçükuysal and Yavuz, 2017). Several cooling and drought events were superimposed on the Holocene warming trend in Anatolia and the Northern Aegean Sea that reflects significant climate instability in the Mid-Holocene (Triantaphyllou et al., 2010; Oçakoğlu et al., 2013; Berger et al., 2016). Arid phases occurred in the Eastern Mediterranean from 5.3 to 5.0 ka cal BP and 4.5 to 4.0 ka cal BP (Nicoll and Küçükuysal, 2013) that are coherent with the findings of Erginal et al. (2013). An increasingly arid phase happened between 4.0 and 3.3 ka cal BP, which was interrupted by a particularly wet phase at about 3.7 ka cal BP (Eastwood et al., 2007; Nicoll and Küçükuysal, 2013; Roberts et al., 2016). The moderate climate in the watershed associated with moderate discharge of Kızılırmak River prevented closing of the lagoon while very dry climate between 4.0 and 3.3 ka cal BP might have led to lagoon closure due to lower sediment retention in the watershed. A contemporary relative regression is expressed in Balabanov (2007) as a steep absolute regression of ca. 10 m terminating at 3.3 ka cal BP, while our estimations and the majority of the other available Black Sea level curves show only small sea-level variations of a few centimetres to a few meters (Figure 3.12). Our sea level estimations (Figure 3.11) indicate a minor regression of less than or ca. 2 m, which is in good agreement with the findings of Erginal et al. (2012, 2013) and

Giosan et al. (2006). Recent research has shown strong indications for a tectonic origin of the so-called Phanagorian Regression (Fouache et al., 2012) and estimated sea level at about 0.35 and 2.35 m below the recent sea level that fits well to our sea-level estimation, although our data indicate a minor regression only. Earlier studies suggested a sea level fall by 5 to 6 m or even more (e.g., Fedorov, 1977; Ostrovsky et al., 1977; Chepalyga, 2002).

The lagoon coincides well with the first and primary inhabitation phase of İkiztepe on the western slope of the delta platform (Figure 3.12). The Late Chalcolithic to Middle Bronze Age town of İkiztepe relied upon fishing, which implies a much closer shoreline than at present (Alkim et al., 1988; Alkim et al., 2003; Turoğlu, 2005; Welton, 2010), as the town is located today 9 km away from the sea and 3 km from the Kızılırmak River. It is possible that this somewhat drier phase created a large-scale delta progradation converting the lagoon to a shallow lake with increasing distance of the settlement to the sea. This period of İkiztepe habitation ended at the latest at 3.75 ka cal BP (Burney, 1956; Alkim et al., 1988; Alkim et al., 2003). We thus infer a contemporaneous development of the lagoon and habitation of İkiztepe. This socio-environmental correlation between lagoonal conditions and the occupation of İkiztepe might imply that the lagoon was an advantageous location for historic settlement as a possible harbour for trade and boat protection.

After the abandonment of İkiztepe, the deltaic lake once more became a shallow marine lagoon. The timing of this phase is unclear. However, the Central Anatolian Plateau experienced a significant arid phase for ca. 300 years between 3.1 and 2.8 ka cal BP (Nicoll and Küçükuysal, 2013; Kaniewski et al., 2015) or even slightly longer from 3.2 to 2.6 ka cal BP according to Roberts et al. (2016). During that time, the water levels and carrying capacity of the Kızılırmak River might have been highly reduced, while sea level rose constantly with ca. 1 mm/yr from 3 ka cal BP onwards (Mater and Turoğlu, 2014) creating a renewed lagoonal phase.

The town of İkiztepe became repopulated between the end of the third millennium BC and 2.65 ka cal BP (Bilgi, 1999) (Figure 3.12). It seems apparent that people re-occupied the town of İkiztepe by taking advantage of the renewed lagoonal phase. Nevertheless, warmer and wetter conditions prevailed in Central Anatolia from the Beyşehir Occupation until Hellenistic period (Bakker et al., 2012) and lead to a final transformation of the lagoon to a swamp environment. Although the lagoon was

eventually silted-up, the people of İkiztepe continued to inhabit the town until at least Hellenistic times, which might have been possible due to a vanishing importance of the lagoon as economic and/or cultural factor.

3.6 Conclusions

Our study of the ostracod associations and salinity reconstruction through sieve pore analysis of *C. torosa* from the sediment core BW depicts the development of the Kızılırmak Delta since ca. 7.9 ka cal BP in Black Sea that had been reconnected to the Mediterranean Sea. The sediment core shows an alternation of marginal marine lagoonal and restricted lacustrine environments indicating variable sea-level changes of several meters during the Mid-Holocene while reaching a near-recent sea level by ca. 5 ka cal BP.

Lagoonal phases with relative water depths up to ca. 5 m are dominated by *C. torosa*. The more open marine lagoonal settings are additionally characterized by a high content of *Loxoconcha* spp., while the riverine (deltaic) influence leads to a dominance of *A. quinetuberculata* and *A. longa*. Limnic phases show a dominance of *C. neglecta* and *H. salina*.

In addition, *P. marchica* appears in settings with oligohaline salinities. The salinity of the lagoon reaches generally α -mesohaline to low-polyhaline levels at ca. 5.3 ka cal BP. The lake environments were frequently connected to the open sea leading to β -mesohaline conditions. Oligohaline conditions evolved with further restriction of the lagoons from the sea.

The sieve pore analysis was successfully applied with the aid of faunal characteristics reconstructing the salinity of the brackish palaeoenvironments. Eventually, a local sea-level reconstruction for the Southern Black Sea was created.

While Holocene delta plain environmental changes until 7 ka cal BP are mainly forced by sea-level variability of the Black Sea under generally wet regional climate, climate variability in the Central Anatolian Plateau became a dominating factor for the delta development by regulating sediment influx. Absolute sea-level variations affected the delta progradation as well. The sediment influx was highest during drier conditions in the elevated Central Anatolian Plateau during the Middle and Late Holocene.

The delta mostly kept pace with sea-level changes during phases of moderate precipitation. Sea level is estimated to have risen rapidly from 7.9 to 7.65 ka cal BP. The delta submerged quickly at 7.65 ka cal BP due to rapid sea-level rise or tectonic submergence with subsequent phases of stagnation or regression until 5.3 ka cal BP when the delta submerged again and sea level reached a near present day position until 5 ka cal BP. Subsequently, sea level fell by up to 2 m and rose slowly until today.

Another lagoon developed during the major drought of the Late Bronze Age (ca. 3.7 to 3 ka cal BP), while a subsequent wet phase during the Iron Age (ca. 2.8 to 2.3 ka cal BP) led to its final restriction, which remains until today. Wetter phases from ca. 7.9 to 7.65 ka cal BP and from 6.8 to 5.0 ka cal BP re-opened the connection to the sea forming lagoonal habitats. Drier phases resulted in restriction and desiccation.

Both lagoonal phases correspond well with the occupation phases of the historic İkištepe. These phases are indicated to be a major economic and/or cultural factor for the historic town of İkištepe. Subsequently, the lagoon was silted-up and converted to the recent delta wetland environment.

4. INTRASPECIFIC LENGTH VARIATION AND SHELL THICKNESS OF THE OSTRACOD *CYPRIDEIS TOROSA* (JONES, 1850) AS A POTENTIAL TOOL FOR PALAEO-SALINITY CHARACTERIZATION³

4.1 Introduction

Ostracoda are small crustaceans (typically 0.5–2.0 mm long in the adult stage) enclosed by a two-valved mineralized carapace. They populate nearly all aquatic realms (Horne et al., 2002). Their highly variable calcareous carapace preserves easily, and thus ostracods show a good geological record since the Palaeozoic times. Based on their wide distribution, often high abundance, and diversity and taxon-specific ecological preferences and tolerances, they are highly suitable for environmental reconstructions (Horne et al., 2002; Boomer et al., 2003). An integral part of every ostracod is its carapace as it protects the animal against predators or harsh environmental conditions, plays an important role for the contact with the surrounding environment, supports its mode of life, and gives stability for the benthonic lifestyle (Hartmann, 1963; Karanovic, 2012). The identification and use of each ostracod species to reconstruct environments in the geological past is highly based on the morphology of their shells (Horne et al., 2002).

Ostracod valves grow discontinuously by molting, i.e., their instars shed their valves and calcify new ones in defined ontological stages. There are eight instar stages, and adults are characterized by a strong sexual dimorphism in *Cyprideis torosa* (Heip, 1976). The carapace of an ostracod is formed by the uptake of Ca-ions from the surrounding water before or after molting, thus producing a new fully-calcified carapace (Turpen and Angell, 1971). In this way, the shell chemistry can only be related to the environmental conditions which prevail in this specific timespan (De Deckker and Forester, 1988). Especially the carbonate availability and construction time determine shell calcification and growth in ostracods as in bivalves alike

³ This chapter is based on the paper “Berndt, C., et al., Intraspecific Length Variation and Shell Thickness of the Ostracod *Cyprideis torosa* (Jones, 1850) as a Potential Tool for Palaeosalinity Characterization. *Geosciences*, 2019, 9(2): p. 83”

(Remane, 1958; Keyser and Walter, 2004), but also the prevailing water temperatures during calcification play a role (Roca and Wansard, 1997). While the intraspecific shell thickness of marine taxa is well known to be significantly larger in marine waters than in brackish waters, such intraspecific changes are recognized mostly in mollusks, i.e., bivalves, so far (Remane, 1958).

A common and widely distributed ostracod species is *Cyprideis torosa* (Jones, 1850). It is recognized as an indicator of environmental changes displayed in its phenotypic morphological adaptation (Meisch, 2000). This species is very common nearly worldwide in marginal marine and paralic environments over a large salinity range from oligohaline to hypersaline water bodies (Heip, 1976; Van Harten, 1975, 1996 and 2000; Mezquita et al., 2000). High population densities up to several tens of thousands of individuals of this plant detritus-feeding species within one-meter square are seen in stressed environments where other ostracod species are absent (Heip, 1976). This brackish species lives preferentially in brackish water environments at water depths of 0.5–30 m while reaching high population densities between 3 and 5 m under 0–25 °C water temperature (Dykan, 2016). It prefers vegetated, silty, and muddy sand substrates (Dykan, 2016).

Several former studies demonstrate a phenotypic salinity-dependency of various morphological shell features in *C. torosa*. After the first descriptions of the ostracod valve structure (Müller, 1900), three other morphologically variable features on the shell of *C. torosa* were found to be related to the ambient salinity of the surrounding waters. A variable noded character of the valve's morphology appears in individuals of this species living in low-salinity environments, which was discussed already in Van Morkhoven (1962). The living cultures of Frenzel et al. (2012) imply their phenotypic appearance with decreasing salinity below 7 ‰. Furthermore, the ratio between rounded and non-rounded sieve pores is related to salinity as well (Rosenfeld and Vesper, 1977). A length variation of the female adult valves was observed by Van Harten (1975). Boomer et al. (2017) gathered new data from modern sediments of different seas for the size-salinity relationship and confirmed the threshold of Harten (1975) at about 8 ‰ with small valves above and larger valves below this point. However, there is still a significant lack of data in between, i.e., between 8 and 13 ‰.

The Kızılırmak Delta is a wave-dominated delta at the central Black Sea coast of Turkey (Erginal and Öztürk, 2010) (Figure 4.1). It is fed by Kızılırmak River, the longest river of Turkey (1355 km long) that flows across the Anatolian Plateau in a large bend and traverses the North Anatolian Fault Zone and Central Pontide Mountains until it mouths into the Sinop Graben in Samsun province where it forms an extensive delta plain. The North Anatolian Fault Zone is indicated to actively uplift the Southern delta plain since the Mid-Pleistocene forming of several terrace levels of palaeo-delta plains (Berndt et al., 2018).

Today, the Eastern delta plain has extensive wetlands (Ramsar site) with nine shallow fresh to brackish lakes (Figure 4.1) as remnants of the Mid- to Late Holocene lagoon in a semi-arid to semi-humid maritime climate (Turoğlu, 2010; Ustaoglu et al., 2012; Köse et al., 2014; Berndt et al., 2019).

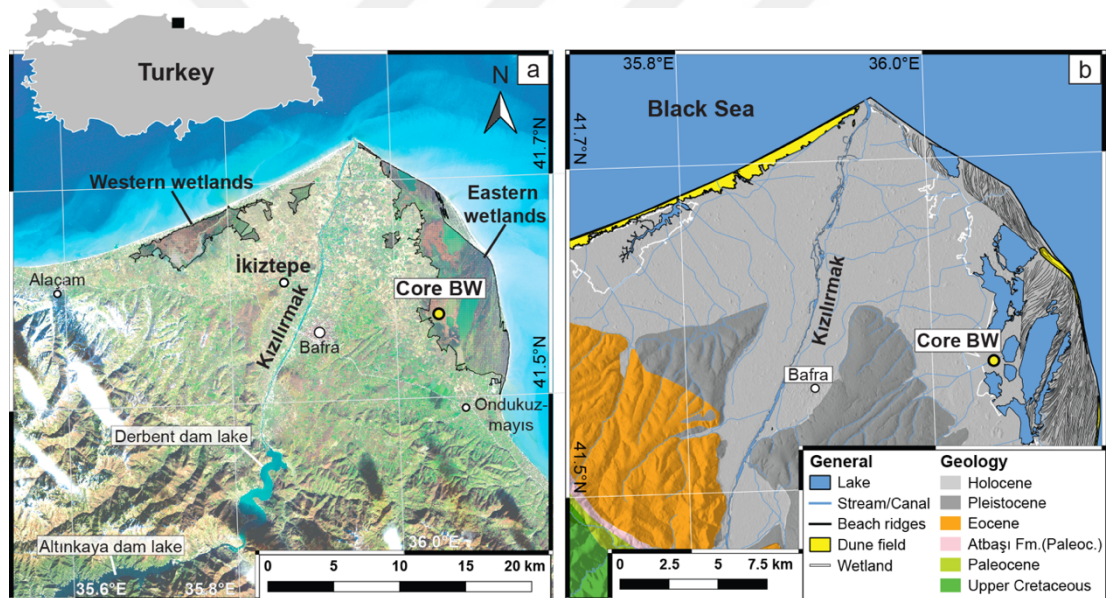


Figure 4.1 : Natural-colored image (a) and geological-geomorphological map (b) of the Kızılırmak Delta with sediment core (BW) (modified from Berndt et al., 2019).

Berndt et al. (2018) gave the first insight into the Quaternary fluvio-deltaic development of the Kızılırmak Delta. Berndt et al. (2019) analyzed the sediment core BW (41°34'40" N and 36°02'51" E) at the Eastern Kızılırmak Delta plain dealing with ostracod associations and sieve pore shape analysis of *C. torosa* to reconstruct the Holocene environmental development of the Kızılırmak Delta (Figure 4.1). The studied sediment core has been radiocarbon-dated by using shells of *Cerastoderma edule* (Linné), wood, and paralic peats. It covers the development of the delta plain since about 7.9 ka cal BP with a major hiatus between 7.0 and 5.3 ka cal BP. The

palaeoenvironment is described to change back-and-forth from a mesohaline to a polyhaline lagoon with up to about 6 m water depth, and to (near-)oligohaline lakes, which were similar to the recent wetland lakes (Berndt et al., 2019). According to Berndt et al. (2019), the main factors controlling the Holocene environments are indicated to be the rising sea level and an increasingly arid regional climate of the Anatolian Plateau. While sea level changes have a major impact until the sea level reached a near-recent level at the latest 5 ka cal BP, the regional climate is the major forcing factor thereafter (Berndt et al., 2019).

Herein, we aim to test the size-salinity relationship of *C. torosa* along the Holocene profile from the Kızılırmak Delta at the Black Sea coast of Turkey to prove its applicability for palaeoenvironmental studies. The reconstructed salinity of the related palaeoenvironments ranges from oligohaline to polyhaline (ca. 6 to 20‰). Thus, our study is covering the range well with the lack of data in the study of Boomer et al. (2017) about the variability of carapace size in *C. torosa* along the salinity gradient. Furthermore, we introduce the thickness of its shells as a new palaeoenvironmental indicator in marginal marine settings. Both potential proxies aim to give important information about palaeoenvironments, especially within low-diversity or even monospecific assemblages dominated by *C. torosa*.

4.2 Materials and Methods

We analyzed 17 of already prepared samples taken from the sediment core BW by Berndt et al. (2019). Sample preparation, species identification, and counting were previously described in Berndt et al. (2019). The samples contain the instars A-3 to A (adult) of *C. torosa* due to the chosen analyzed fraction of the samples (> 200 µm). Thus, smaller individuals were excluded during the sieving process.

For the analyses, all available valves of *C. torosa* of the largest two stages were used. The samples along the core are of changing quality for the used methodology. The occurrence of adult valves is limited in many samples; hence, we chose to merge the size data of right and left valves of female individuals, although a size difference of about 3% was observed that is consistent with the results of Boomer et al. (2017). Nine samples in the lower and upper units were excluded from the analysis because of the very low content of usable valves of *C. torosa*.

We measured lengths and heights of all A-1 (penultimate ontogenetic stage) and A (adult) valves in 19 samples by using a light microscope with an ocular scale. Size differences were visible between the adult male and female specimens, but only tentative in the A-1 stage like already observed in Boomer et al. (2017). We thus used only the female adult individuals to receive results comparable to the studies of Van Harten (1975) and Boomer et al. (2017), and all specimens of the stage A-1. A linear regression model for the salinity-length relationship was performed using PAST (Hammer et al., 2001).

During the sieve pore analysis of Berndt et al. (2019), apparent color differences between the valves were recognized using a transmitted light microscope. The adult valves were grouped into three classes according to their translucence. To measure the shell thickness and to exclude a dissolution effect, we took SEM images of two broken valves per valve type.

4.3 Results

4.3.1 Length variation

The length of an ostracod is the distance from anterior to posterior margin and the height is the distance from ventral to dorsal margin (Bradley, 1941). The adult specimens of our material vary in size and have mean lengths between 0.77 and 1.036 mm (female) and 0.903 and 1.106 mm (male). The measurement error is about ± 2 to 3%.

The mean length of instar A-1 varies between 0.58 and 0.76 mm and the mean height between 0.36 and 0.44 mm (Figure 4.2). The measurement error ranges between ± 3 and 4%. The largest specimens of this instar are seen in BW-3M and BW-11A, while BW-10C contains the smallest. The deviation between length and height shows a similar pattern like the pure length variations at both instars, although there are small differences—the length deviation of A-1 remains at constant during the middle to upper unit, while the length is slightly increased and the length deviation of the adult specimens is slightly lower in the lowermost two samples and higher at the base of the middle unit with transition to the upper unit. However, there are neither clear patterns nor large deviations recognizable (Figure 4.2).

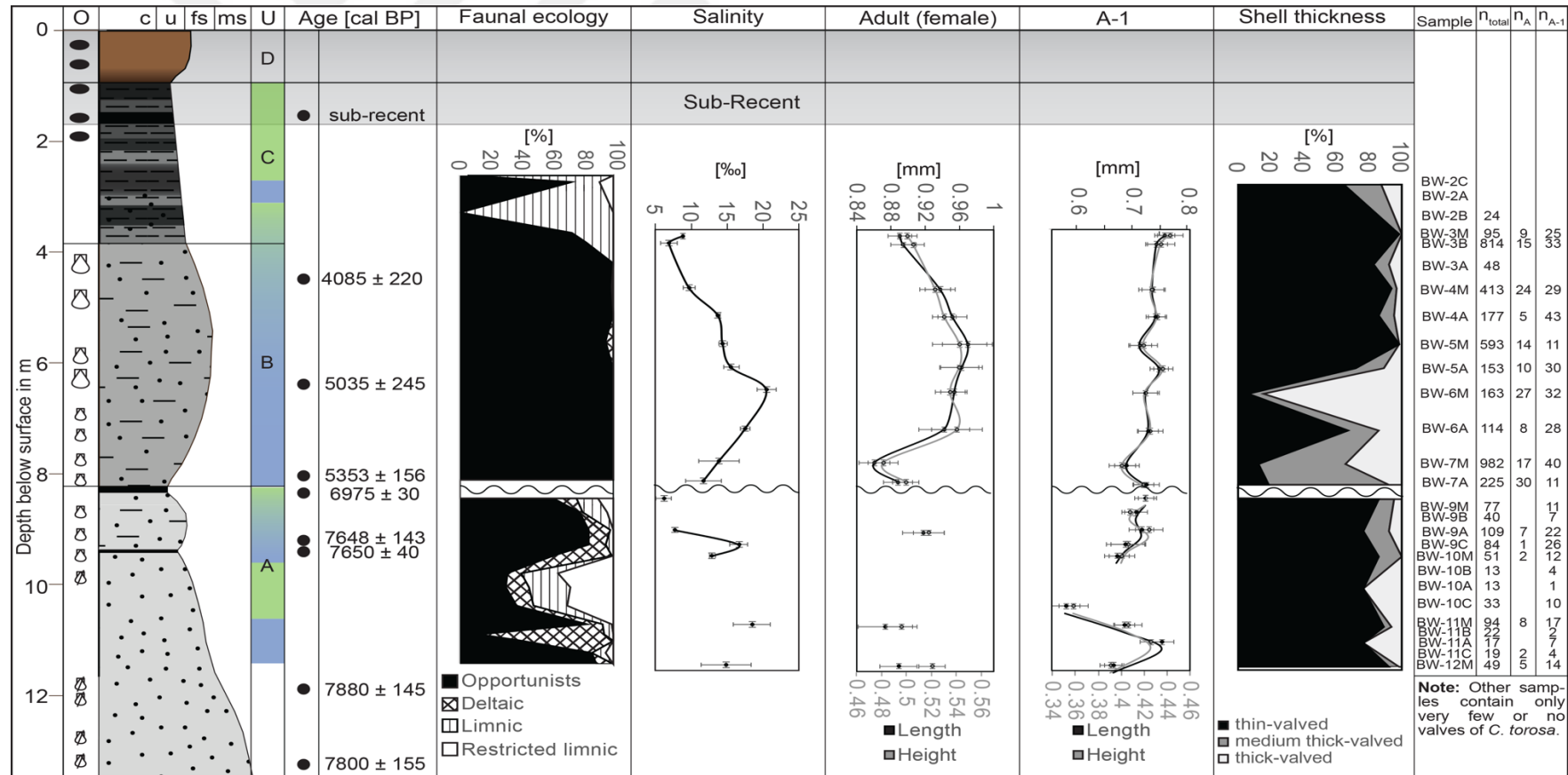


Figure 4.2 : Sediment core BW with lithology appearance of larger shells of *C. edule* and gravel, sedimentological (A–D) and ecological zonation (blue: Marine, green: Lacustrine), radiocarbon ages, ostracod ecology, reconstructed salinity, length and height measurements of female adult and instar A-1 *C. torosa* valves, valves thickness variation, sample names according to their depth below surface, total number of *C. torosa* valves (n_{total}), number of adult *C. torosa* valves (n_A) and number of valves of the instar A-1 (n_{A-1}) (modified from Berndt et al., 2019 and combined with new data of this study).

4.3.2 Valve thickness

The observation using SEM revealed that the colorless-translucent valves are the thinnest with about 12–13 μm , the brown ones are of intermediate thickness with 18–19 μm , and the opaque ones had a thickness with a relatively large range of about 21–30 μm (Figure 4.3). The threshold between translucent and opaque valves is thus indicated to be at about 20 μm . The translucent valve type is separated from a brown-translucent valve type by its absence of a distinct/continuous colored appearance (brown) of the valve although this change is rather gradual. Valves with slightly brownish central areas, while the rest of the valve is colorless, are still counted as colorless (Figure 4.3).

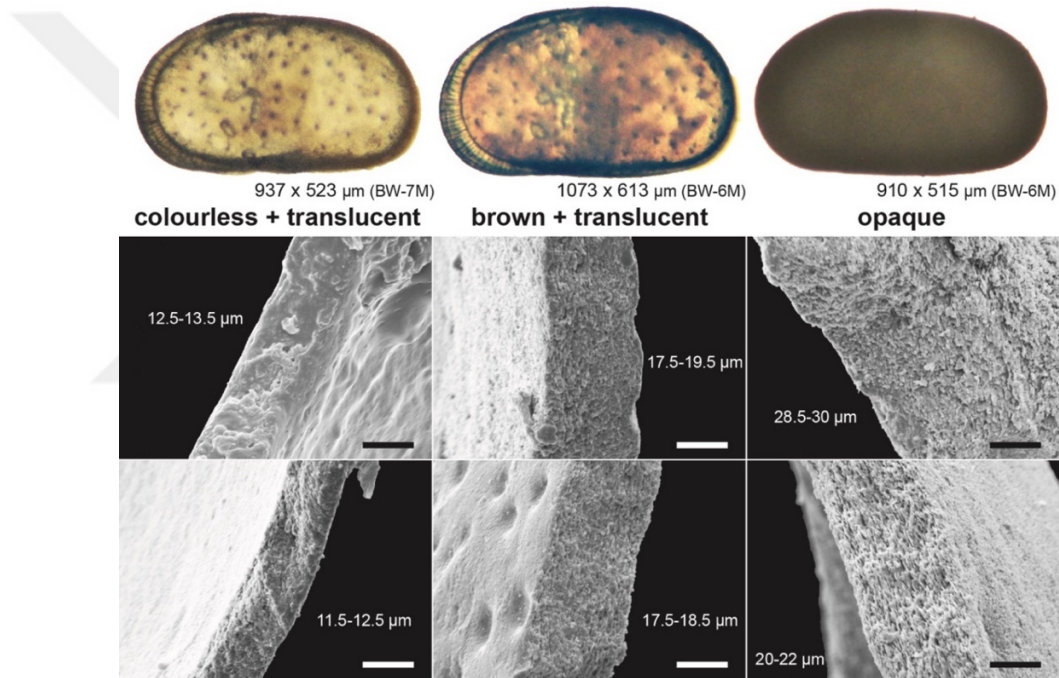


Figure 4.3 : Examples of valve microstructure of female adult valves of *C. torosa*. All scales: 10 μm .

The preservation of the identified valves inspected with the aid of SEM was good, except the thinner ones of the translucent-brown and opaque valves, which have valve surface-parallel dissolution traces (lower middle and lower right images of Figure 4.3). The opaque valves are two–three times thicker than the colorless translucent valves. We therefore name the categories as thin-walled (colorless-translucent), medium thick-walled (brown translucent), and thick-walled (opaque) specimens. The brownish coloring of translucent valves seems to be rather variable between the valves, but it is always particularly intense in the back of the central

muscle scars. None of the shells showed internal sub-layering under the SEM. Dissolution traces were absent in the thin shells and occur only in the medium-thick and thick valves.

The amounts of the different thickness classes are shown in Figure 4.2. Throughout the lower unit (11.4–8.2 m below surface), the number of thin valves is predominating with about $83 \pm 6\%$, while thicker valves are less abundant ($7.2 \pm 6.2\%$ for medium thick valves and $9.5 \pm 9.3\%$). While the number of thick-walled specimens is generally higher than the medium thick-walled ones from the base to BW-10A, the number of medium thick valves is higher above until the top of the lower unit. The middle unit (8.2–3.9 m) shows two samples (BW-7M and BW-6M) with very low amounts (13 and 6.7%, respectively) of thin-walled specimens and a high amount of medium thick-walled specimens (BW-6A). In samples with very low amounts of thin-walled specimens, the amount of medium thick-walled specimens is highest in BW-7M and low in BW-6M. The amounts of thick-walled specimen are increased throughout the lower part of the middle unit up to 85%.

Above a transitional sample with 73% of thin-walled specimens accompanied by a slightly increased proportion of medium thick-walled specimens (BW-5A at 5.93 m), the amounts of thin-walled specimens are strongly dominant until the upper unit (above 3.9 m below surface) again (between 83 and 98%). The top sample (BW-2A at 2.58 m) shows slightly lower amounts (63%) of thin-walled specimens, but the number of analyzed valves is low (8 valves).

4.4 Discussion

This study is a pioneering attempt to apply the size and thickness variation of the valves of *C. torosa* in a natural setting in a fossil (Holocene) succession and the first study using length and height variations of the A-1 (oldest juvenile) and adult instars.

The length and height variations of both instar A-1 and adult specimens along the section show significant changes. In contrast to the studies of Van Harten (1975) and Boomer et al. (2017), our samples contained only short adult female individuals, and despite the reconstructions of Berndt et al. (2019) indicated salinities of about 6–7‰ for at least two samples (Figures 4.2 and 4.4). The intraspecific valve thickness of this species was not described as a phenotypic feature of *C. torosa* so far. This

thickness appears to be highly sensitive to environmental changes throughout the regarded period of the Holocene (Figure 4.2).

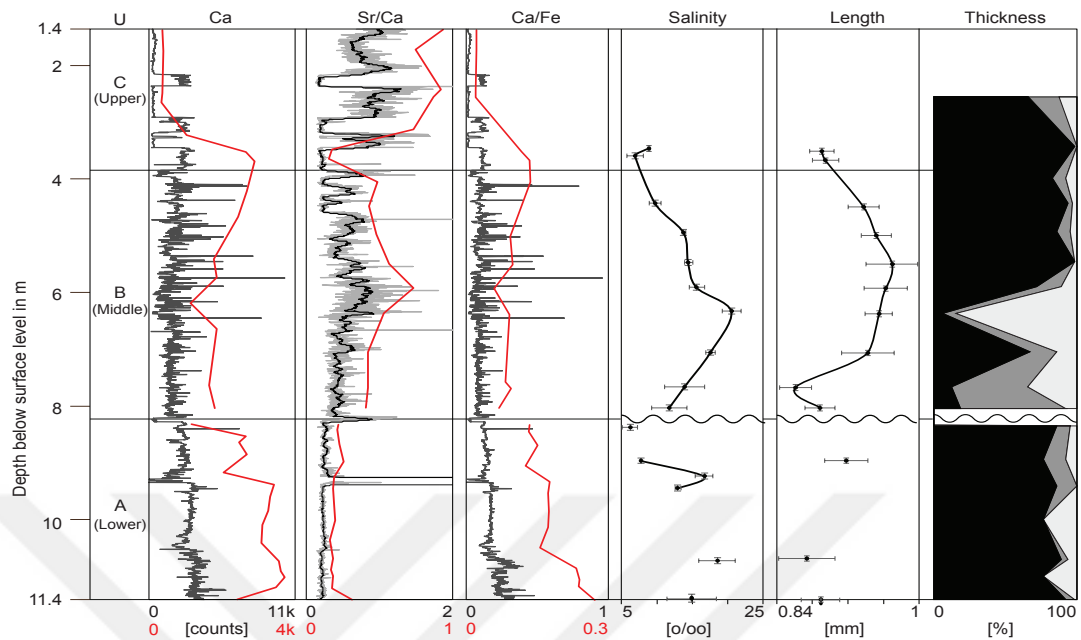


Figure 4.4 : ITRAX-XRF (Ca, Sr/Ca and Ca/Fe) measurements (XRF data from Berndt et al., 2019), valve length and thickness of *C. torosa* (this study). Red lines are mean XRF values for the ostracod sampling ranges. Remark: There are different scales between the ITRAX-XRF record and subsampled mean values.

4.4.1 Valve size-salinity relationship

The length and height on both A-1 and adult specimens correlate very well at 98% (A-1) and 91% (female adult) with each other. This implies a primary total size variation instead of a nearly pure lengthening of adult individuals within errors (Figure 4.5) and is in rough agreement with Van Harten (1975) and Boomer et al. (2017).

By comparing the size measurements of adults with the salinity reconstruction of Berndt et al. (2019), we neglected the lower unit measurements due to their punctual character in a highly variable environment (Figure 4.5). The numbers of individuals of the lower unit and within the two lowermost samples of the middle unit are small, and the salinity reconstruction of Berndt et al. (2019) shows larger errors. The studied period for the analysis is thus from 5.3 ka cal BP to about 4 ka cal BP in which a major lagoonal phase was prevailing at the eastern part of the Kızılırmak Delta covering the middle to upper units of the sediment core (Berndt et al., 2019). This phase contains two environmental shifts. At first, the lagoon formed with an

extension of a barrier leading to higher salinities due to evaporation exceeding the open sea conditions at about 5 ka cal BP. Subsequently, the lagoon was highly restricted and an increasing freshwater impact lead to low salinities with a final β -mesohaline to oligohaline lake phase starting at about 4 ka cal BP (Berndt et al., 2019).

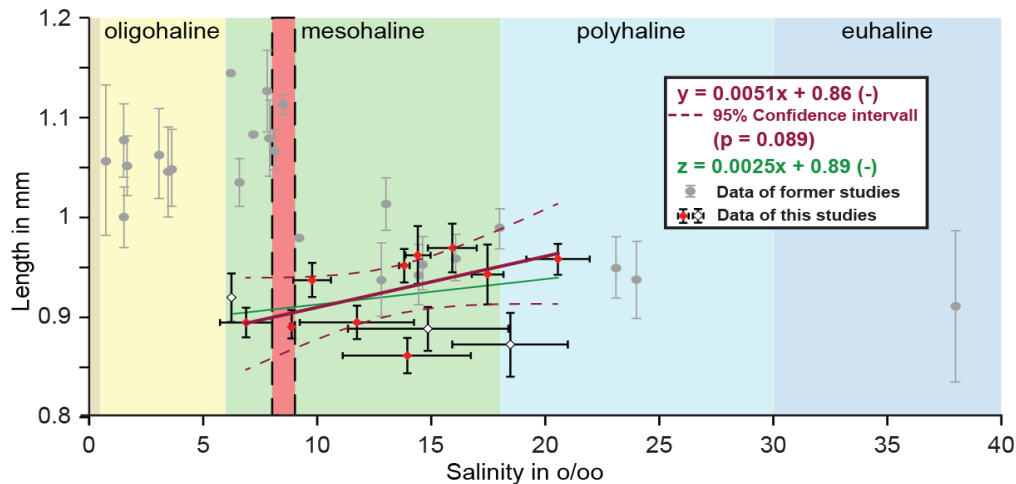


Figure 4.5 : The valve length-salinity relationship with data of former studies in grey (data from Van Harten, 1975 and Boomer et al., 2017). The trend line y excludes our whole dataset and the trend line z includes data from the lower unit.

In this part of the sediment core, the average sizes of the female adult individuals correlate well with the salinity in a positive way (Pearson correlation coefficient for height and salinity: 0.54; length and salinity: 0.56), while the size variations of instar A-1 are insignificant, and thus only the size results of female adult measurements are regarded below (Figure 4.2). Above salinities of 15‰, the length of adults is rather variable within a similar range (Figure 4.2). The error due to size differences between the left and right female valves is lower than the measurement error so that we neglect this potential error. The p-value (0.089) of the salinity-length relationship is only slightly above 0.05, indicating that other factors might influence this relationship as well. The linear regression model accepted a slope equal to zero with a p-value of $1.26 \cdot 10^{-8}$. We thus cannot exclude an independent result. However, we explain this high p-value with the low sample number and an indicated temporal offset between salinity and size. The palaeo-environment might still reach (seasonally?) previous temporal salinity values after its reconstructed salinity maximum.

The Sr/Ca ratio is related to evaporation that increases the prevailing salinity but is temperature-dependent as well (Rothwell and Croudace, 2015; Berndt et al., 2019) and correlates positively with the reconstructed salinity and length measurements (with a Pearson correlation coefficient of about 0.7 for each) (Figure 4.4). In contrast, the Ca content and Ca/Fe ratio as indicators for marine influence are negatively correlated to the salinity and Sr/Ca in a similar way and to the length to a lower degree (with a Pearson correlation coefficient of -0.3) as well (Figure 4.4). This indicates that the evaporation rates mainly control the salinity of the lagoon. This is explained as an effect of the restriction caused by increased freshwater or lower saline seawater input (Berndt et al., 2019).

The riverine freshwater input, and thus a decrease in salinity, had no significant impact on the size before the salinity dropped below 15.9‰ (Figure 4.2). The difference between sieve pore shapes and size variability might be caused by a different formation time. While the size of the valves is determined during its growth period within the molting process (Turpen and Angell, 1971; Martens, 1985), the sieve pore shape is finalized during the subsequent valve calcification process (De Deckker, 2002). This relationship additionally rules out a major impact of food availability on the size of the detritivorous species.

The deltaic plain system experienced rapid water mass changes due to mainly intra-annual to inter-annual precipitation and insolation changes and storms. Ustaoglu et al. (2012) shows that the Kızılırmak Delta plain lakes experience large salinity fluctuations between freshwater and intermediate mesohaline conditions in the recent deltaic lakes. This means that the osmoregulation of the local population of *C. torosa* is capable of managing or adapting to such low salinities and transforms its sieve pores accordingly. This high variability may lead to short-term salinities up to about 8‰ as well (Figures 4.2, 4.4 and 4.5). It is thus possible that *C. torosa* might molt preferentially to smaller-sized adult individuals, which are not expressed in juvenile instars in higher saline conditions while the mean salinity drops below 15‰.

Aladin (1989) described two kinds of osmotic regulation styles within the euryhaline species *C. torosa*: Amphiosmotic (oligohaline origin) and confohyperosmotic (brackish with marine origin). This separation agrees well with the former differentiation between *C. torosa* forma *torosa*, which displays a reaction to low saline environments, and *C. torosa* forma *littoralis*, which is dominant in marine

environments (Meisch, 2000; Frenzel et al., 2012). The individuals of our study are smallest during (near-)oligohaline conditions and at significantly lower salinities than the size-break (Boomer et al., 2017). This might confirm Aladin (1989), which mentions that *C. torosa* of the Black Sea is mainly amphiosmotic (*C. torosa* forma *torosa*). This further implies that both morphotypes are phenotypic variations of one species in shifting salinities by changing their style of osmoregulation (Frenzel et al., 2012), or that the populations of different water bodies developed specific osmoregulation (Aladin, 1989). This could explain the discrepancy between the results of Van Harten (1975), Boomer et al. (2017) and ours. However, nodes that appear regularly in *C. torosa* forma *torosa* are absent in our study, which might be caused by the lower salinity contrast between marine and terrestrial environments, which show a salinity rarely below 7‰, or environments giving sufficient time to molt in preferred conditions (Frenzel et al., 2012).

Based on these results, the salinity or the conditions bound to salinity have a significant impact on size variation. For example, Roca and Wansard (1997) showed a strong temperature relationship of *Herpetocypris brevicaudata* Kaufmann 1900 in a laboratory experiment. During the evolution of the Kızılırmak lagoon, the restriction seems to promote an increase in salinity and increasing variability of surface temperatures in the shallower and smaller water body (compare Den Hartog, 1964). Adult *C. torosa* seem to form larger valves under α -mesohaline and more stable conditions (Boomer et al., 2017). Smaller, oligohaline water bodies with increased seasonal salinity and temperature variability are expected to produce smaller valves instead. In addition, the restriction of the lagoon might cause an oxygen deficiency, which is known to be a critical factor in the growth of mollusks, e.g., Hamburger et al. (1983) and McClain and Rex (2001). However, dominance of *C. torosa* is seen in sub- to anoxic environments like harbor basins (Delile et al., 2013; Berndt, 2014), indicating a high ability to withstand oxygen deficiency. The smaller-sized adults in the lower part of the lagoonal phase of the sediment core BW with an interpreted good connection to the open sea (Berndt et al., 2019) seem to disagree with the major influence of oxygenation on size as well. Furthermore, Van Harten (1975) mentioned a possible dependency on increased environmental stress that is concurrent with the approximation of low saline environments. This seems to be plausible as a cause of

smaller valves and a final replacement by other taxa when the salinity becomes too low.

Overall, we observed a positive size feedback on salinity changes in the mesohaline range. This finding is in good agreement with the studies done on mollusks (Remane 1934; Trahms, 1939). These results fill partly the salinity gap of the former studies of Van Harten (1975) and Boomer et al. (2017). In contrast to those studies, no break in size variation by salinity was observed, although the mean salinities decreased to even near-oligohaline conditions (Berndt et al., 2019) (Figure 4.4). The absence of this size break observed by Van Harten (1975) and Boomer et al. (2017) seems to be caused by the adaptation ability of the local population or high variability of the environment. The reconstructed salinity by Berndt et al. (2019) must be taken as a mean value over a multi-decadal to multi-centennial time period so that a high variability of the salinity can be expected. Nevertheless, a causal dependency between size and osmoregulatory capabilities or stresses of this species in lower salinities needs to be tested in laboratory studies. Furthermore, the sample size is relatively low, and this study deals with material from only one location, so both should be expanded in future studies to test the applicability of this proxy further.

4.4.2 Valve thickness

The thickness of ostracod shells has been already recognized to be environmentally caused by Scott (1961). Carbonel (1988) pointed out that the ornamentation of ostracods is primarily controlled by physiology (intensity of the ornamentation) and genetics (shape of the ornamentation). In addition, Carbonel and Pinson (1979) and Carbonel (1980) described a positive correlation of the reticulation intensity of *Cyprideis* with an increased ionic concentration in the water (evaporation).

The differentiation of three different classes of valves thicknesses (translucent, brownish-less translucent, and opaque valves) unraveled significant differences along the Holocene sediment record and reflects some of the major ecological variations (Figures 4.2 and 4.3). The samples are dominated by thin-walled specimens throughout the lower and beginning in the upper middle unit to the top. Both units of the sediment core show mainly freshwater-influenced, highly variable, and more restricted environments (Berndt et al., 2019). The thicker valves dominate largely the marine lower part of the lagoon, although some variability prevails.

The pattern of the occurrence of the thicker valves reflects a good connection to the open sea, while rather restricted environments are populated by thinner specimens (Berndt et al., 2019) (Figure 4.2). Medium-thickness valves appear in large amounts in the more stable, but lower saline part of the lagoon, while thick valves dominate increasingly until the highest salinity caused by a further restriction of the lagoon and lack of freshwater influx. This agrees well with the positive valve thickness correlation and ionic concentration of the water (Remane, 1958; Carbonel, 1988). In agreement with Keyser and Walter (2004), a better connection to the higher saline open sea and its salinization improves the conditions to form thicker shells, especially in regard to ion concentration, which is crucial for the shell calcification, like calcium. In addition, the available time to calcify the shell is longest within periods of good connection to the sea, and shortest in the highly variable brackish delta plain environment. Both might explain further the dominance of thick-shelled individuals in the lower part of the middle unit. An abundance maximum of thin specimens in between might relate to an increased freshwater input/seasonality of the lagoon.

Furthermore, a good connection to the open sea implies higher oxygenation and lower but more stable temperatures. Both might be necessary to form thicker valves as well. The upper part of the lagoon is indicated to be more restricted so that periods of oxygen deficiency increase due to higher oxygen consumption following high primary productivity and restricted water mass exchange with the open sea. Lower water temperatures trigger a higher solubility of calcium carbonate (Frear and Johnston, 1929) so that the calcium ion availability is higher and more constant. This could support an easier, and thus thicker, shell calcification.

In addition, taphonomic processes like mechanical destruction and transport effects due to sorting by weight can affect preferably thin and thus more fragile and lighter specimens (Kaesler et al., 1993). This can lead to an under-representation of thinner specimens compared to the thicker, more robust ones. The lower part of the lagoonal phase is more exposed to currents, which might rework, carry away, and crush fragile specimens. Indeed, this part of the core contains a sample with a skewed assemblage (BW-6M) and plenty of broken valves (BW-7A). However, other samples showed none of both effects, thus making strong taphonomic alteration improbable.

Based on these implications, the valve thickness might be a good proxy for the differentiation of estuarine water bodies with freshwater influx and marine realms and appears to be a continuation of the loss in ornamentation by decreasing salinity within the mesohaline salinity range. This finding aims to extend the range of the application of the semi-quantitative approach of Carbonel and Pinson (1979) to reconstruct the (palaeo-)salinity by the surface characteristic of this species to mesohaline salinities, especially because the salinity range is characterized by a very low ostracod diversity that makes additional proxies necessary for environmental reconstructions. The number of samples and specimens in our study is relatively low so that future studies with more samples and comparisons between different settings are necessary to validate these preliminary interpretations, which might lead to a reliable and fast quantitative proxy to improve palaeo-reconstructions using fossil *Cyprideis*-dominated associations.

4.5 Conclusions

The current study shows a phenotypic reaction of *C. torosa* in a marginal marine environment driven by the transformation of a relatively open to a restricted lagoon and deltaic lakes in the Eastern Kızılırmak Delta. Good positive coupling of the size of adult specimens of this species in the local population and salinity was observed between about 6 and 20 ‰ (correlation coefficient of salinity to length: 0.56). This coupling seems to originate either directly from salinity changes as the main driving factor or stress that arises in more variable environments. A size break in lower mesohaline salinities, as suggested by former studies, could not be observed. That might be an osmoregulatory effect or result of molting preferences of the local population. Surprisingly, instar A-1 sizes seem to be independent of the surrounding salinity and change in significant levels only in highly variable environments.

The valve thickness seems to work as a simple proxy for evaluating marginal marine environments dominated by freshwater (thin) or marine (thick) influence. Our results imply a similar reaction of *C. torosa* like mollusks to decreasing or shorter availabilities of sufficient calcium ion concentrations in the habitat by forming thinner shells.



6. CONCLUSIONS AND FUTURE PROSPECTS

River deltas are one of the most variable environments of the world. Those landforms are affected by several factors determining their shape and appearance. The deposited sediments are recorders for local, regional and global environmental changes over different timescales so that those bear a wealth of information about the geological past. The aim of the study was to understand the processes impacting on the development of the Kızılırmak Delta at the northern margin Central Anatolian Plateau to the Black Sea. In this thesis, I studied the Late Quaternary tectonic impact of the North Anatolian Fault on the Kızılırmak Delta, the palaeoenvironmental evolution of this delta during Holocene and how the environmental factors, in turn, modified the morphometric appearance on ostracod species.

In the first part of the thesis I focused on the tectonic impact of the North Anatolian Fault on the Kızılırmak Delta. Mapping of fluvial, marine and delta terraces along the lower stream of Kızılırmak River revealed the presence of nine terrace levels up to 123 m above the river; the lowermost one being equal to the recent river plain and three of them forming major delta terraces. In addition, the sea sculpted coastal terraces at three levels into the northern fringe of the delta terrace platform. The OSL-dating of the terrace sediments together with a newly developed best-fit uplift model revealed that those terraces have formed by a relatively constant uplift of 0.28 m/ka since 545 ka. This tectonic displacement even raised up two terrace levels, which were formed during MIS 12 and MIS 10 lowstands of the Black Sea. The uplift rate together with regional information from northern and central Turkey indicate a differential uplift with distance to the main strand of the North Anatolian Fault, which causes compressive accelerated regional uplift compared to the slowly uplifting Central Anatolian Plateau. The relatively constant and sub-horizontal movement implies a deep-rooted source forcing this uplift.

The second part of the thesis addresses the Holocene evolution of the Kızılırmak Delta by using ostracod assemblages and morphometries in the sediment core BW supported by the sediment's geochemistry. This study revealed a

palaeoenvironmental development since 7.9 ka cal BP at the eastern part of the delta plain. The environments were α -mesohaline to polyhaline and up to 5 m deep palaeo-lagoons while freshwater impact during restrictive periods leads to β -mesohaline and eventually oligohaline conditions similar to the delta lakes at present. The two major influencing factors affecting the ostracod associations are the restriction from the open sea and the stability of the lake habitats. Lagoonal environments are represented predominantly by the appearance of *Cyprideis torosa* (Jones). This species co-inhabits the palaeo-lagoons with *Loxoconcha* spp. in phases with better connection to the open sea and *Amnicythere* spp. in phases of increased fluvial water impact. The transformation to limnic environments lead to a dominance of *Candona* sp. and *Pseudocandona* sp. dominates in an oligohaline lake environment.

Lagoonal restrictions and openings between 7.9 and 7 ka cal BP are forced primarily by frequent sea level variations accompanied by high sedimentation rates and fluvial impact. An apparent 1700 year-long hiatus with questionable origin occurs from 7 to 5.3 ka cal BP. The plateau became drier over time triggering a relatively stable lagoonal environment. Salinity of the palaeo-lagoon increases to polyhaline conditions until about 5 ka cal BP due to increased restriction, while the Black Sea sea level reached near-recent levels. Freshwater influence reduces the salinity and progressive restriction from the open sea transforms the palaeo-lagoon to a mesohaline lake short after 4 ka cal BP. Another short-term lagoon forms presumably as a result of the 'Late Bronze Age megadrought' between 3.7 and 3 ka cal BP. A correlation of the historic population phases of İkiştepe with the lagoonal phases indicates a cultural or economic dependency on the prevailing palaeogeographic setting during Late Chalcolithic and Bronze Ages.

The third part of the thesis deals with the retro-action of the environmental factors on the species. The valve size and shell thickness of *Cyprideis torosa* were studied along a Holocene sediment core section. The size variability of adult individuals shows a good positive correlation to salinity changes along the sediment core BW within the mesohaline range. A lack of large-sized individuals is interpreted as the effect of the local population. The size of individuals of the penultimate ontogenetic stage lacks of a clear correlation to the salinity variations. The shell thickness is rather thin throughout most of the studied core section, but thick within a relatively stable lagoon phase with increased marine influence. This presence of mainly thick-

shelled individuals indicates a similar relation of the intraspecific shell thickness to a marine environment like mollusks.

In conclusion, the Kızılırmak Delta is highly affected by the tectonic activity of the North Anatolian Fault Zone. The delta's environment is shaped by the climate of Anatolia and sea level variations during Holocene. In turn, those environmental factors modify also the morphological appearance of ostracod species.

However, the studied delta terrace platform and lower stream of the Kızılırmak River represents a rather narrow area within the orogenic wedge of the Central Pontides and no significant uplift variation was observed. More spatial and long-term data need to be acquired, especially from higher elevated geomorphological features (e.g., wind gaps). Those future investigations will help to examine the evolution of the northern margin of the Central Anatolian Plateau in relation with the impact of the North Anatolian Fault.

Future studies might be able to recover deeper sediments of the Kızılırmak Delta to examine the delta development before and during the highly-disputed last reconnection of the Black Sea. Furthermore, the 1700 year-long hiatus (7 to 5.3 ka cal BP) remains of questionable origin and this should be further investigated. In addition, a high-resolved study of the sediment core BW might give an important insight into the climate of Anatolia, its future and the degree of antropogenic impact.

Finally, the phenotypic morphological variability of this species has been recognized as a valuable proxy over the last decades for environmental changes. Because of that, the morphological variability seems to show a good potential to create a future transfer function of the size and shell thickness of this or other species to environmental parameters. Such quantification could expand the ostracodological toolbox for palaeoenvironmental reconstructions and can give valuable information of (palaeo-) environments containing a low diverse ostracod fauna.



REFERENCES

- Akçer Ön, S.** (2011). *Late Holocene climatic records from Küçükçekmece Lagoon, Yeniçağa, Uludağ glacial and Bafa lakes (western turkey): Comparison with records from Europe and Middle East* (Ph. D. thesis). Istanbul Technical University, EMCOL and Eurasia Institute of Earth Sciences, Istanbul.
- Akkan, E.** (1970). Geomorphology of the Kızılırmak Valley. *Publications of the Faculty of Language and History–Geography of Ankara University*, **191**, 158pp.
- Aksu, A. E., Hiscott, R. N., Mudie, P. J., Rochon, A., Kaminski, M. A., Abrajano, T., and Yaar, D.** (2002). Persistent Holocene outflow from the Black Sea to the Eastern Mediterranean contradicts Noah's Flood hypothesis. *GSA Today*, **12(5)**, 4-10.
- Aladin, N.V.** (1989). Osmoregulation in *Cyprideis torosa* from various seas of the USSR. *Zool. Zhurnal*, **68**, 40–50.
- Alkim, U. B., Alkim, H., and Bilgi, Ö.** (1988). İkiztepe. Ankara, *Türk Tarih Kurumu Basımevi*.
- Alkim, U. B., Alkim, H., and Bilgi, Ö.** (2003). İkiztepe: üçüncü, dördüncü, beşinci, altıncı, yedinci dönem kazıları (1976-1980). Ankara, *Türk Tarih Kurumu Basımevi*.
- Allen, J. R.** (2000). Morphodynamics of Holocene salt marshes: a review sketch from the Atlantic and Southern North Sea coasts of Europe. *Quaternary Science Reviews*, **19(12)**, 1155-1231.
- Allen, M. B., Saville, C., Blanc, E., Talebian, M., and Nissen, E.** (2013). Orogenic plateau growth: Expansion of the Turkish-Iranian Plateau across the Zagros fold-and-thrust belt. *Tectonics*, **32(2)**, 171-190.
- Allmendinger, R. W., Jordan, T. E., Kay, S. M., and Isacks, B. L.** (1997). The evolution of the Altiplano-Puna plateau of the Central Andes. *Annu. Rev. Earth Planet. Sci.* **25(1)**, 139-174.
- Almogi-Labin, A., Perelis-Grossovicz, L., and Raab, M.** (1992). Note: *Ammonia beccarii tepida* - a doubtful indicator of a Pliocene marine ingression into the southern Jordan Valley. *Israel Journal Earth Sciences*, **40**, 255-256.
- Alpar, B.** (2009). Vulnerability of Turkish coasts to accelerated sea-level rise. *Geomorphology*, **107(1-2)**, 58-63.
- Alpar, B., Dogan, E., Yuce, H., and Altıok, H.** (2000). Sea level changes along the Turkish coasts of the Black Sea, the Aegean Sea and the Eastern Mediterranean. *Mediterranean Marine Science*, **1(1)**, 141-156.

- Arslan, H., Guler, M., Cemek, B., and Demir, Y.** (2007). Assessment of groundwater quality in Bafra plain for irrigation. *Journal of Tekirdağ Agricultural Faculty*, 4(2), 219–226.
- Aydar, E., Cubukcu, H. E., Şen, E., and Akın, L.** (2013). Central Anatolian Plateau, Turkey: incision and paleoaltimetry recorded from volcanic rocks. *Turkish J Earth Sci*, 22, 739-746.
- Badertscher, S., Fleitmann, D., Cheng, H., Edwards, R. L., Göktürk, O. M., Zumbühl, A., ...Tüysüz, O.** (2011). Pleistocene water intrusions from the Mediterranean and Caspian seas into the Black Sea. *Nature Geoscience*, 4(4), 236-239.
- Bahr, A., Lamy, F., Arz, H., Kuhlmann, H., and Wefer, G.** (2005). Late glacial to Holocene climate and sedimentation history in the NW Black Sea. *Marine Geology*, 214(4), 309-322.
- Bahr, A., Lamy, F., Arz, H. W., Major, C., Kwiecien, O., and Wefer, G.** (2008). Abrupt changes of temperature and water chemistry in the late Pleistocene and early Holocene Black Sea. *Geochemistry, Geophysics, Geosystems*, 9(1).
- Bakker, J., Paulissen, E., Kaniewski, D., De Laet, V., Verstraeten, G., and Waelkens, M.** (2012). Man, vegetation and climate during the Holocene in the territory of Sagalassos, Western Taurus Mountains, SW Turkey. *Vegetation history and archaeobotany*, 21(4-5), 249-266.
- Balabanov, I. P.** (2007). Holocene sea-level changes of the Black Sea. In Yanko-Hombach, V., Gilbert, A. S., Panin, N., Dolukhanov, P. M. (Eds.), *The Black Sea Flood Question: Changes in Coastline, Climate, and Human Settlement*. Dordrecht : Springer Science and Business Media. 711-730.
- Banerjee, D., Bøtter-Jensen, L., and Murray A.S.** (1999). Retrospective Dosimetry: preliminary use of the single aliquot regeneration (SAR) protocol for the measurement of quartz dose in young house bricks. *Radiat. Prot. Dosime.*, 84, 421-426.
- Bard, E., Hamelin, B., Arnold, M., Montaggioni, L., Cabioch, G., Faure, G., and Rougerie, F.** (1996). Deglacial sea-level record from Tahiti corals and the timing of global meltwater discharge. *Nature*, 382(6588), 241.
- Bartol, J., and Govers, R.** (2009). Flexure due to the Messinian-Pontian sea level drop in the Black Sea. *Geochemistry, Geophysics, Geosystems*, 10(10).
- Behre K.-E.** (2003). Eine neue Meeresspiegelkurve für die südliche Nordsee. Transgressionen und Regressionen in den letzten 10.000 Jahren. In Strahl, E., Bungenstock, F., Ey, J., Wolters, S., Kiepe, R., Spath, L. (Eds.), *Probleme der Küstenforschung im südlichen Nordseegebiet*. Iseensee, Oldenburg, Lower Saxony Institute for Historical Coastal Research, 28, 9-63.
- Berger, J. F., Lespez, L., Kuzucuoğlu, C., Glais, A., Hourani, F., Barra, A., and Guilaine J.** (2016). Interactions between climate change and human

activities during the early to mid-Holocene in the eastern Mediterranean basins. *Climate of the Past*, 12(9).

- Berndt, C.** (2014). Combined Micropalaeontological and Heavy Mineral Investigation of Holocene Sediments from Elaia, the Ancient Harbour City of Pergamum (Turkey). Master's Thesis, Institute of Earth Sciences, Friedrich Schiller University Jena, Jena, Germany.
- Berndt, C., Yıldırım, C., Çiner, A., Strecker, M. R., A., Ertunç, G., Sarıkaya, M. A., ... and Kiyak, N. G.** (2018). Quaternary uplift of the northern margin of the Central Anatolian Plateau: New OSL dates of fluvial and delta-terrace deposits of the Kızılırmak River, Black Sea coast, Turkey. *Quaternary Science Reviews*, 201, 446-469.
- Berndt, C., Frenzel, P., Çiner, A., Ertunç, G., and Yıldırım, C.** (2019). Holocene marginal marine ostracod successions from the Kızılırmak River delta; Implications for depositional environments and sea level changes at the southern Black Sea coast. *Sediment. Geology*, 382, 103-121.
- Berndt, C., Frenzel, P., and Çiner, A.** (2019). Intraspecific length variation and shell thickness of the ostracod *Cyprideis torosa* (Jones, 1850) as a potential tool for palaeosalinity characterization. *Geosciences*, 9, 83.
- Bhattacharya, J. P.** (2003). Deltas and estuaries. In Middleton, G.V. (Ed.), *Encyclopedia of Sediments and Sedimentary Rocks*, Kluwer, Dordrecht, 195–203.
- Bilgi, Ö.** (1999). İkiztepe in the Late Iron Age. *Anatolian studies*, 49, 27-54.
- Bilgin, T.** (1963). Ünye batısında Akçay Pleistosen taraçaları. *Istanb. Üniv. Coğraf. Enst. Derg.*, 7(13), 3.
- Bintanja, R., van de Wal, R. S., and Oerlemans, J.** (2005). Modelled atmospheric temperatures and global sea levels over the past million years. *Nature*, 437(7055), 125-128.
- Blum, M. D., and Törnqvist, T. E.** (2000). Fluvial responses to climate and sea-level change: a review and look forward. *Sedimentology*, 47, 2-48.
- Boğaziçi University Kandilli Observatory and Earthquake Research Institute** (2017). International Federation of Digital Seismograph Networks. *Other/Seismic Network*. 10.7914/SN/KO.
- Bohnhoff, M., Martínez-Garzón, P., Bulut, F., Stierle, E., and Ben-Zion, Y.** (2016). Maximum earthquake magnitudes along different sections of the North Anatolian fault zone. *Tectonophysics*, 674, 147-165.
- Bolikhovskaya, N. S., Porotov, A. V., Richards, K., Kaitamba, M. D., Faustov, S. S., and Korotaev, V. N.** (2018). Detailed reconstructions of Holocene climate and environmental changes in the Taman Peninsula (Kuban River delta region) and their correlation with rapid sea-level fluctuations of the Black Sea. *Quaternary International*, 465, 22-36.
- Bony, G., Morhange, C., Marriner, N., Baralis, A., Kaniewski, D., Rossignol, I., and Lungu, V.** (2015). History and influence of the Danube delta lobes on the evolution of the ancient harbour of Orgame (Dobrogea, Romania). *Journal of Archaeological Science*, 61, 186-203.

- Boomer, I., and Eisenhauer, G.** (2002). Ostracod faunas as palaeoenvironmental indicators in marginal marine environments. In Holmes, J. A., Chivas, A. R. (Eds.), *The Ostracoda: applications in Quaternary research*. American Geophysical Union, Geophysical Monograph Series, 131. 135-149.
- Boomer, I., Horne, D.J., Slipper, I.J.** (2003). The use of ostracods in palaeoenvironmental studies, or what can you do with an ostracod shell? *Paleontol. Soc. Pap.*, 9, 153–180.
- Boomer, I., Guichard, F., and Lericolais, G.** (2010). Late Pleistocene to Recent ostracod assemblages from the western Black Sea. *Journal of Micropalaeontology*, 29(2), 119-133.
- Boomer, I., Frenzel, P., Feike, M.** (2017). Salinity-driven size variability in *Cyprideis torosa* (Ostracoda, Crustacea). *J. Micropalaeontol.*, 36, 63–69.
- Bottema, S., Woldring, H., and Aytug, B.** (1995). Late Quaternary vegetation history of northern Turkey. *Palaeohistoria*, 35–36, 13–72.
- Bøtter-Jensen, L.** (1997). Luminescence techniques: instrumentation and methods. *Radiation Measurements*, 17, 749-768.
- Bradley, P.S.** (1941). The shell structure of the Ostracoda and its Application to their Palaeontological investigation. *Ann. Mag. Nat. Hist.*, 8, 1–33.
- Bradley, R.S.** (2015). *Paleoclimatology (Third Edition): Reconstructing Climates of the Quaternary*. Elsevier Academic Press, San Diego (675 pp.).
- Brandão, S. N., Angel, M. V., Karanovic, I., Perrier, V., and Meidla, T.** (2018). World Ostracoda Database. Access: 30 October, 2018. <http://www.marinespecies.org>.
- Brückner, H., Kelterbaum, D., Marunchak, O., Porotov, A., and Vött, A.** (2010). The Holocene sea level story since 7500 BP—Lessons from the Eastern Mediterranean, the Black and the Azov Seas. *Quaternary International*, 225(2), 160-179.
- Bull, W. B.** (1991). Geomorphic responses to climatic change. U.S. Department of Energy.
- Burbank, D. W., and Anderson, R. S.** (2011). *Tectonic geomorphology*. John Wiley & Sons.
- Burney, C. A.** (1956). Northern Anatolia before Classical Times. *Anatolian Studies*, 6, 179-203.
- Butler, S.** (1907). Atlas of Ancient and Classical Geography. J. M. Dent & Sons Ltd., London, E.P. Dutton & Co. Inc., New York.
- Çağatay, M. N., Öğretmen, N., Damcı, E., Stockhecke, M., Sancar, Ü., Eriş, K. K., and Özeren, S.** (2014). Lake level and climate records of the last 90ka from the Northern Basin of Lake Van, eastern Turkey. *Quaternary Science Reviews*, 104, 97-116.
- Can, Ö., and Taş, B.** (2012). RAMSAR alanı içinde yer alan Cernek Gölü ve sulak alanının (Kızılırmak Deltası, Samsun) Ekolojik ve sosyo-ekonomik önemi. Türk Bilim Araştırma Vakfı, *Bilim Dergisi*, 5(2), 1-11.

- Carbonel, P.** (1980). Les Ostracodes et Leur Intérêt Dans la Définition des Écosystèmes Estuariens et de Plateforme Continentale: Essais D'application à des Domaines Anciens. Mémoires de l'Institut de Géologie du Bassin d'Aquitaine, Université de Bordeaux I, Bordeaux, France, *11*.
- Carbonel, P.** (1988). Ostracods and the transition between fresh and saline waters. In *Ostracoda in the Earth Sciences*, Amsterdam, The Netherlands: Elsevier, 157–173.
- Carbonel, P. and Pinson, J.** (1979). Les Cyprideis Témoins de L'évolution des Sels en Milieu Laguno-Lacustre Sous Climat Semi-Aride; In Krstic, N. (Ed.) *Taxonomy, Biostratigraphy and Distribution of Ostracodes*, Proceedings of the 7th International Symposium on Ostracoda, Serbian Geological Society: Belgrade, SFR Yugoslavia, 211-217.
- Cavazza, W., Cattò, S., Zattin, M., Okay, A. I., and Reiners, P.** (2018). Thermochronology of the Miocene Arabia-Eurasia collision zone of southeastern Turkey. *Geosphere*, *14*, 2277-2293.
- Champion, D. E., Dalrymple, G. B., and Kuntz, M. A.** (1981). Radiometric and palaeomagnetic evidence for the Emperor Reversed Polarity Event at 0.46 ± 0.05 M.Y. in basalt lava flows from the eastern Snake River Plain, Idaho. *Geophysical Research Letters*, *8*, 1055-1058.
- Chekhovskaya M. P., Khusid T.A., Matul A. S., Stepanova A. Y., and Rakowski A. Z.** (2014). Late Pleistocene-Holocene ostracod assemblages of the northern Caspian Sea shelf. *Oceanology*, *54*(2), 212-221.
- Çiner, A., Strecker, M.R., and Bertotti, G.** (2013). Late Cenozoic Evolution of the Central Anatolia Plateau: Preface. *Turkish Journal of Earth Sciences*, *22*, i-ii.
- Çiner, A., Doğan, U., Yıldırım, C., Akçar, N., Ivy-Ochs, S., Alfimov, V., ... and Schlüchter, C.** (2015). Quaternary uplift rates of the Central Anatolia Plateau, Turkey: Insights from cosmogenic isochron-burial nuclide dating of the Kızılırmak River terraces. *Quaternary Science Reviews*, *107*, 81-97.
- CloudCompare (version 2.8.0) [GPL software]** (2016). Retrieved from <http://www.cloudcompare.org/>
- Cosentino, D., Schildgen, T. F., Cipollari, P., Faranda, C., Gliozzi, E., Hudáčeková, N., ... and Strecker, M. R.** (2012). Late Miocene surface uplift of the southern margin of the Central Anatolian Plateau, Central Taurides, Turkey. *GSA Bulletin*, *124*(1-2), 133-145.
- Dabkowski, P., Buczynski, P., Zawal, A., Stepień, E., Buczyńska, E., Stryjecki, R., ... and Szenejko, M.** (2016). The impact of dredging of a small lowland river on water beetle fauna (Coleoptera). *Journal of Limnology*, *75*(3).
- De Deckker, P., Forester, R. M.** (1988). The use of ostracods to reconstruct continental palaeoenvironmental records. In *Ostracoda in the Earth Sciences*, Amsterdam, The Netherlands: Elsevier, 175–199.

- De Deckker, P.** (2002). Ostracod palaeoecology. In Holmes, J.A., Chivas, A.R., (Eds.) *The Ostracoda: Applications in Quaternary Research*, n: Washington D. C., USA: Geophysical Monograph Series; American Geophysical Union, 131, 121–134.
- Defant, A.** (1961). *Physical Oceanography. Volume II*. Oxford : Pergamon Press, 598 pp.
- Demir, O.** (2005). Jeoloji Haritası 1/25.000. *Türkiye Petrolleri Anonim Ortaklığı (TPAO) (Turkish Petroleum Corporation)*.
- Demir, T., Yeşilnacar, İ., and Westaway, R.** (2004). River terrace sequences in Turkey: Sources of evidence for lateral variations in regional uplift. *Proceedings of the Geologists' Association*, 115(4), 289-311.
- Demirkalp, F. Y., Çağlar, S. S., Saygı, Y., Gündüz, E., Kaynaş, S., and Kılınç, S.** (2004). Preliminary limnological survey on the shallow lagoon Lake Çernek (Samsun, Turkey): Phytoplankton and zooplankton community structure, in relation to physical and chemical variables. *Fresenius Environmental Bulletin*, 13(6), 508-518.
- Demirkalp, F. Y., Gündüz, E., Çağlar, S. S., Saygı, Y., and Bayarı, S.** (2006). Liman Gölü limnolojisi ve ekonomik öneme sahip balık populasyonları üzerine araştırmalar. Project: TBAG-2196, Final report, Ankara : Türkiye Bilimsel ve Teknolojik Araştırma Kurumu.
- Demirkalp, F. Y., Saygı, Y., Gündüz, E., Çağlar, S. S., Kılınç, S.** (2010). Limnological assessment on the brackish shallow Liman Lake from Kızılırmak Delta (Turkey). *Journal of Animal and Veterinary Advances*, 9(16), 2132-2139.
- Den Hartog, C.** (1964). Typologie des Brackwassers. *Helgoländer Wiss. Meeresunters.*, 10, 377.
- Doğan, U.** (2010). Fluvial response to climate change during and after the Last Glacial Maximum in Central Anatolia, Turkey. *Quaternary International*, 222(1-2), 221-229.
- Doğan, U.** (2011). Climate-controlled river terrace formation in the Kızılırmak Valley, Cappadocia section, Turkey: inferred from Ar–Ar dating of Quaternary basalts and terraces stratigraphy. *Geomorphology*, 126(1-2), 66-81.
- Duman, T.Y., Çan, T., and Emre, Ö.** (2011). 1:1,500,000 scale Landslide Inventory Map of Turkey. Ankara-Turkey, *General Directorate of Mineral Research and Exploration, Special Publication Series*, 27.
- Dykan, N.** (2016). *Neogene–Quaternary ostracodes of the Northern part of the Black Sea*. Publishing House “Chetverta Hvylyja”, Kiev (272 pp.).
- Eastwood, W. J., Leng, M. J., Roberts, N., and Davis, B.** (2007). Holocene climate change in the eastern Mediterranean region: a comparison of stable isotope and pollen data from Lake Gölhisar, southwest Turkey. *Journal of Quaternary Science*, 22(4), 327-341.
- Emre, Ö., O. Tüysüz, and C. Yildirim** (2009). Uplift of Pontide orogenic belt since the late Miocene, paper presented at 2nd International Symposium on

the Geology of the Black Sea Region, Maden Tetk. ve Arama Congress Cent., Ankara, 5–9 Oct.

- Emre, Ö., Özalp, S., Duman, T. Y., and Kondo, H.** (2012). 1:250.000 Scale Active Fault Map Series of Turkey, Sinop (NK 36-12) and Samsun (NK 37-9) Quadrangles. Ankara, *General Directorate of Mineral Research and Exploration, Serial Number: 29*.
- Engel, M., Brückner, H., Pint, A., Wellbrock, K., Ginau, A., Voss, P., ... and Frenzel, P.** (2012). The early Holocene humid period in NW Saudi Arabia–Sediments, microfossils and paleo-hydrological modelling. *Quaternary International*, 266, 131-141.
- Erginal, A. E. and Öztürk, M. Z.** (2010). Kızılırmak Deltası plaj sırtlarının taramalı elektron mikroskobu analizleri ve tane boyu parametreleri ile incelenmesi (An assessment of beach ridges on the Kızılırmak delta based on scanning electron microscopy analyses and grain size parameters). *Türk Coğrafya Derg.*, 54, 43–51.
- Erginal, A. E., Ekinci, Y. L., Demirci, A., Elmas, E. K., and Kaya, H.** (2012). First note on Holocene coquinite on Thrace (Black Sea) coast of Turkey. *Sedimentary Geology*, 267, 55–62.
- Erginal, A. E., Ekinci, Y. L., Demirci, A., Bozcu, M., Ozturk, M. Z., Avcioglu, M., and Oztura, E.** (2013). First record of beachrock on Black Sea coast of Turkey: implications for Late Holocene sea-level fluctuations. *Sedimentary Geology*, 294, 294-302.
- Eriş, K. K., Ryan, W. B. F., Çağatay, M. N., Sancar, U., Lericolais, G., Menot, G., and Bard, E.** (2007). The timing and evolution of the post-glacial transgression across the Sea of Marmara shelf south of İstanbul. *Marine Geology*, 243, 57-76.
- Eriş, K. K., Çağatay, M. N., Akçer, S., Gasperini, L., and Mart, Y.** (2011). Late glacial to Holocene sea-level changes in the Sea of Marmara: new evidence from high-resolution seismics and core studies. *Geo-Marine Letters*, 31(1), 1-18.
- Espurt, N., Hippolyte, J. C., Kaymakci, N., and Sangu, E.** (2014). Lithospheric structural control on inversion of the southern margin of the Black Sea Basin, Central Pontides, Turkey. *Lithosphere*, 6(1), 26-34.
- Fedorov, P.V.** (1977). Pozdnechetvertichnaia istoriia Chernogo moria i razvitie iuzhnykh morei Evropy [Late Quaternary history of the Black Sea and evolution of the southern seas of Europe]. In Kaplin, P.A., Shcherbakov, F.A. (Eds.), *Paleogeografiia i otlozheniia pleistotsena iuzhnykh morei SSSR [Pleistocene Paleogeography and Sediments of the Southern Seas of the USSR]*. Nauka, Moscow, 25–32 (In Russian).
- Filipova-Marinova, M.** (2007). Archaeological and palaeontological evidence of climate dynamics, sea-level change, and coastline migration in the Bulgarian sector of the Circum-Pontic region. In Yanko-Hombach, V., Gilbert, A. S., Panin, N., and Dolukhanov, P. M. (Eds.), *The Black Sea Flood Question: Changes in Coastline, Climate and Human Settlement*. Dordrecht: Springer Science and Business Media.

- Fouache, E., Kelterbaum, D., Brückner, H., Lericolais, G., Porotov, A., and Dikarev, V.** (2012). The Late Holocene evolution of the Black Sea—a critical view on the so-called Phanagorian regression. *Quaternary International*, 266, 162–174.
- Frear, G. L., and Johnston, J.** (1929). The solubility of calcium carbonate (calcite) in certain aqueous solutions at 25°. *J. Am. Chem. Soc.*, 51, 2082–2093.
- Frenzel, P., and Boomer, I.** (2005). The use of ostracods from marginal marine, brackish waters as bioindicators of modern and Quaternary environmental change. *Palaeogeography, Palaeoclimatology, Palaeoecology*, 225(1-4), 68-92.
- Frenzel, P., Keyser, D., and Viehberg, F. A.** (2010). An illustrated key and (palaeo) ecological primer for Postglacial to Recent Ostracoda (Crustacea) of the Baltic Sea. *Boreas*, 39(3), 567-575.
- Frenzel, P., Schulze, I., Pint, A., Boomer, I., and Feike, M.** (2011). Salinity dependant morphological variation in *Cyprideis torosa*. *Joannea Geologie und Paläontologie*, 11, 59–61.
- Frenzel, P., Schulze, I., and Pint, A.** (2012). Noding of *Cyprideis torosa* valves (Ostracoda)—A proxy for salinity? New data from field observations and a long-term microcosm experiment. *Int. Rev. Hydrobiol.*, 97, 314–329.
- Frenzel, P., Ewald, J., and Pint, A.** (2016). Salinity-dependent sieve pore variability in *Cyprideis torosa*: an experiment. *Journal of Micropalaeontology*, 36(1), 57-62.
- Fulton, J. M., Arthur, M. A., and Freeman, K. H.** (2012). Black Sea nitrogen cycling and the preservation of phytoplankton $\delta^{15}\text{N}$ signals during the Holocene. *Global Biogeochemical Cycles*, 26(2).
- Fürstenberg, S., Frenzel, P., Peng, P., Henkel, K., and Wrozyna, C.** (2015). Phenotypical variation in *Leucocytherella sinensis* Huang, 1982 (Ostracoda): a new proxy for palaeosalinity in Tibetan lakes. *Hydrobiologia*, 751(1), 55-72.
- Garziona, C. N., McQuarrie, N., Perez, N. D., Ehlers, T. A., Beck, S. L., Kar, N., ... and Horton, B. K.** (2017). Tectonic evolution of the Central Andean plateau and implications for the growth of plateaus. *Annual Review of Earth and Planetary Sciences*, 45, 529-559.
- Giosan, L., Donnelly, J. P., Constantinescu, S., Filip, F., Ovejanu, I., Vespremeanu-Stroe, A., ... and Duller, G. A.** (2006). Young Danube delta documents stable Black Sea level since the middle Holocene: Morphodynamic, palaeogeographic, and archaeological implications. *Geology*, 34(9), 757-760.
- Giosan, L., Syvitski, J., Constantinescu, S., and Day, J.** (2014). Climate change: protect the world's deltas. *Nature News*, 516(7529), 31.
- Gofman, E. A.** (1966). Ecology of Modern and Novocaspian Ostracods of the Caspian Sea. *Akademie NAUK*, Moscow, USSR. 183 pp.

- Göktürk, O. M.** (2011). *Climate in the Eastern Mediterranean through the Holocene inferred from Turkish stalagmites* (Ph. D. thesis), University of Bern, Institute of Geological Sciences, Bern, Switzerland (113 pp.).
- Göktürk, O. M., Fleitmann, D., Badertscher, S., Cheng, H., Edwards, R. L., Leuenberger, M., ... and Kramers, J.** (2011). Climate on the southern Black Sea coast during the Holocene: implications from the Sofular Cave record. *Quaternary Science Reviews*, 30(19-20), 2433-2445.
- Görür, N.** (1988). Timing of opening of the Black Sea basin. *Tectonophysics*, 147, 247-262.
- Görür, N., Tüysüz, O., and Celal Şengör, A. M.** (1998). Tectonic evolution of the central Anatolian basins. *International Geology Review*, 40(9), 831-850.
- Görür, N., Çağatay, M. N., Emre, Ö., Alpar, B., Sakıncı, M., İslamoğlu, Y., ... and Karlık, G.** (2001). Is the abrupt drowning of the Black Sea shelf at 7150 yr BP a myth? *Marine Geology*, 176, 65–73.
- Grigorovich, I. A., Therriault, T. W., and MacIsaac, H. J.** (2003). History of aquatic invertebrate invasions in the Caspian Sea. *Biological Invasions*, 5(1), 103-115.
- Grimm, E. C.** (1987). CONISS: a FORTRAN 77 program for stratigraphically constrained cluster analysis by the method of incremental sum of squares. *Computers and Geosciences*, 13(1), 13-35.
- Gündüz, E., Saygi, Y., Demirkalp, F. Y., Çağlar, S. S., Atasagun, S., and Kilinc, S.** (2013). Seasonal composition and population density of zooplankton in Lake Karaboğaz from the Kızılırmak Delta (Samsun, Turkey). *Turkish Journal of Zoology*, 37(5), 544-553.
- Hamburger, K., Møhlenberg, F., Randløv, A., Riisgård, H.U.** (1983). Size, oxygen consumption and growth in the mussel *Mytilus edulis*. *Mar. Boil.*, 75, 303–306.
- Hammer, Ø., Harper, D. A. T., and Ryan, P. D.** (2001). PAST: paleontological statistics software package for education and data analysis. *Palaeontologia Electronica*, 4, 1–9. http://palaeo-electronica.org/2001_1/past/issue1_01.htm.
- Handl, M., Mostafawi, N., and Brückner, H.** (1999). Ostracodenforschung als Werkzeug der Paläogeographie. *Marburger Geographische Schriften*, 134, 116-153.
- Hartmann, G.** (1963). Zur Morphologie und Ökologie rezenter Ostracoden und deren Bedeutung bei der Unterscheidung mariner und nichtmariner Sedimente. *Fortschr. Der Geol. Rheinl. Westfal.*, 10, 67–80.
- Haşimoğlu, B. Y., Çifçi, G., Lacassin, R., Fernández-Blanco, D., and Özel, Ö.** (2016). Tectonics of the Kızılırmak Delta and Sinop Basin, offshore Pontides, evidence from new, high resolution seismic and bathymetric data. American Geophysical Union, Fall Meeting 2016, 12-16 December, 2016, Abstracts.

- Hay, B. J., Arthur, M. A., Dean, W. E., Neff, E. D., and Honjo, S.** (1991). Sediment deposition in the Late Holocene abyssal Black Sea with climatic and chronological implications. *Deep Sea Research Part A. Oceanographic Research Papers*, 38, 1211-1235.
- Heip, C.** (1976). The life-cycle of *Cyprideis torosa* (Crustacea, Ostracoda). *Oecologia*, 24, 229–245.
- Herrle, J. O., Bollmann, J., Gebühr, C., Schulz, H., Sheward, R. M., and Giesenberg, A.** (2018). Black Sea outflow response to Holocene meltwater events. *Scientific reports*, 8(1), 4081.
- Hippolyte, J. C., Espurt, N., Kaymakci, N., Sangu, E., and Müller, C.** (2016). Cross-sectional anatomy and geodynamic evolution of the Central Pontide orogenic belt (northern Turkey). *International Journal of Earth Sciences*, 105(1), 81-106.
- Hoefs, J.** (2009). *Stable Isotope Geochemistry*. 6th edition. Springer, Berlin (285 pp.).
- Holmes, J. A.** (1992). Nonmarine ostracods as Quaternary palaeoenvironmental indicators. *Progress in Physical Geography*, 16(4), 405-431.
- Horne, D.J., Cohen, A., Martens, K.** (2002). Taxonomy, morphology and biology of Quaternary and living Ostracoda. In Holmes, J.A., Chivas, A.R. (Eds.) *The Ostracoda: Applications in Quaternary*, Research Washington D. C., USA: Geophysical Monograph Series; American Geophysical Union, Volume 131, 5–36.
- Howard, A. D., Dietrich, W. E., and Seidl, M. A.** (1994). Modeling fluvial erosion on regional to continental scales. *Journal of Geophysical Research: Solid Earth*, 99(B7), 13971-13986.
- Hubert-Ferrari, A., Armijo, R., King, G., Meyer, B., and Barka, A.** (2002). Morphology, displacement, and slip rates along the North Anatolian Fault, Turkey. *Journal of Geophysical Research: Solid Earth*, 107(B10), ETG-9.
- Huntley, D. J.** (1985). On the zeroing of the thermoluminescence of sediments. *Phys. Chem. Miner.*, 12, 122-127.
- Isacks, B. L.** (1988). Uplift of the central Andean plateau and bending of the Bolivian orocline. *Journal of Geophysical Research: Solid Earth*, 93(B4), 3211-3231.
- Ivanova, E. V., Marret, F., Zenina, M. A., Murdmaa, I. O., Chepalyga, A. L., Bradley, L. R., ... and Zyryanova, M. I.** (2015). The Holocene Black Sea reconnection to the Mediterranean Sea: new insights from the northeastern Caucasian shelf. *Palaeogeography, Palaeoclimatology, Palaeoecology*, 427, 41-61.
- Jara-Muñoz, J., Melnick, D., and Strecker, M. R.** (2016). TerraceM: A MATLAB® tool to analyze marine and lacustrine terraces using high-resolution topography. *Geosphere*, 12(1), 176-195.
- Juggins, S.** (2012). Rioja: analysis of Quaternary Science Data. version 0.7-3. Retrieved from: <https://cran.r-project.org/web/packages/rioja/index.html>.

- Kaesler, R. L., Kontrovitz, M. and Taunton, S.** (1993). Crushing strength of *Puriana pacifica* (Ostracoda), an experimental approach to taphonomy. *J. Paleontol.*, 67, 1005–1010.
- Kalafat, D., and Toksöz, N. M.** (2017). Seismicity and Tectonics of the Black Sea. *Int. J. Earth Sci. Geophys.*, 3, 011.
- Kaniewski, D., Guiot, J., and Van Campo, E.** (2015). Drought and societal collapse 3200 years ago in the Eastern Mediterranean: a review. *Wiley Interdisciplinary Reviews: Climate Change*, 6(4), 369-382.
- Karanovic, I.** (2012). *Recent Freshwater Ostracods of the World: Crustacea, Ostracoda, Podocopida*, The Hague, The Netherlands: Springer Science & Business Media.
- Karimova, S.** (2011). Eddy statistics for the Black Sea by visible and infrared remote sensing. In Tang, D. L. (Ed.). *Remote Sensing of the Changing Oceans*, Berlin, Heidelberg: Springer, 61-75.
- Keith, M.L., and Parker, R.H.** (1965). Local variation of ^{13}C and ^{18}O content of mollusk shells and the relatively minor temperature effect in marginal marine environments. *Marine Geology*, 3, 115–129.
- Keskin, S., Pedroja, K., and Bektaş, O.** (2011). Coastal uplift along the eastern Black Sea coast: New marine terrace data from Eastern Pontides, Trabzon (Turkey) and a review. *Journal of Coastal Research*, 27(6A), 63-73.
- Ketin, İ.** (1948). Über die tektonisch-mechanischen Folgerungen aus den großen anatolischen Erdbeben des letzten Dezenniums: *Geologische Rundschau*, 36, 77-83.
- Keyser, D., Walter, R.** (2004). Calcification in ostracodes, *Rev. Española Micropaleontol.*, 36, 1–11.
- Kihn, G. R., Crespo, F., and Pall, L. J.** (2017). Ostracods of shallow lakes of the central region of Argentina: Paleolimnological implications. *Revista brasileira de palaeontologia*, 20(3), 373-382.
- Kochegura, V. V., and Zubakov, V. A.** (1978). Palaeomagnetic time scale of the Ponto-Caspian Plio-Pleistocene deposits. *Palaeogeography, Palaeoclimatology, Palaeoecology*, 23, 151-160.
- Korotaev, G., Oğuz, T., Nikiforov, A., and Koblinsky, C.** (2003). Seasonal, interannual, and mesoscale variability of the Black Sea upper layer circulation derived from altimeter data. *Journal of Geophysical Research: Oceans*, 108(C4).
- Köse, B., Ateş, S., and ÇelİK, H.** (2014). Determination of late spring frost affections on some grape varieties grown in Samsun. *Türkiye Tarımsal Araştırmalar Dergisi*, 1(2), 162-169.
- Kremenetski, C. V., Chichagova, O. A., and Shishlina, N. I.** (1999). Palaeoecological evidence for Holocene vegetation, climate and land-use change in the low Don basin and Kalmuk area, southern Russia. *Vegetation History and Archaeobotany*, 8(4), 233-246.

- Küçükuysal, C., and Yavuz, N.** (2017). Multi-proxy records of Quaternary fluvio-lacustrine sediments around Lakes Eymir and Mogan, Ankara (Central Anatolia, Turkey). *Environmental Earth Sciences*, 76(16), 587.
- Kuzucuoğlu, C.** (2015). The Rise and Fall of the Hittite State in Central Anatolia, How, When, Where, Did Climate Intervene? In Beyer, D., Henry, O., Tibet, A. (Eds.), *La Cappadoce Méridionale de la préhistoire à la période Byzantine.*, Istanbul : Institut Français d'Études Anatoliennes. 17-41.
- Kuzucuoğlu, C., and Roberts, N.** (1997). Évolution de l'environnement en Anatolie de 20 000 à 6 000 BP. *Paléorient*, 23, 7–24.
- Kuzucuoğlu, C., Dörfler, W., Kunesch, S., and Goupille, F.** (2011). Mid-to late-Holocene climate change in central Turkey: the Tecer Lake record. *The Holocene*, 21(1), 173-188.
- Kuzucuoğlu, C., Çiner, A., and Kazancı, N.** (2019). Introduction to Landscapes and Landforms of Turkey. In Kuzucuoğlu, C., Çiner, A., and Kazancı, N. (Eds.), *Landscapes and Landforms of Turkey*. Cham : Springer, 3-5.
- Kwiecien, O., Arz, H.W., Lamy, F., Wulf, S., Bahr, A., Röhl, U., and Haug, G.H.** (2008). Estimated reservoir ages of the Black Sea since the last glacial. *Radiocarbon*, 50, 99–118.
- Laermans, H., Kelterbaum, D., May, S. M., Elashvili, M., Opitz, S., Hülle, D., ... and Brückner, H.** (2018). Mid-to Late Holocene landscape changes in the Rioni delta area (Kolkheti lowlands, W Georgia). *Quaternary International*, 465, 85-98.
- Landmann, G., Reimer, A., and Kempe, S.** (1996). Climatically induced lake level changes at Lake Van, Turkey, during the Pleistocene/Holocene transition. *Global Biogeochemical Cycles*, 10(4), 797-808.
- Langbein, W. B., and Schumm, S. A.** (1958). Yield of sediment in relation to mean annual precipitation. *American Geophysical Union Transactions*, 39(6), 1076-1084.
- Lavé, J., and Avouac, J. P.** (2001). Fluvial incision and tectonic uplift across the Himalayas of central Nepal. *Journal of Geophysical Research: Solid Earth*, 106(B11), 26561-26591.
- Leeder, M. R., Harris, T., and Kirkby, M. J.** (1998). Sediment supply and climate change: implications for basin stratigraphy. *Basin Research*, 10(1), 7-18.
- Lisiecki, L. E., and Raymo, M. E.** (2005). A Pliocene-Pleistocene stack of 57 globally distributed benthic $\delta^{18}\text{O}$ records. *Paleoceanography*, 20(1).
- Maddy, D., Bridgland, D., and Westaway, R.** (2001). Uplift-driven valley incision and climate-controlled river terrace development in the Thames Valley, UK. *Quaternary International*, 79(1), 23-36.
- Martens, K.** (1985). Effects of temperature and salinity on postembryonic growth in *Mytilocypris henricae* (Chapman) (Crustacea, Ostracoda). *J. Crustac. Boil.*, 5, 258–272.

- Masek, J. G., Isacks, B. L., Gubbels, T. L., and Fielding, E. J.** (1994). Erosion and tectonics at the margins of continental plateaus. *Journal of Geophysical Research: Solid Earth*, 99(B7), 13941-13956.
- Mater, B., and Turoğlu, H.** (2014). Outlines of the Holocene Geomorphology of Anatolia. In Wawruschka, C. (Ed.). *Prehistoric Economies of Anatolia: Subsistence Practices and Exchange*. Workshop at the Austrian Academy of Sciences, 13-14. November, 2009, Vienna.
- McClain, C. and Rex, M.** (2001). The relationship between dissolved oxygen concentration and maximum size in deep-sea turrid gastropods: An application of quantile regression. *Mar. Boil.*, 139, 681–685.
- McClain, K., Yıldırım, C., Çiner, A., Sarıkaya, M.A., Şahin, S., Özcan, O., ... and Ozturk, T.** (2018) Quantification of fluvial response to tectonic deformation in the Central Pontides, Turkey; inferences from OSL dating (updated results and interpretations). *VIII. Quaternary Symposium of Turkey*, Istanbul, May 2-5, 2018.
- Meade, R. H.** (1996). River-sediment inputs to major deltas. In Milliman, J. D., and Haq, B. U. (Eds.), *Sea-level rise and coastal subsidence*, Springer, Dordrecht, 63-85.
- Meijers, M. J. M., Kaymakci, N., Van Hinsbergen, D. J., Langereis, C. G., Stephenson, R. A., and Hippolyte, J. C.** (2010). Late Cretaceous to Paleocene oroclinal bending in the central Pontides (Turkey). *Tectonics*, 29, TC4016.
- Meisch, C.** (2000). Crustacea: Ostracoda. In Schwoerbel, J., and Zwick, P. (Eds.), *Süßwasserfauna von Mitteleuropa*. Heidelberg, Berlin: Spektrum Akademischer Verlag, 8(3), 522 pp.
- Melnick, D., Yıldırım, C., Hillemann, C., Garcin, Y., Çiner, A., Pérez-Gussinyé, M., and Strecker, M. R.** (2017). Slip along the Sultanhanı Fault in Central Anatolia from deformed Pleistocene shorelines of palaeo-lake Konya and implications for seismic hazards in low-strain regions. *Geophysical Journal International*, 209, 3, 1431-1454.
- Merritts, D. J., and Bull, W. B.** (1989). Interpreting Quaternary uplift rates at the Mendocino triple junction, northern California, from uplifted marine terraces. *Geology*, 17(11), 1020-1024.
- Merritts, D. J., Vincent, K. R., and Wohl, E. E.** (1994). Long river profiles, tectonism, and eustasy: A guide to interpreting fluvial terraces. *Journal of Geophysical Research: Solid Earth*, 99(B7), 14031-14050.
- Mertens, K. N., Bradley, L. R., Takano, Y., Mudie, P. J., Marret, F., Aksu, A. E., ... and Matsuoka, K.** (2012). Quantitative estimation of Holocene surface salinity variation in the Black Sea using dinoflagellate cyst process length. *Quaternary Science Reviews*, 39, 45–59.
- Métivier, F., Gaudemer, Y., Tapponnier, P., and Meyer, B.** (1998). Northeastward growth of the Tibet plateau deduced from balanced reconstruction of two depositional areas: The Qaidam and Hexi Corridor basins, China. *Tectonics*, 17(6), 823-842.

- Mezquita, F., Olmos, V., and Oltra, R.** (2000). Population ecology of *Cyprideis torosa* (Jones, 1850) in a hypersaline environment of the Western Mediterranean (Santa Pola, Alacant) (Crustacea: Ostracoda). *Ophelia*, *53*, 119–130.
- Mudie, P. J., Marret, F., Aksu, A. E., Hiscott, R. N., and Gillespie, H.** (2007). Palynological evidence for climatic change, anthropogenic activity and outflow of Black Sea water during the late Pleistocene and Holocene: centennial-to decadal-scale records from the Black and Marmara Seas. *Quaternary International*, *167*, 73-90.
- Müller, G.W.** (1900). Deutschlands Süßwasser-Ostracoden. In Chun, C. (Ed.) *Originalabhandlungen aus dem Gesamtgebiete der Zoologie*, Zoologica, *30*, Leipzig, Germany: Schweizerbart Science Publishers, 1900.
- Murray A. S., and Wintle A. G.** (2000). Luminescence dating of quartz using an improved single-aliquot regenerative-dose protocol. *Radiation Measurements*, *32*, 57-73.
- Murray, J. W., Top, Z., and Özsoy, E.** (1991). Hydrographic properties and ventilation of the Black Sea. *Deep Sea Research Part A: Oceanographic Research*, *38*, 663-689.
- Nicoll, K., and Küçükuysal, C.** (2013). Emerging multi-proxy records of Late Quaternary Palaeoclimate dynamics in Turkey and the surrounding region. *Turkish Journal of Earth Sciences*, *22(1)*, 126-142.
- Nikishin, A. M., Okay, A. I., Tüysüz, O., Demirer, A., Wannier, M., Amelin, N., and Petrov, E.** (2015). The Black Sea Basins structure and history: new model based on new deep penetration regional seismic data. Part 2: Tectonic history and palaeogeography. *Marine and Petroleum Geology*, *59*, 656-670.
- Ocakoğlu, F., Kır, O., Yılmaz, İ. Ö., Açıkalın, S., Erayık, C., Tunoğlu, C., and Leroy, S. A.** (2013). Early to Mid-Holocene Lake level and temperature records from the terraces of Lake Sünnet in NW Turkey. *Palaeogeography, Palaeoclimatology, Palaeoecology*, *369*, 175-184.
- Oğuz, T., La Violette, P. E., and Ünlüata, Ü.** (1992). The upper layer circulation of the Black Sea: Its variability as inferred from hydrographic and satellite observations. *Journal of Geophysical Research: Oceans*, *97(C8)*, 12569-12584.
- Okay, A. I., and Tüysüz, O.** (1999). Tethyan sutures of northern Turkey. Geological Society, London, *Special Publications*, *156(1)*, 475-515.
- Okay, A. I., Siyako, M., and Bürkan, K. A.** (1991). Geology and tectonic evolution of the Biga Peninsula, northwest Turkey. *Bulletin of the Technical University of Istanbul*, *44(1-2)*, 191-256.
- Okay, A. I., Sengor, A. M. C., and Görür, N.** (1994). Kinematic history of the opening of the Black Sea and its effect on the surrounding regions. *Geology*, *22(3)*, 267-270.

- Olley, J. M., Murray A. S., and Robert R. G.** (1996). The effects of disequilibria in the uranium and thorium decay chain on burial dose rates in fluvial sediments. *Quaternary Science Reviews*, 15, 751-760.
- Opreanu, P. A.** (2008). Ostracode relicte Ponto-Caspice in sectorul Romanecs Aal Marii Negre. *GeoEcoMarina*, 14(Suppl 1), 57-62.
- Ostrovsky, A. B., Izmailov, Y. A., Balabanov, I. P., Skiba, S. I., Skryabina, N. G., Arslanov, K. A., ... and Suprunova, N. I.** (1977). Novye dannye o palaeogidrologicheskom rezhime Chernogo moria v verkhnem pleistotsene i golosene [New data on the palaeogeographical regime of the Black Sea in the Late Pleistocene and Holocene]. In Kaplin, P. A., Shcherbakov, F. A. (Eds.), *Paleogeografiia i otlozheniia pleistotsena iuzhnykh morei SSSR [Pleistocene palaeogeography and sediments of the southern seas of the USSR]*, Nauka, Moscow, 131-140.
- Özbal, H. N., Pehlivan, B., E., and Gedik, B.** (2002). Metallurgy at İkiztepe. In Yalçın, Ü. (ed.) *Anatolian Metal II*. Bochum: Deutsches Bergbau-Museum Publications. 39-48.
- Özden, S., Over, S., Kavak, K. S., and Inal, S. S.** (2008). Late Cenozoic stress states around the Bolu basin along the north Anatolian fault, NW Turkey. *Journal of Geodynamics*, 46(1), 48-62.
- Ozener, H., Arpat, E., Ergintav, S., Dogru, A., Cakmak, R., Turgut, B., and Dogan, U.** (2010). Kinematics of the eastern part of the North Anatolian Fault Zone. *Journal of Geodynamics*, 49(3-4), 141-150.
- Özsoy, E., and Ünlüata, Ü.** (1997). Oceanography of the Black Sea: a review of some Recent results. *Earth-Science Reviews*, 42(4), 231-272.
- Öztürk, D., and Sesli, F. A.** (2015). Shoreline change analysis of the Kizilirmak Lagoon Series. *Ocean & Coastal Management*, 118, 290-308.
- Palcu, D. V., Vasiliev, I., Stoica, M., and Krijgsman, W.** (2018). The end of the Great Khersonian Drying of Eurasia: Magnetostratigraphic dating of the Maeotian transgression in the Eastern Paratethys. *Basin Research*, 31(1), 33-58.
- Panin, N., and Popescu, I.** (2007). The northwestern Black Sea: climatic and sea level changes in the Upper Quaternary. In V. Yanko-Hombach, A.S. Gilbert, N. Panin and P.M. Dolukhanov (Eds), *The Black Sea Flood Question: Changes in Coastline, Climate, and Human Settlement.*, New York: Springer, 387-404.
- Placzek, C., Quade, J., Betancourt, J. L., Patchett, P. J., Rech, J. A., Latorre, C., ... and English, N. B.** (2009). Climate in the dry central Andes over Geologic, Millennial, and Interannual Timescales. *Annals of the Missouri Botanical Garden*, 96(3), 386-397.
- Polanyi, K.** (1963). Ports of trade in early societies. *The Journal of Economic History*, 23(1), 30-45.
- Posamentier, H. W., and Morris, W. R.** (2000). Aspects of the stratal architecture of forced regressive deposits. Geological Society of London, *Special Publications*, 172(1), 19-46.

- Prescott J. R., and Hutton J. T.** (1988). Cosmic ray and gamma ray dosimetry for TL and ESR. *Nuclear Tracks Radiation Measurements*, 14, 223-227.
- Prescott J. R., and Hutton J. T.** (1994). Cosmic ray contribution to dose rates for luminescence and ESR dating: large depths and long-term time variations. *Radiation Measurements*, 23, 497-500.
- Purcell, J. E., Shiganova, T. A., Decker, M. B., and Houde, E. D.** (2001). The ctenophore *Mnemiopsis* in native and exotic habitats: US estuaries versus the Black Sea basin. *Hydrobiologia*, 451(1-3), 145-176.
- Radeff, G., Schildgen, T. F., Cosentino, D., Strecker, M. R., Cipollari, P., Darbaş, G., and Gürbüz, K.** (2017). Sedimentary evidence for late Messinian uplift of the SE margin of the Central Anatolian Plateau: Adana Basin, southern Turkey. *Basin Research*, 29(S1), 488-514.
- Ramos, L. Y., Alperin, M., Pérez, A. P., Coviaga, C. A., Schwalb, A., and Cusminsky, G. C.** (2015). *Eucypris fontana* (Graf, 1931) (Crustacea, Ostracoda) in permanent environments of Patagonia Argentina: a geometric morphometric approach. *International Journal of Limnology*, 51(2), 125-138.
- Ramsey, K. W., and Baxter, S. J.** (1996). Reports of Investigations, 54(1). Delaware Geological Survey, Reports of Investigations 54, 1–18.
- Ramstein, G., Fluteau, F., Besse, J., and Joussaume, S.** (1997). Effect of orogeny, plate motion and land-sea distribution on Eurasian climate change over the past 30 million years. *Nature*, 386(6627), 788-795.
- Rangin, C., Bader, A. G., Pascal, G., Ecevitoglu, B., and Görür, N.** (2002). Deep structure of the Mid Black Sea High (offshore Turkey) imaged by multi-channel seismic survey (BLACKSIS cruise) 1, 2. *Marine Geology*, 182(3-4), 265-278.
- Reimer, P. J., Bard, E., Bayliss, A., Beck, J. W., Blackwell, P. G., Ramsey, C. B., ... and van der Plicht, J.** (2013). IntCal13 and Marine13 radiocarbon age calibration curves 0–50,000 years cal BP. *Radiocarbon*, 55(4), 1869-1887.
- Reineck, H. E., and Singh, I. B.** (1980). Tidal flats. In *Depositional Sedimentary Environments: With Reference to Terrigenous Clastics*. Berlin, Heidelberg: Springer,, 430-456.
- Remane, A.** (1934). Die Brackwasserfauna. *Verhandlungen der Deutschen zoologischen Gesellschaft*, 36, 34-74.
- Remane, A.** (1958). Die Biologischen Grenzen Meer—Süßwasser und Meer—Land, *Geol. Rundsch.*, 47, 11–24.
- Remane, A., and Schlieper, C.** (1971). Biology of brackish water. *Die Binnengewässer*, 25, Schweizerbart Science Publishers.
- Riller, U., and Oncken, O.** (2003). Growth of the Central Andean Plateau by tectonic segmentation is controlled by the gradient in crustal shortening. *The Journal of Geology*, 111(3), 367-384.
- Roberts, N., Reed, J. M., Leng, M. J., Kuzucuoğlu, C., Fontugne, M., Bertaux, J., ... and Karabiyikoğlu, M.** (2001). The tempo of Holocene

climatic change in the eastern Mediterranean region: new high-resolution crater-lake sediment data from central Turkey. *The Holocene*, 11(6), 721-736.

- Roberts, N., Eastwood, W. J., Kuzucuoğlu, C., Fiorentino, G., and Caracuta, V.** (2011). Climatic, vegetation and cultural change in the eastern Mediterranean during the mid-Holocene environmental transition. *The Holocene*, 21(1), 147-162.
- Roberts, N., Allcock, S. L., Arnaud, F., Dean, J. R., Eastwood, W. J., Jones, M. D., ... and Yiğitbaşıoğlu, H.** (2016). A tale of two lakes: a multi-proxy comparison of Lateglacial and Holocene environmental change in Cappadocia, Turkey. *Journal of Quaternary Science*, 31(4), 348-362.
- Robertson, A. H., Parlak, O., and Ustaömer, T.** (2012). Overview of the Palaeozoic–Neogene evolution of neotethys in the Eastern Mediterranean region (southern turkey, cyprus, Syria). *Petroleum Geoscience*, 18(4), 381-404.
- Robinson, A. G., Rudat, J. H., Banks, C. J., and Wiles, R. L. F.** (1996). Petroleum geology of the Black Sea. *Marine and Petroleum Geology*, 13(2), 195-223.
- Rögl, F.** (1999). Mediterranean and Paratethys. Facts and hypotheses of an Oligocene to Miocene paleogeography (short overview). *Geologica carpathica*, 50(4), 339-349.
- Rosenfeld, A., and Vesper, B.** (1977). The variability of the sieve-pores in Recent and fossil species of *Cyprideis torosa* (Jones, 1850) as an indicator for salinity and palaeosalinity. In Löffler, H., Danielopol, D. (Eds.), *Aspects of ecology and zoogeography of Recent and fossil ostracoda*. Dordrecht : Springer Science and Business Media, 1978, 55–67.
- Rossi, V.** (2009). Ostracod assemblages from Holocene subsurface deposits of modern Po Delta: a palaeoenvironmental proxy record. *Bollettino della Società Paleontologica Italiana*, 48(2), 95-103.
- Rothwell, R. G. and Croudace, I. W.** (2015). Twenty years of XRF core scanning marine sediments: What do geochemical proxies tell us? In Croudace, I.W., Rothwell, R.G., (Eds.) *Micro-XRF Studies of Sediment Cores*. Springer, Berlin, 25–102.
- Ruddiman, W. F., and Kutzbach, J. E.** (1991). Plateau uplift and climatic change. *Scientific American*, 264(3), 66-75.
- Ryan, W. B. F., Major, C. O., Lericolais, G., and Goldstein, S. L.** (2003). Catastrophic flooding of the Black Sea. *Annual Review of Earth and Planetary Sciences*, 31(1), 525-554.
- Samsunlu, A., Akca, L., Kinaci, C., Findik, N., and Tanik, A.** (2002). Significance of wetlands in water quality management-past and present situation of Kizilirmak Delta, Turkey. *Water science and technology*, 46(8), 145-152.
- Sarıkaya, M. A., Zreda, M., and Çiner, A.** (2009). Glaciations and palaeoclimate of Mount Erciyes, central Turkey, since the Last Glacial Maximum,

inferred from ^{36}Cl cosmogenic dating and glacier modeling. *Quaternary Science Reviews*, 28(23-24), 2326-2341.

- Sarıkaya, M.A., and Çiner, A.** (2015). Late Pleistocene glaciations and palaeoclimate of Turkey. *Bulletin of Mineral Research and Exploration (MTA Journal)*, 151, 107-127.
- Sarıkaya, M. A., and Çiner, A.** (2017). Late Quaternary glaciations in the eastern Mediterranean. Geological Society of London, *Special Publications*, 433(1), 289-305.
- Sarıkaya, M.A., Zreda, M., and Çiner, A.** (2009). Glaciations and palaeoclimate of Mount Erciyes, central Turkey, since the Last Glacial Maximum, inferred from ^{36}Cl cosmogenic dating and glacier modelling. *Quaternary Science Reviews*, 28, 2326–2341.
- Saygı, Y., Gündüz, E., Demirkalp, F. Y., and Çağlar, S. S.** (2011). Seasonal patterns of the zooplankton community in the shallow, brackish Liman Lake in Kızılırmak Delta, Turkey. *Turkish Journal of Zoology*, 35(6), 783-792.
- Schildgen, T. F., Cosentino, D., Bookhagen, B., Niedermann, S., Yıldırım, C., Echtler, H., ... and Strecker, M. R.** (2012). Multi-phased uplift of the southern margin of the Central Anatolian plateau, Turkey: A record of tectonic and upper mantle processes. *Earth and Planetary Science Letters*, 317, 85-95.
- Schildgen, T. F., Yıldırım, C., Cosentino, D., and Strecker, M. R.** (2014). Linking slab break-off, Hellenic trench retreat, and uplift of the Central and Eastern Anatolian plateaus. *Earth Science Reviews*, 128, 147-168.
- Schönwiese, C.** (1995). *Klimaänderungen: Daten, Fakten, Analysen*. Heidelberg, Berlin : Springer.
- Schornikov, E. I.** (1972). *Ecology of Azov and Black Sea ostracodes*. Biologiya morya, 26(5), Kiev.
- Scott, H. W.** (1961). Shell morphology of Ostracoda. *Arthropoda*, 3, 21–37.
- Seeliger, M., Pint, A., Frenzel, P., Feuser, S., Pirson, F., Riedesel, S., and Brückner, H.** (2017). Foraminifera as markers of Holocene sea-level fluctuations and water depths of ancient harbours—A case study from the Bay of Elaia (W Turkey). *Palaeogeography, Palaeoclimatology, Palaeoecology*, 482, 17-29.
- Şengör A. M. C.** (1979). The North Anatolian Transform Fault: its age, offset and tectonic significance, London, *Journal of the Geological Society*, 136, 269-282.
- Şengör, A. M. C., and Yılmaz, Y.** (1981). Tethyan evolution of Turkey: a plate tectonic approach. *Tectonophysics*, 75(3-4), 181-190, 193-199, 203-241.
- Şengör, A. M. C., Tüysüz, O., İmren, C., Sakınç, M., Eyidoğan, H., Görür, N., ... and Rangin, C.** (2005). The North Anatolian fault: A new look. *Annu. Rev. Earth Planet. Sci.*, 33, 37-112.

- Şensoy, S., Demircan, M., Ulupinar, U., and Balta, I.** (2008). The climate of Turkey. *Turkish State Meteorological Services*. <http://www.dmi.gov.tr/iklim/iklim.aspx>.
- Shmuratko, V.** (2001). Gravitatsionno-rezonansnaia ekzotektonika [Gravity-resonance exotectonic]. *Astroprint*, Odessa.
- Siani, G., Paterne, M., Arnold, M., Bard, E., Métivier, B., Tisnerat, N., and Bassinot, F.** (2000). Radiocarbon reservoir ages in the Mediterranean Sea and Black Sea. *Radiocarbon*, 42, 271–280.
- Sivan, D., Wdowinski, S., Lambeck, K., Galili, E., and Raban, A.** (2001). Holocene sea-level changes along the Mediterranean coast of Israel, based on archaeological observations and numerical model. *Palaeogeography, Palaeoclimatology, Palaeoecology*, 167(1-2), 101-117.
- Smith, A.J., and Horne, D. J.** (2002). Ecology of marine, marginal marine and nonmarine Ostracodes, p. 37-64. In Holmes, J. A., Chivas, A. R. (Eds.). *The Ostracoda: Applications in Quaternary Research*. Geophysical Monograph, 131. American Geophysical Union, Washington D.C., USA.
- Snaveley, N., Seitz, S. M., and Szeliski, R.** (2007). Modelling the World from Internet Photo Collections. *International Journal of Computer Vision*, 80(2), 189-210.
- Sobel, E. R., Hilley, G. E., and Strecker, M. R.** (2003). Formation of internally drained contractional basins by aridity-limited bedrock incision. *Journal of Geophysical Research: Solid Earth*, 108(B7).
- Stephenson, R., and Schellart, W. P.** (2010). The Black Sea back-arc basin: insights to its origin from geodynamic models of modern analogues. Geological Society, London, *Special Publications*, 340(1), 11-21.
- Strecker, M. R., Alonso, R. N., Bookhagen, B., Carrapa, B., Hilley, G. E., Sobel, E. R., and Trauth, M. H.** (2007). Tectonics and climate of the southern central Andes. *Annu. Rev. Earth Planet. Sci.*, 35, 747-787.
- Strecker, M. R., Alonso, R., Bookhagen, B., Carrapa, B., Coutand, I., Hain, M. P., ... and Sobel, E. R.** (2009). Does the topographic distribution of the central Andean Puna Plateau result from climatic or geodynamic processes?. *Geology*, 37(7), 643-646.
- Svitoch, A. A., Selivanov, A. O., and Yanina, T. A.** (2000). Paleohydrology of the Black Sea Pleistocene basins. *Water Resources*, 27(6), 594-603.
- Swift, D. J.** (1968). Coastal erosion and transgressive stratigraphy. *The Journal of Geology*, 76, 444–456.
- Symposium on the Classification of Brackish Waters** (1958). The Venice system for the classification of marine waters according to salinity. *Oikos*, 9, 311–312.
- Tapponnier, P., Zhiqin, X., Roger, F., Meyer, B., Arnaud, N., Wittlinger, G., and Jingsui, Y.** (2001). Oblique stepwise rise and growth of the Tibet Plateau. *Science*, 294(5547), 1671-1677.

- Tatar, O., Poyraz, F., Gürsoy, H., Cakir, Z., Ergintav, S., Akpınar, Z., ... and Yavaşoğlu, H.** (2012). Crustal deformation and kinematics of the Eastern Part of the North Anatolian Fault Zone (Turkey) from GPS measurements. *Tectonophysics*, 518, 55-62.
- Törnqvist, T. E., and Hijma, M. P.** (2012). Links between early Holocene ice-sheet decay, sea-level rise and abrupt climate change. *Nature Geoscience*, 5(9), 601.
- Trahms, O.K.** (1939). Beiträge zur Ökologie küstennaher Brackwasser. 2. Die Bodenfauna und Bodenflora des Großen Jasmunder Boddens. *Arch. Hydrobiol.*, 36, 1–35.
- Triantaphyllou, M., Dimiza, M., Krasakopoulou, E., Malinverno, E., Lianou, V., and Souvermezoglou, E.** (2010). Seasonal variation in *Emiliana huxleyi* coccolith morphology and calcification in the Aegean Sea (Eastern Mediterranean). *Geobios*, 43(1), 99-110.
- Tunoğlu, C.** (2001). Pontian aged *Loxococoncha* (Ostracoda) from eastern Black Sea region of Turkey. *Yerbilmeri*, 24, 127-142.
- Turner, R., Roberts, N., and Jones, M. D.** (2008). Climatic pacing of Mediterranean fire histories from lake sedimentary microcharcoal. *Global and Planetary Change*, 63(4), 317-324.
- Turoğlu, H.** (2005). Kızılırmak Deltası ve Yakın Çevresinin Jeomorfolojik Özellikleri ve İnsan Yaşamındaki Etkileri. İstanbul Üniversitesi, *İkiztepe Kazılarının, 30. Yılı Sempozyumu*, 1-4 September 2005, Samsun.
- Turoğlu, H.** (2010). Kızılırmak Deltası ve yakın çevresinin jeomorfolojik özellikleri ve insan yaşamındaki etkileri. *Anadolu Araştırmaları*, İstanbul: İstanbul University Publications, 4903, 98-111.
- Tüysüz, O.** (1999). Geology of the Cretaceous sedimentary basins of the Western Pontides. *Geological Journal*, 34(1-2), 75-93.
- Tyuleneva, N., Suchkov, I., and Fedoronchuk, N.** (2014). Changes in coastline positions during the Holocene in the shelf of the Northwestern Black Sea. *Quaternary International*, 345, 77-87.
- Uğuz, M. F., and Sevin, M.** (2007). Geology map of Sinop: E35. Ankara Maden Tetkik Arama Genel Müdürlüğü. Scale 1:100,000.
- Uğuz, M. F., and Sevin, M.** (2009). Geology map of Sinop: F35. Ankara Maden Tetkik Arama Genel Müdürlüğü. Scale 1:100,000.
- Ustaoğlu, M. R., Mis, D. Ö., and Aygen, C.** (2012). Observations on zooplankton in some lagoons in Turkey. *Journal of Black Sea/Mediterranean Environment*, 18(2).
- Van Baak, C. G. C.** (2015). *Mediterranean-Paratethys connectivity during the late Miocene to Recent: Unraveling geodynamic and paleoclimatic causes of sea-level change* (Ph. D. thesis), University Utrecht.
- Van Baak, C. G., Grothe, A., Richards, K., Stoica, M., Aliyeva, E., Davies, G. R., ... and Krijgsman, W.** (2019). Flooding of the Caspian Sea at the

intensification of Northern Hemisphere Glaciations. *Global and Planetary Change*, 174, 153-163.

- Van Harten, D.** (1975) Size and environmental salinity in the modern euryhaline ostracod *Cyprideis torosa* (Jones, 1850), a biometrical study. *Palaeogeogr. Palaeoclimatol. Palaeoecol.*, 17, 35–48.
- Van Harten, D.** (1996) *Cyprideis torosa* (Ostracoda) revisited. Of salinity, nodes and shell size. In *Proceedings of the Second European Ostracodologists' Meeting*, London, UK: British Micropalaeontological Society, 191, 194.
- Van Harten, D.** (2000) Variable nodding in *Cyprideis torosa* (Ostracoda, Crustacea): An overview, experimental results and a model from Catastrophe Theory. *Hydrobiologia*, 419, 131–139.
- Van Hinsbergen, D. J., Maffione, M., Plunder, A., Kaymakçı, N., Ganerød, M., Hendriks, B. W., ... and Vissers, R. L. M.** (2016). Tectonic evolution and paleogeography of the Kırşehir Block and the Central Anatolian Ophiolites, Turkey. *Tectonics*, 35(4), 983-1014.
- Van Morkhoven, F.P.** (1962). *Post-Palaeozoic Ostracoda: Their Morphology, Taxonomy, and Economic Use: 1. General*, Amsterdam, The Netherlands: Elsevier, (204 pp.).
- Van Zeist, W., Woldring, H., and Stapert, D.** (1975). Late Quaternary vegetation and climate of southwestern Turkey. *Palaeohistoria*, 17, 53–143.
- Vandenberghe, J.** (2008). The fluvial cycle at cold–warm–cold transitions in lowland regions: a refinement of theory. *Geomorphology*, 98(3-4), 275-284.
- Vesper, B.** (1972). Zum Problem der Buckelbildung bei *Cyprideis torosa* (Jones, 1850) (Crustacea, Ostracoda, Cytheridae). *Mitteilungen aus dem Hamburgischen Zoologischen Museum und Institut*, 68(79), 94.
- Vött, A.** (2007). Relative sea level changes and regional tectonic evolution of seven coastal areas in NW Greece since the mid-Holocene. *Quaternary Science Reviews*, 26(7-8), 894-919.
- Welton, M. L.** (2010). *Mobility and social organization on the ancient Anatolian Black Sea coast: An archaeological, spatial and isotopic investigation of the cemetery at İkiztepe, Turkey*. PhD Thesis, University of Toronto (597 pp.).
- Whipple, K. X., and Tucker, G. E.** (1999). Dynamics of the stream-power river incision model: Implications for height limits of mountain ranges, landscape response timescales, and research needs. *Journal of Geophysical Research: Solid Earth*, 104(B8), 17661-17674.
- Whipple, K. X., Kirby, E., and Brocklehurst, S. H.** (1999). Geomorphic limits to climate-induced increases in topographic relief. *Nature*, 401(6748), 39.
- Wick, L., Lemcke, G., and Sturm, M.** (2003). Evidence of Lateglacial and Holocene climatic change and human impact in eastern Anatolia: high-resolution pollen, charcoal, isotopic and geochemical records

from the laminated sediments of Lake Van, Turkey. *The Holocene*, 13(5), 665-675.

- Yanko-Hombach, V. V.** (2007). Controversy over Noah's Flood in the Black Sea: geological and foraminiferal evidence from the shelf. In Yanko-Hombach, V., Gilbert, A. S., Panin, N., Dolukhanov, P. (Eds.), *The Black Sea Flood Question: Changes in Coastline, Climate, and Human Settlement*. Springer, Dordrecht, pp. 149–204.
- Yanko-Hombach, V. V., Yanina, T. A., and Motnenko, I.** (2013). Neopleistocene stratigraphy of the Ponto-Caspian Corridors. *IGCP 610 First Plenary Conference and Field Trip*, Tbilisi, Georgia, 12-19 October.
- Yanko-Hombach, V., Gilbert, A. S., Panin, N., and Dolukhanov, P. M.** (2007). *The Black Sea Flood Question: Changes in Coastline, Climate and Human Settlement*. Dordrecht : Springer Science and Business Media.
- Yıldırım, C., Schildgen, T. F., Echtler, H., Melnick, D., and Strecker, M. R.** (2011). Late Neogene and active orogenic uplift in the Central Pontides associated with the North Anatolian Fault: Implications for the northern margin of the Central Anatolia Plateau, Turkey. *Tectonics*, 30(5).
- Yıldırım, C., Melnick, D., Ballato, P., Schildgen, T. F., Echtler, H., Erginal, A. E., ... and Strecker, M. R.** (2013a). Differential uplift along the northern margin of the Central Anatolia Plateau: inferences from marine terraces. *Quaternary Science Reviews*, 81, 12-28.
- Yıldırım, C., Schildgen, T. F., Echtler, H., Melnick, D., Bookhagen, B., Çiner, A., ... and Strecker, M. R.** (2013b.) Tectonic implications of fluvial incision and pediment deformation at the northern margin of the Central Anatolia Plateau based on multiple cosmogenic nuclides. *Tectonics*, 32(5), 1107-1120.
- Yılmaz, C.** (2005). Kızılırmak Deltası'nda meydana gelen erozyonun coğrafi analizi. In Tüysüz, O. (Ed.), *Türkiye Kuvaterner Sempozyumu (TURQUA)*, Istanbul Technical University, Eurasia Institute for Earth Sciences, 2-5 June 2005, Istanbul, 227–234.
- Yin, Y., Geiger, W., and Martens, K.** (1999). Effects of genotype and environment on phenotypic variability in *Limnocythere inopinata* (Crustacea: Ostracoda). *Hydrobiologia*, 400, 85-114.
- Zaitsev, Y., and Mamaev, V.** (1997). Marine biological diversity in the Black Sea - A study of change and decline. New York, *United Nations Publications*, 208.
- Zhai, D., Xiao, J., Zhou, L., Wen, R., Chang, Z., and Pang, Q.** (2010). Similar distribution pattern of different phenotypes of *Limnocythere inopinata* (Baird) in a brackish-water lake in Inner Mongolia. *Hydrobiologia*, 651(1), 185-197.
- Zhang, W., Qi, J., Wan, P., Wang, H., Xie, D., Wang, X., and Yan, G.** (2016). An Easy-to-Use Airborne LiDAR Data Filtering Method Based on Cloth Simulation. *Remote Sensing*, 8(6), 501 p.

Zubakov, V. A., and Borzenkova, I. I. (1990). Global palaeoclimate of the late Cenozoic. *Developments in Paleontology and Stratigraphy, 12*, Amsterdam, Netherlands : Elsevier.





APPENDIX

OSL dating

Optically Stimulated Luminescence dating of sedimentary deposits is based on the following equation: $OSL\ age = D_e / D_r$ where the equivalent dose (D_e) is the absorbed radiation dose (Huntley, 1985) and the radiation dose rate (D_r) is calculated from measurements of the radioactive isotopes within the sample and its surroundings plus the radiation dose rate from cosmic rays.

Sample preparation

The samples were prepared under subdued red light at the Istanbul OSL Research and Archeometry Lab. The center portions of the sediment tubes were wet-sieved, and the 90-180 μ m fraction was used for further analysis. The sediment was washed and treated with 10% HCl to remove carbonate particles, with 30% H₂O₂ to remove organic material, with 36-38% HF to remove feldspar grains and to etch the quartz grains twice, and with 10% HCl to remove possible remnant carbonate particles. Finally, the etched quartz grains were dried at 50°C.

These quartz grains were scattered over a 9 mm stainless steel disc with a silicon spray for OSL measurements. The OSL equivalent dose was measured using an automated Risø DA-15 TL-OSL system (equipped with an internal ⁹⁰Sr-⁹⁰Y beta source giving a dose rate of 89 mGy/s and 40 mW/cm² to the sample) and detected by an EMI 9635QA photomultiplier tube fitted with 7.5-mm-thick Hoya U-340 filters (Bøtter-Jensen, 1997).

Equivalent dose measurement

Banerjee et al. (1999) and Murray and Wintle (2000) presented the Single-Aliquot Regenerative Dose (SAR) protocol after an earlier proposal by Huntley (1985) to obtain estimates of absorbed natural radiation doses of samples. These samples contain light-emitting minerals such as quartz, feldspar, and calcite, making the method suitable for dating particularly sandy samples. The radiation dose absorbed

by the material during its burial time in the natural environment is proportional to the intensity of the emitted light. Equivalent doses of quartz grains were determined using the OSL- SAR protocol (A. Table; Murray and Wintle, 2000).

A. Table : The sequence of the Single-Aliquot Regenerative Dose (SAR) protocol

1.	Regenerative Dose (D_i)
2.	Preheating at 260 °C for 10 s
3.	OSL measurement at 125 °C for 40 s (L_i)
4.	Test dose (T_D)
5.	TL to 180 °C
6.	Test dose OSL measurement at 125 °C for 40 s (T_i)

The SAR protocol used involves six measurement cycles, including one natural dose, three regenerative doses, one zero-dose cycle, and a repeat of the first regenerative dose. The fixed-test dose (T_D) was employed prior to cut-heat temperature to test sensitivity correction, with the aim of building a dose-response curve using the corrected dose points. Subsequently, the equivalent dose was determined by interpolating the natural OSL signal over the dose- effect curve (A.1).

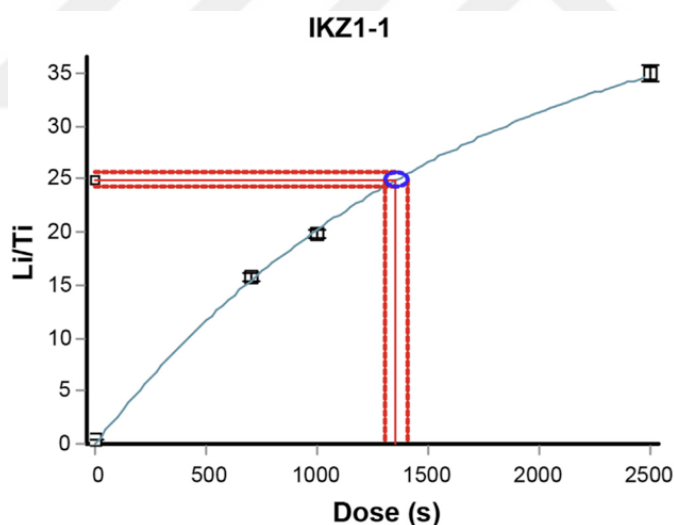


Figure A.1 : OSL dose-response curve constructed for the sample IKZ1-1 using sensitivity-corrected dose points.

The fixed test dose (T_D) was employed prior to the cut-heat temperature for the sensitivity correction and build-up of dose-response curves based on the corrected dose points, and the equivalent dose was determined by interpolating the natural OSL over the dose-effect curve. Precision analysis based on the Analyst program is presented in A.2 for representative samples of IKZ1-3 and KOL-1. The equivalent

dose used in age calculation was the arithmetic mean of the values obtained for aliquots (subsamples) using the SAR protocol as described above.

Dose-rate estimate

Concentrations of the radioactive isotopes U, Th, and ⁴⁰K and the moisture content of the samples were measured at Acme Analytical Laboratories Ltd. (Vancouver, Canada) to estimate the dose rate. Cosmic radiation contributions were measured using the sampling depth, elevation, and location (Olley et al., 1996; Prescott and Hutton, 1988, 1994). External alpha contributions to the dose rates were neglected for the quartz grains.

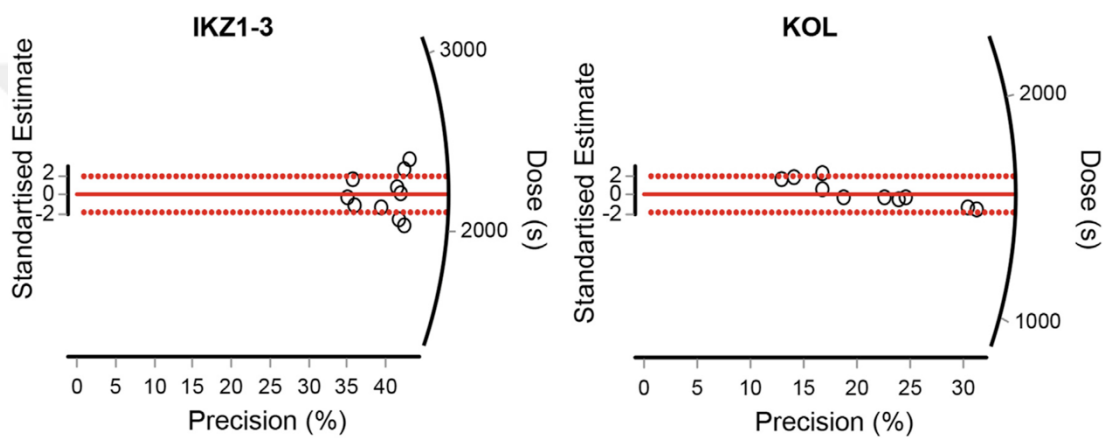


Figure A.2 : Precision analyses based on the Analyst program for representative samples of IKZ1-3 and KOL-1 (ten aliquots for each sample).



CURRICULUM VITAE



Name Surname : Christopher Berndt

Place and Date of Birth : Gera / 25.08.1989

E-Mail : berndt@itu.edu.tr

EDUCATION

B.Sc. : 2011, Freiberg University of Mining and Technology, Faculty of Geosciences, Geoengineering and Mining, Institute for Geology

M.Sc. : 2014, Friedrich Schiller University, Faculty of Chemistry of Earth Sciences, Institute for Geosciences

PUBLICATIONS ON THE THESIS

- **Berndt, C.**, Yıldırım, C., Çiner, A., Strecker, M., Ertunç, G., Sarıkaya, M. A., Özcan, O., Öztürk, T., Güneç Kıyak, N. 2018. Quaternary uplift of the northern margin of the Central Anatolian Plateau: New OSL dates of fluvial and delta-terrace deposits of the Kızılırmak River, Black Sea coast, Turkey, *Quaternary Science Reviews*, **201**, 446-469. DOI:10.1016/j.quascirev.2018.10.029
- **Berndt, C.**, Frenzel, P., Ertunç, G., Çiner, A., Yıldırım, C. 2019. Holocene marginal marine ostracod successions from the Kızılırmak River delta; Implications for depositional environments and sea-level changes at the Southern Black Sea coast. *Sedimentary Geology*, **382**, p. 103-121.
- **Berndt, C.**, Frenzel, P., Çiner, A., Yıldırım, C. 2019. Intraspecific Length Variation and Shell Thickness of the Ostracod *Cyprideis torosa* (Jones, 1850) as a Potential Tool for Palaeosalinity Characterization. *Geosciences*, **9(2)**, p. 83.

PRESENTATIONS ON THE THESIS

- **Berndt, C.**, Ertunç, G., Yıldırım, C., Çiner, A., Sarıkaya, M. A., Öztürk, T., and Kıyak, N. G. 2016: OSL dating of fluvial strath terrace levels of the Kızılırmak River: Implications for the Uplift of the Central Pontides. Congrès des Doctorants, Institute de Physique de Globe, March 14-18, 2016, Paris, France.
- **Berndt, C.**, Ertunç, G., Yıldırım, C., Çiner, A., Sarıkaya, M. A., Öztürk, T., Kıyak, N. G. 2016: OSL Dating of fluvial strath terraces and paleo- delta levels of

the Kızılırmak River: Implications for the Uplift of the Central Pontides. 69th Geological Congress of Turkey, 11-15 April, Ankara, 477.

- **Berndt, C.**, Ertunç, G., Çiner, A., Yıldırım, C., Sarıkaya, M. A. 2016: Post-glacial development of the Black Sea level during Kızılırmak Delta build-up: Insights from microfaunal analysis. 69th Geological Congress of Turkey, 11-15 April, Ankara, Turkey, 598.
- **Berndt, C.**, Ertunç, G., Yıldırım, C., Çiner, A., Sarıkaya, M. A., Öztürk, T., Kıyak, N. G. 2016: OSl Dating of fluvial strath terraces and paleo-delta levels of the Kızılırmak River: Implications for the Uplift of the Central Pontides. TURQUA, Istanbul Technical University, 24.
- **Berndt, C.**, Ertunç, G., Yıldırım, C., Çiner, A., Sarıkaya, M. A., Öztürk, T., Kıyak, N. G., Özcan, O. 2016: OSL Dating of Fluvial Strath and Delta Terrace Levels of the Kızılırmak River: Implications for the Uplift of the Central Pontides. AGU General Assembly, 12-16 December 2016, San Francisco, EP11B-1008.
- **Berndt, C.**, Yıldırım, C., Çiner, A., Ertunç, G., Sarıkaya, M. A., Özcan, O., Kıyak, N. G., Öztürk, T. 2017: Timing and development of Late Quaternary fluvial terraces of the lower course of Kızılırmak River (Northern Turkey). EGU General Assembly, Vienna, Geophysical Research Abstracts, Vol. 19, EGU2017-1173.
- **Berndt, C.**, Ertunç, G., Çiner, A., Yıldırım, C., Frenzel, P. 2017: Late Quaternary paleoenvironmental development of the Kızılırmak delta plain (Northern Turkey). EGU General Assembly, Vienna, Geophysical Research Abstracts, Vol. 19, EGU2017-1259.